LAPPEENRANTA UNIVERSITY OF TECHNOLOGY
LUT School of Energy
Electrical Engineering

Eduard Ignatev

PERFORMANCE DEGRADATION MODELLING AND TECHNO-ECONOMIC ANALYSIS OF LITHIUM-ION BATTERY ENERGY STORAGE SYSTEMS

First examiner Professor Jarmo Partanen
Second examiner Associate Professor Jukka Lassila
Supervisor Mikko Honkaniemi, ABB Power Grids, Vaasa

ABSTRACT

Lappeenranta University of Technology
LUT School of Energy
Electrical Engineering

Eduard Ignatev

Performance Degradation Modelling and Techno-Economic Analysis of Lithium-Ion Battery Energy Storage Systems

Master's thesis

2016

88 pages, 52 figures, 11 tables and 7 appendices

First examiner Professor Jarmo Partanen
Second examiner Associate Professor Jukka Lassila
Supervisor Mikko Honkaniemi, ABB Power Grids, Vaasa

Keywords: Lithium-ion, Lifetime, Battery energy storage system, Frequency Containment Reserves, Net present value.

Transmission system operators and distribution system operators are experiencing new challenges in terms of reliability, power quality, and cost efficiency. Although the potential of energy storages to face those challenges is recognized, the economic implications are still obscure, which introduce the risk into the business models.

This thesis aims to investigate the technical and economic value indicators of lithium-ion battery energy storage systems (BESS) in grid-scale applications. In order to do that, a comprehensive performance lithium-ion BESS model with degradation effects estimation is developed. The model development process implies literature review on lifetime modelling, use, and modification of previous study progress, building the additional system parts and integrating it into a complete tool. The constructed model is capable of describing the dynamic behavior of the BESS voltage, state of charge, temperature and capacity loss.

Five control strategies for BESS unit providing primary frequency regulation are implemented, in addition to the model. The questions related to BESS dimensioning and the end of life (EoL) criterion are addressed. Simulations are performed with one-month real frequency data acquired from Fingrid. The lifetime and cost-benefit analysis of the simulation results allow to compare and determine the preferable control strategy. Finally, the study performs the sensitivity analysis of economic profitability with variable size, EoL and system price. The research reports that BESS can be profitable in certain cases and presents the recommendations.

ACKNOWLEDGMENTS

This master's thesis was carried out at the department of Electrical Engineering at Lappeenranta University of Technology (LUT) School of Energy as part of the Double Degree program with Moscow Power Engineering Institute (MPEI). I would like to thank all persons, who are responsible for the existence of Double Degree program and making such an experience possible.

I would like to give special thanks to my research supervisor Jukka Lassila, for his guidance throughout the thesis and valuable comments, which helped to improve the work. I would also like to thank my home university supervisor Alexander Polyakov for early stage discussions and original suggestion to research the lithium-ion battery storages.

This work was also arranged with ABB Oy, Vaasa. I express my gratitude to Dmitry Vinokurov, Mikko Honkaniemi, Seppo Pasto, and Julia Vauterin-Pyrhönen, who gave me this opportunity to work on my thesis and get an inside look at Power Grids division in Vaasa.

Thanks to all my friends at Russia for sincere affection and missing me. I am also very grateful for meeting a lot of pleasant people in Lappeenranta and making a connection with them.

Finally, I would like to acknowledge my family, especially my mother and father, for their encouragement and enormous support over the years of my study. This thesis would not be possible without them, and I infinitely appreciate it.

Eduard Ignatev
Lappeenranta, May 2016

TABLE OF CONTENTS

LIST OF SYMBOLS

Ah_{th}	Ampere-hour throughput [Ah]
b	Complex balancing factor
B	Pre-exponent factor
C_0	Initial investment [EUR]
C_1	Short time transient capacity [F]
C_2	Long time transient capacity [F]
c_e	Electricity price [EUR/MWh]
C_e	Loss due to efficiency [EUR]
C_{rate}	Current rate
C_t	Cash flow [EUR]
DoD	Depth of discharge
Ea	Activation energy [$kJ \times mol^{-1}$]
E_{BESS}	Total BESS capacity [MWh]
I_{cell}	Cell throughput current [A]
k_i	Kinetic dependence of the capacity fade evolution
N_{cyc}	Number of cycles
NPV	Net Present Value [EUR]
$P_{FCR\text{-}N}$	FCR-N maximum bidding power [MW]
$P_{rec\ charge}$	Charge power during recovery [p.u.]
$P_{rec\ discharge}$	Discharge power during recovery [p.u.]
$Q_{cycling}$	Capacity loss due to cycling [%]
Q_{loss}	Total capacity loss [%]
Q_{nom}	Cell nominal capacity [Ah]
$Q_{storage}$	Capacity loss dues to storage [%]
r	Discount rate
r	Number of years for analysis
R	Universal gas constant [$J \times mol^{-1}K^{-1}$]

R_0	Cell internal resistance [Ohm]
R_1	Short time transient resistance [Ohm]
R_2	Long time transient resistance [Ohm]
R_2	Long time transient resistance [Ohm]
SoC	State of charge
SoC_{max}	State of charge maximum limit
SoC_{min}	State of charge minimum limit
SoC_{ref}	State of charge set point
t	Number of cash flow year
t	Time
T	Temperature [K]
t_{15min}	Full activation time period requirement [h]
T_{ref}	Reference temperature [K]
V_{cell}	Cell terminal voltage [V]
V_{OC}	Open-circuit voltage [V]
α_{3-4}	Constant fitting parameters
α	Parameter of the severity factor function
β	Parameter of the severity factor function
β_{3-4}	Constant fitting parameters
γ_{1-3}	Constant fitting parameters
γ_{1-3}	Constant fitting parameters
η	Battery efficiency [%] [Ohm]
λ	Transport properties of solvent molecule through SEI layer

LIST OF ABBREVIATIONS

BESS	Battery Energy Storage System
CAES	Compressed Air Energy Storage
CE	Continental Europe
DoD	Depth of Discharge
EIS	Electrochemical Impedance Spectroscopy
ENTSO-E	European Network of Transmission System Operators for Electricity
ESS	Energy Storage System
FCR	Frequency Containment Reserves
FCR-D	Frequency Containment Reserve for Disturbances
FCR-N	Frequency Containment Reserve for Normal operation
FES	Flywheel Energy Storage
FRR	Frequency Restoration Reserves
LCO	Lithium Cobalt Oxide
LCP	Lithium Cobalt Phosphate
LFP	Lithium Iron Phosphate
LMO	Lithium Manganese Oxide
LMP	Lithium Manganese Phosphate
LNO	Lithium Nickel Oxide
LTO	Lithium Titanium Oxide
NC LFCR	Network Code on Load-Frequency Control and Reserves
NCA	Nickel Cobalt Aluminum Oxide
NMC	Nickel Manganese Cobalt Oxide
NMO	Nickel Manganese Oxide
NPV	Net Present Value
OCV	Open-circuit Voltage
PHS	Pumped Hydroelectric Storage
RC	Resistor-Capacitor

RR	Replacement Reserves
SEI	Solid Electrolyte Interphase
SMES	Superconducting Magnetic Energy Storage
SoC	State of Charge
SoH	State of Health
TSO	Transmission System Operator

1 INTRODUCTION

A substantial amount of global electricity generation growth took place over the last decade. The effect of population growth and progress in industrial technology is becoming a threat since it clearly impacts the growing energy demands of a society which have to be satisfied. Main sources of energy today are fossil fuels, nuclear energy, and renewable sources. Fossil fuels contribute almost 70% of global electricity generation. Unfortunately, the complication with fossil fuels is that their amount in the world is limited. Also, they produce a considerable amount of CO2 emissions to the atmosphere. To limit the level of pollution by burning fossil fuels, future electrical energy generation will have to develop a bigger reliance on renewable energy sources, thus contributing to the environment improvement (Skea 2008, 8). High penetration of variable generation such as solar and wind energy brings uncertainty and instability to the grid due to their intermittent nature. The uncertainty creates challenges for system operators to balance electricity generation and demand while instability can manifest itself in frequency fluctuations. Energy Storage Systems (ESS) has been identified as one of the most rational option to overcome those issues. ESS has always received a lot of attention from power systems stakeholders as part of various applications to improve operating conditions and increase their profits. A numerous amount of EES applications review papers are getting published on a regular basis (Zidar et al. 2016, Luo et al. 2015, Medina et al. 2014) which indicates the continuous progress, certain future prospects, and unresolved research questions.

The range of different ESS is very broad. There is no a particular best storage solution, and the choice is always depending on requirements. Recent advances in battery technology have induced keen interest in Battery Energy Storage Systems (BESS). A large body of data was dedicated to the development of advanced cell component materials (Gulbinska (ed.) 2014; Zhuang et al. 2014; Prosini 2011) and promising ways of BESS applications for system operators, utility and customers services (Fitzgerald et al. 2015; Eyer and Corey 2010). For many years, lead-acid and nickel-cadmium technologies have been the only viable options as a secondary stationary battery until the early 1990s appearance of lithium-ion cell chemistry. By

this moment, Lithium-ion has undergone huge improvement development and considered to be one of the leading battery technology candidate available. It is also expected that Lithium-ion batteries will play a bigger role in the future formation of electric grid due to technical, economic and policy advantageous aspects. A place of the lithium-ion batteries among other energy storage technologies is demonstrated in Figure 1.1.

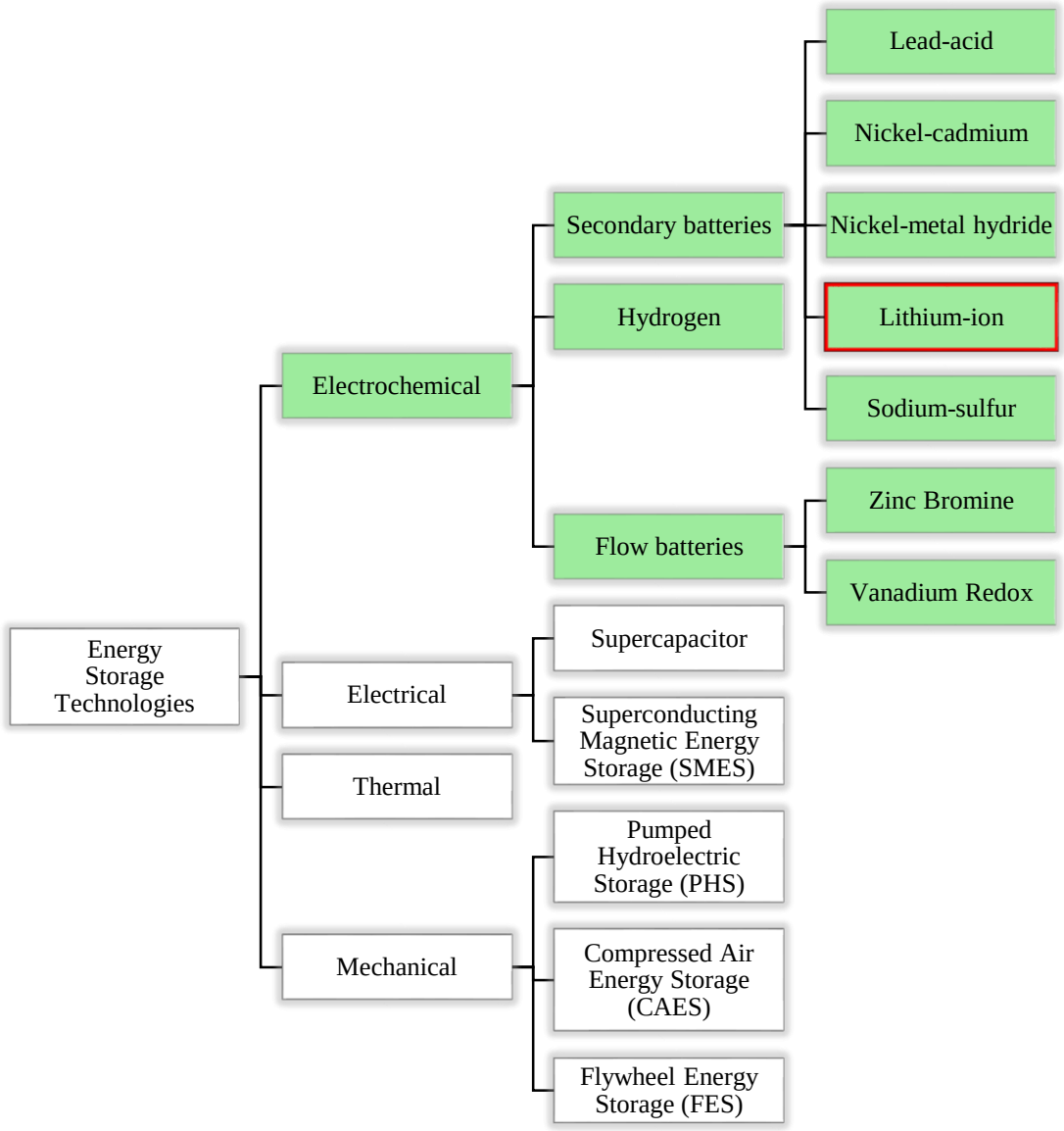

Figure 1.1. ESS technologies hierarchy.

Battery system operators, developers, and decision makers must have access to reliable information about the performance and lifetime of a lithium-ion battery, as well as optimal operational strategies of BESS. A better understanding of aging mechanisms and cell behavior modelling is an effective way to reduce life-cycle costs of BESS, which is the key aspect for the feasibility of integrating it in ancillary services. For these reasons, comprehensive analysis of different sources that have been investigating degradation effects caused by various factors with respect to the cell chemistry is needed. Moreover, additional studies dedicated to techno–economic analysis of battery storages have to be carried out due to changing power industry regulations and cell price reduction. Based on that knowledge, certain recommendations for decision making could be made such as selecting, sizing, location and operating conditions of the BESS.

1.1 Research problem and objectives of the work

The main objectives of the research in this thesis are:

- Aggregate recently reported findings and provide an updated picture of the BESS technology state of art;
- Investigate lithium-ion cell ageing phenomena and compare available degradation models;
- Develop a practical lithium-ion BESS model with ability to describe dynamic performance behavior and to estimate degradation effects;
- Design and conduct a series of simulations to analyse techno-economic feasibility of BESS providing primary frequency regulation service;

1.2 Outline of the work

This thesis is structured as follows: Chapter 2 introduces a comparison of available battery technologies with an in-depth view of lithium-ion chemistry and also presents the analysis of promising BESS applications. Chapter 3 provides a literature review trying to cover the topic of

lithium-ion cell ageing mechanisms. Further, the reported lifetime models are compared, and one of them is selected. Chapter 4 represent the development process of performance degradation BESS model based on LFP chemistry. Chapter 5 addresses the feasibility of frequency regulation service provided by BESS in Finland.

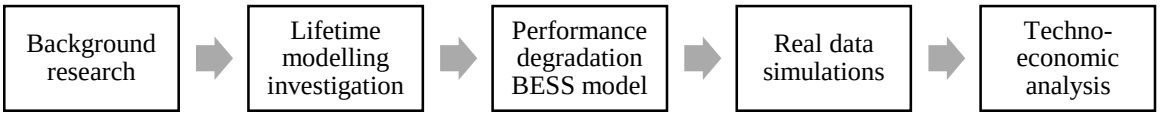

Figure 1.1. Research process plan.

2 OVERVIEW OF BESS TECHNOLOGIES AND THEIR APPLICATIONS

In this chapter, a range of electrochemical energy storage technologies is discussed. Main technical characteristics of secondary batteries are compared. Lithium-based batteries selection is justified, and further classification regarding component materials is carried out. It was done in order to emphasize the contrast of batteries which belong to the same type.

2.1. Comparison of battery technologies

It goes without saying that main component of battery storage is an electrochemical cell. For several decades' batteries have been one of the most common direct current sources for many industrial applications and power utilities. A term battery refers to the range of secondary electrochemical cells connected in series and parallel. Cell produce electricity as a result of the electrochemical reaction. Constant efforts are being made to advance the battery performance characteristics, prolong their lifetime and decrease manufacturing costs. The most commonly used battery cell technologies comparison is presented in Table 2.1.

Table 2.1. Technical comparison of battery storage technologies (Luo et al. 2015, Mahlia et al. 2014).

Technology	Development	Energy density (Wh/kg)	Cycle efficiency (%)	Lifetime (full equivalent cycles)	Capital cost (€/kWh)	Special features
Lead-acid	Mature	20-35	60-90	200-2000	50-400	Low cost, poor characteristics
Nickel-cadmium	Commercialized	40-120	60-83	500-2500	800-2400	"Memory effect", toxic
Nickel-metal hydride	Commercialized	60-80	66	3000	300	Poor efficiency and limited application
Lithium-ion	Commercialized	100-200	90-100	1000-6000	450-3800	High cost
Sodium-sulfur	Developing	150-240	>86	2000	280	High temperature operating
Zinc-Bromine Flow	Developing	37	75	>2000	900	Low energy density
Vanadium Flow	Developing	25	85	"unlimited number of cycles" < 20 years	1280	Low energy density

From Figure 2.1, it can be seen that lithium-ion batteries outperform other battery technologies in terms of ability to combine high gravimetric energy and power density. Most of the time density characteristics are not so valuable for stationary batteries, unlike for portable applications. However, in certain cases high specific power and energy values of the battery could result in considerable savings from reduced footprint of the system, if for instance the price of land is very expensive. Next section provides a more detailed analysis of Lithium-ion cell subtypes and their state-of-art.

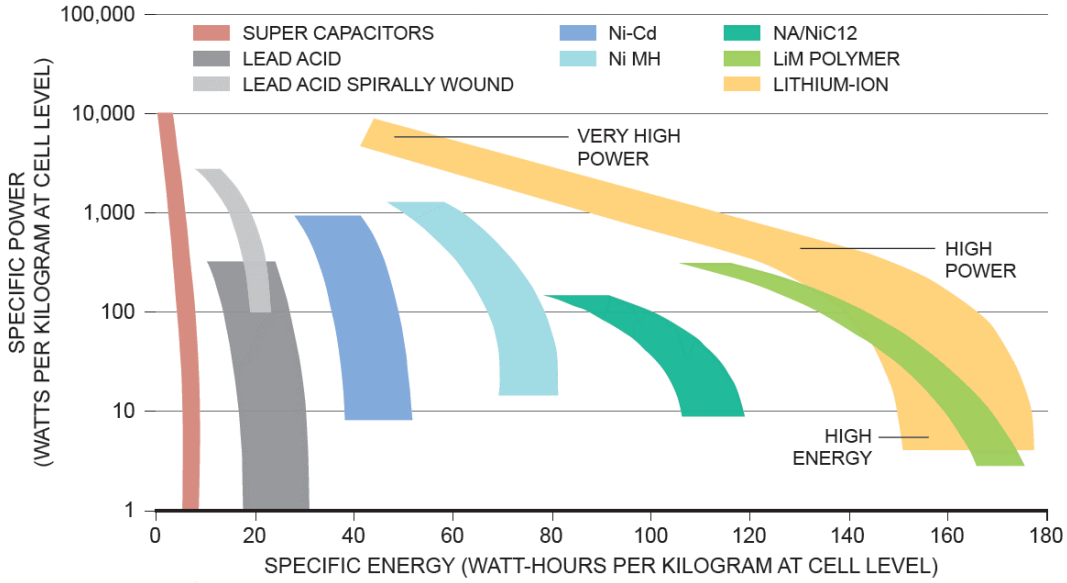

Figure 2.1. Ragone chart for various cell type (Advancing technology for America's transportation future 2013, 14).

2.2. Lithium-ion batteries

Lithium battery cells is a collective term for cells that are composed of lithium metal or lithium compounds. A lithium-ion battery cell consists of two electrodes, cathode and anode, a separator in between, and current collectors on each side of the electrodes. Figure 2.2 shows a schematic representation of lithium-ion battery cell.

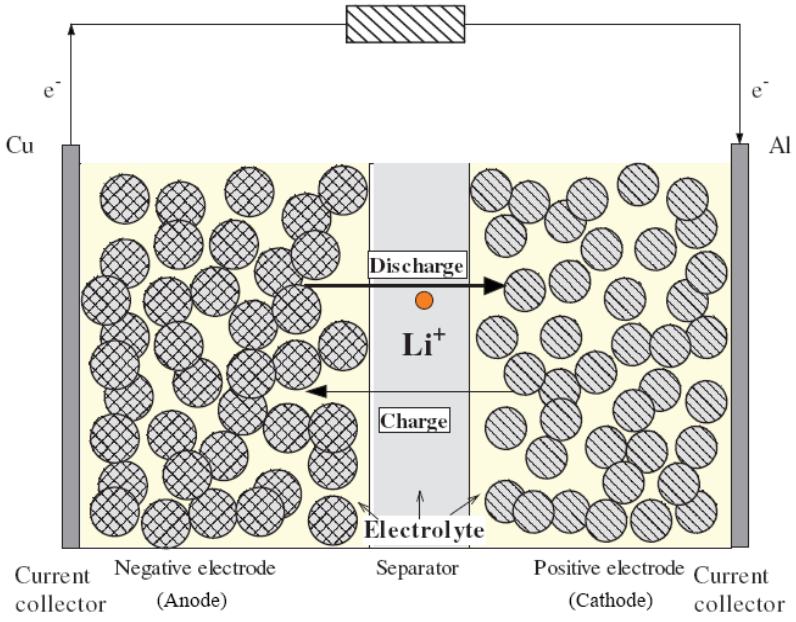

Figure 2.2. A schematic representation of a lithium-ion battery cell (Fang et al. 2010).

Lithium-ion cells have common advantages such as a unmatchable combination of high energy and power density, high coulombic efficiency, low self-discharge rate, no memory effect, comparatively long lifetime, high charge and discharge current possibility and relatively mature state-of-art.

On the other hand, lithium cells still represent a relatively high cost, certain modifications and chemistries have safety issues, and the SoC estimation can be more complicated than in other types of electrochemical cells.

The current research related to lithium batteries mostly focused on improving battery characteristics by developing advanced electrode materials and electrolyte solutions, as well as enhancing safety and reducing manufacturing costs. Next subsections are providing an overview and comparison of lithium-ion materials without entering into deep chemical details, but rather with a focus on operational characteristics differences.

2.2.1. Development of cell components and materials

The choice of components and materials greatly affects the performance and cost of a lithium-ion cell, for example, it mainly defines the energy density, average cell potential and obviously, different materials costs are not the same. The four major components of the lithium-ion battery are the cathode, anode, electrolyte, and separator.

Cathode materials currently in use or under development are described in accordance with the following three morphologies:

- Layered Rock Salt Structure Materials (two-dimensional)
- Spinel Structure Materials (three-dimensional)
- Olivine Structure Materials (one dimensional)

The first practical lithium-ion battery was developed by Goodenough et al. (1980) and it was based on lithium cobalt oxide (LCO) $LiCoO_2$ cathode material. LCO represents the two-dimensional group. Although LCO demonstrates good performance characteristics, the main drawbacks are high cost, low thermal stability, and fast capacity fade. Lithium nickel oxide (LNO) $LiNiO_2$ has a crystal structure with LCO, it has relatively high energy density and lower cost than cobalt, but poor cycle life and even worse thermal stability. Lithium manganese oxide (LMO) $LiMnO_2$ is another material from the same group, it is also much cheaper and less toxic compared to cobalt or nickel. However, the cycling performance of LMO is not satisfactory too. Despite the fact that $LiNiO_2$ and $LiMnO_2$ turned out to be unsuitable in their simple form, the formulation of advanced materials such as $LiNi_{0.8}Co_{0.15}Al_{0.05}O_2$ (NCA), $LiNi_{0.5}Mn_{0.5}O_2$ (NMO) and $LiNi_{0.33}Co_{0.33}Mn_{0.33}O_2$ (NMC) introduced considerable performance improvements. (Nitta et al. 2015)

The three-dimensional spinel structure enables lithium ions to diffuse in all three dimensions, thus benefiting in terms of lower cost and high stability, but reducing discharge capacity. The most known compounds in this group are $Li_2Mn_2O_4$ (LMO) and $Li_2Co_2O_4$ (LCO).

A new class of compounds was developed by Padhi et al. (1997) which restricts lithium ions diffusion to a single linear dimension. The limited ion mobility was minimized through the development of nanoparticles and other techniques. Thus, modern representative material $LiFePO_4$ (LFP) presents relatively low energy density and average voltage, compared to other lithium-ion chemistries, while surpassing them in thermal stability, lifetime and cost. Other novel olivines such as $LiMnPO_4$ (LMP) and $LiCoPO_4$ (LCP) that provide 4.1 V and 4.8 V, respectively are therefore gaining attention but have not reached market yet.

Cathode material mainly determines the discharge profile of the lithium-ion battery. Typical profiles for three types of cathode structures are presented in Figure 2.3.

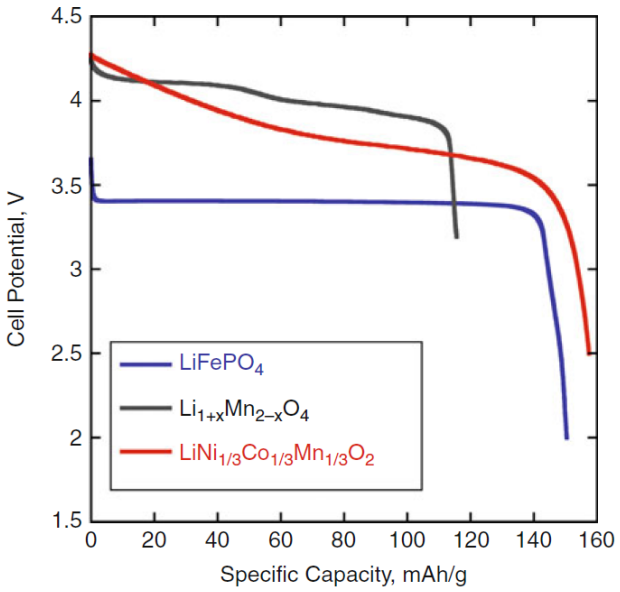

Figure 2.3. Discharge profiles of different lithium-ion cathode structures (Brodd ed. 2013, Chapter 2, 10).

Natural graphite is the most inexpensive graphite material available, but its high reactivity to electrolyte prevents its use as anode without modification. Technology to coat the graphite surface with thin carbon layer has become widely used, enabling modified natural graphite to replace mesophase graphite as the leading anode material.

As there is little scope to increase the capacity of graphite anode further, research has turned to other new materials including metal oxides and alloying materials. For example, lithium titanium oxide (LTO) compound $Li_4Ti_5O_{12}$ provides a combination of excellent thermal stability, high rate capability, rather high volumetric capacity and also long cycle life. Unfortunately, LTO has much higher cost because of Ti and reduces the cell voltage. Alloying materials provide much higher capacity than graphite, but a serious drawback is the large expansion and contraction of volume which occurs during the charge–discharge process. Volume change can cause cracking of the material and loss of electrical contact. Thus, it is common for alloying anodes to have short cycle life and fast increasing cell impedance.

The electrolyte in a lithium-ion battery is a mixture of organic solvents and an electrolyte salt compound. The common solvents are a mixture of cyclic carbonate esters, such as ethylene carbonate and propylene carbonate, and linear carbonate esters, such as dimethyl carbonate and diethyl carbonate. The solution is completed with the addition of a salt compound such as LiPF6 or LiBF4. Electrolyte solutions must enable the Li ions to transport freely, which requires both high dielectric constant and low viscosity. For electrolyte salt, both LiPF6 and LiBF4 were widely used, but LiPF6 has come to dominate the market as shown in Figure 2.4.

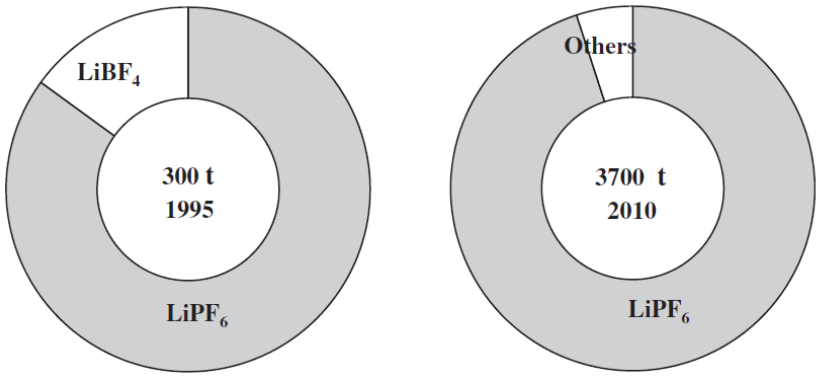

Figure 2.4. Lithium-ion battery electrolyte salt market (Yoshino 2014)

Research on the electrolyte solution is generally focused on one of three areas: functional electrolyte additives, flame-resistant or nonflammable electrolyte solutions, and new electrolyte

salts. For instance, flame-resistance is usually provided by employing phosphate compounds in some way, and salt like lithium bis(oxalate) borate, in particular, is considered to be very promising due to low-cost.

All commercial separators so far have been made of polyolefins, but they provide only limited heat resistance. New separators are expected to offer not only high temperature stability and safety but also improved ion transportation for better rate capability at high current discharge.

2.2.2. Comparison of lithium-based chemistries

Relative comparison of the most promising lithium-ion chemistries is shown in Figure 2.5, and a more detailed list can be found in Table 2.2.

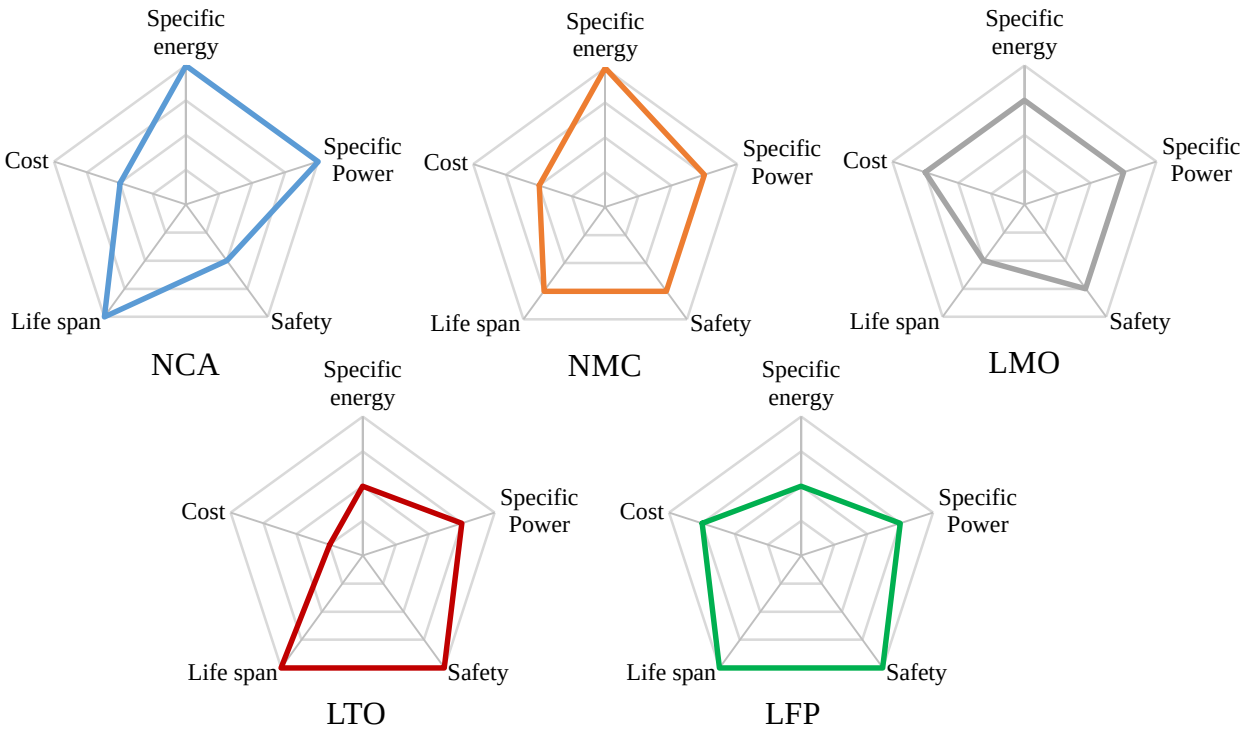

Figure 2.5. Comparison of the most promising lithium-ion battery chemistries (Dinger et al. 2010, De-Leon 2010).

Table 2.2. Technical comparison of lithium-ion battery chemistries (De-Leon 2010, Nitta et al. 2015).

Cathode	Anode	Average voltage, V	Average energy density	Average power density	Lifetime	Safety	Cost
Lithium Cobalt Oxide (LCO)	Graphite	3.7	High	Fair	Fair	Fair	High
Nickel Cobalt Aluminum Oxide (NCA)	Graphite	3.7	High	High	Fair	Fair	High
Lithium Iron Phosphate (LFP)	Graphite	3.3	Low	High	High	Very good	Fair
Lithium Manganese Oxide (LMO)	Graphite	3.8	High	High	Fair	Very good	Fair
Lithium Manganese Oxide Spinel (LMO)	Graphite	3.8	High	High	Fair	Good	Low
Lithium Manganese Oxide Spinel Polymer (LMO)	Graphite	3.8	High	High	Fair	Good	Low
Nickel Manganese Cobalt Oxide (NMC)	Graphite	3.7	High	Fair	Low	Fair	High
Lithium Manganese Oxide Spinel (LMO)	Lithium Titanate Oxide (LTO)	2.5	Low	Low	High	Good	High
Lithium Nickel Oxide (LNO)	Graphite	3.8	High	Fair	Fair	Fair	Fair
Lithium Manganese Nickel Oxide Spinel (LMNS)	Graphite	4.8	High	High	Fair	Fair	Low
Lithium Manganese Nickel Oxide Spinel (LMNS)	Lithium Titanate Oxide (LTO)	3.2	Fair	High	High	Good	Low

To select a particular chemistry for further study, the specific priorities of battery characteristics for particular BESS application must be defined.

2.3. Analysis and potential assessment of BESS applications

Many studies have been conducted investigating the possible value that BESS can provide to the energy system over the past years. Some services and their definitions vary across all reports. To demonstrate the value, services were categorized according to the stakeholder group that receives the biggest part of benefits from each service. The stakeholder groups were identified as supply, grid, and end-users. The supply group represents various energy generators, as well as ancillary services requires by Transmission System Operators (TSO) to maintain a constant

balance between electricity supply and demand. The grid includes transmission and distribution networks. End-users are located behind the meter where BESS can provide them a direct benefit. The separation between stakeholder groups are rather vague, and should not be considered as precise. Table 2.3 presents possible benefit values and basic technical characteristics of BESS applications.

Table 2.3. BESS service values and key characteristics for particular applications (Fitzgerald et al. 2015; Lazard 2015; Eyer and Corey 2010; Technology Roadmap: Energy storage 2014)

Stakeholder group	Service	Possible size, MW	Estimated response time	Service value, $/kW-year
Supply	Spin / non-spin reserves	1 to 500	< 15 min	0 to 70
	Load following	0.1 to 500	< 15 min	60 to 150
	Energy arbitrage	1 to 500	hours	0 to 100
	Black start	0.1 to 10	< 1 hour	10
	Frequency regulation	0.1 to 10	seconds/minutes	10 to 200
Grid	Congestion relief	1 to 100	hours	10
	Investments deferral	1 to 100	hours	50 to 150
	Voltage support	1 to 10	seconds	50
End-user	Renewables integration	0.01 to 10	< 15 min	10
	Time-of-use energy cost management	0.01 to 1	hours	200
	Demand charge reduction	0.01 to 1	< 15 min	20 to 200
	Backup power	0.01 to 1	minutes	180 to 300

It has to be emphasized that values presented above are a very rough estimation and should not be treated as an authoritative framework for resource planning or decision-making. This considerable values uncertainty results from a great number of variables such as electricity markets conditions, regulatory directions, and technical constraints.

Many studies highlighted the frequency regulation service as one of the most high-valued application for BESS (Oudalov et al. 2007; Walawalkar et al. 2007). Moreover, Lazard's

Levelized Cost of Storage Analysis (2015) claims that BESS based on lithium-ion technology are already cost-competitive with their conventional alternative (gas turbine peaker). Frequency regulation is characterized by short duration, but highly frequent BESS operation profile throughout the lifetime. Specific power and energy density are not so critical for that application. Consequently, the most important factors are a lifetime, safety and costs. In that case, the most appropriate lithium-ion chemistry appears to be LFP and graphite anode. As a matter of fact, the battery market researches by Bernhart and Kruger (2012) and by Pillot (2015) predict lithium-ion cathode materials market grow double from 2015 through 2020 and triple through 2025, while LFP is considerably increasing the overall share. The mentioned researches results are shown in Figure 2.6.

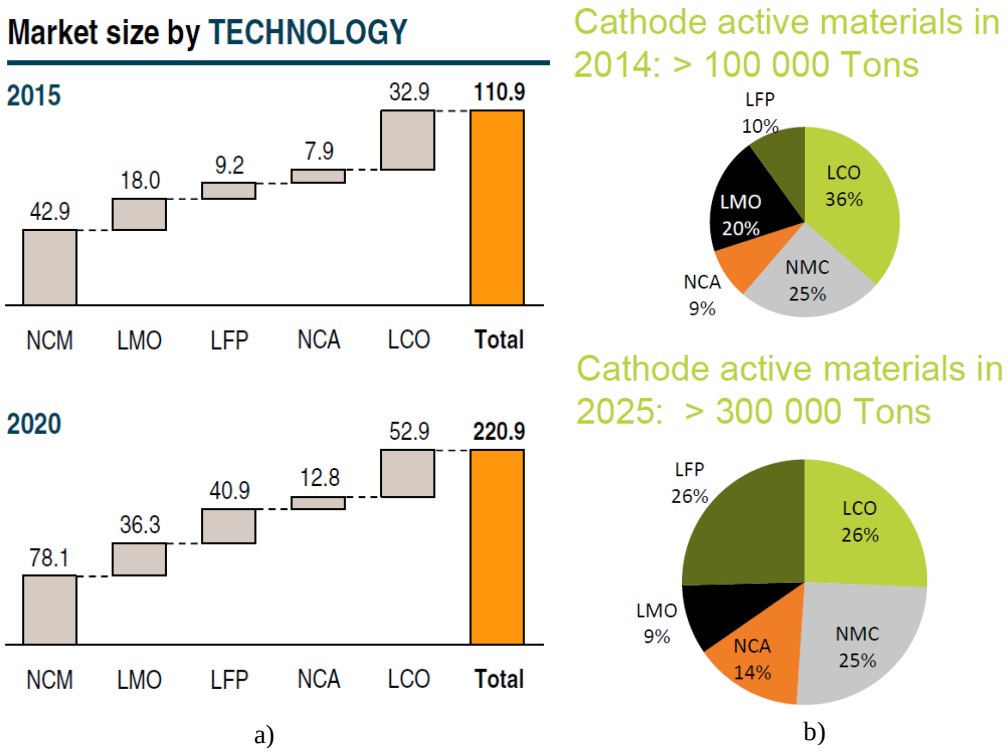

Figure 2.6. Cathode market size forecast a) Bernhart and Kruger (2012); b) Pillot (2015).

Accordingly, next chapters of the thesis will present a development of BESS model based on LFP cells and techno-economic evaluation of frequency regulation service in Finland.

3 LIFETIME MODELING OF LITHIUM-ION CELL

Lifetime modeling plays the critical role when the optimal type and optimal operation of BESS are planned. At first in this chapter, a literature review of lithium-ion battery aging mechanisms and stress factors will be conducted. Then some relevant capacity fading models will undergo a comparison and finally a brief summary with final model selection will conclude the chapter.

Battery cell has many terms and definitions which describe its state and parameters. So in order to clear the ambiguity and to avoid possible misinterpretation, the important cell terms used in this thesis are explained in Appendix I.

3.1 Lithium-ion battery aging mechanisms

Understanding the details of lithium-ion batteries operation is not an easy task and comprehension of aging mechanisms is even more complicated (Vetter et al. 2005, 1). The problem is that factors contributing to aging process are not independent but rather have a synergetic effect and occur at similar timescale. That creates a great effort for researchers who tried to explore above mentioned phenomena throughout the years (Cheng Lin 2015, 1).

Since in this thesis LFP cathode and graphite anode are materials that were chosen as the primary, following findings are related only to mentioned chemistry. For example, studies by Li et al. (2016), Schlasza et al. (2014) and Liu et al. (2010) were focused to the particularity of lithium iron phosphate electrode aging.

The results of battery degradation process include a decrease in remaining capacity (i.e. capacity fade) and internal resistance rise. The aging mechanisms of cathode, anode, electrolyte and separator differ significantly and therefore presented separately. Table 3.1 provides a summary of aging mechanisms according to cell components, conditions that are enhancing the process and the possible measures that reduce the effects.

Table 3.1. Aging mechanisms in LFP/graphite cells according to cell components (Lin et al. 2015; Schlasza et al. 2014; Vetter et al. 2005).

Cell component	Failure subgroup	Aging mechanism	Result	Reduced by	Enhanced by
Cathode	Current collector corrosion	Corrosion of Al in combination with LiPF6	Impedance rise Overpotential	Current collector pre-treatment	Low SoC
	Morphological changes	Change in surface porosity Crystal distortion Mechanical stress	Capacity fading	Control charge cutoff voltage	Overcharge
	Decomposition of binder	Binder dissolution	Capacity fading	Proper binder choice	High temp High SoC
	Dissolution of soluble species	Precipitation of new phases Loss of active material	Capacity fading Impedance rise	Temperature control	High temp
	Moisture intrusion	Reaction of cell materials with water	Delithiation of the surface layer	Climate control	High moisture
Anode	Morphological changes	Change in volume, surface peeling of graphite, cracking	Capacity fading	Charge control cutoff voltage	Overcharge (very high SoC)
	Lithium plating	Lithium deposits and growth of dendrites (loss of lithium)	Capacity fading Impedance rise	Temperature control	Low temp High C-rate Bad design
	SEI-layer* growth	Consumption of lithium Resistive behavior becomes more pronounced	Capacity fading Impedance rise	Stable SEI-layer* (additives)	High C-rate High SoC High DoD
	SEI-layer* decomposition	Decomposition due to high temperatures	Impedance rise	Stable SEI-layer* (additives)	High temp
Electrolyte	Electrolyte decomposition	Stability of electrolyte and conduction salt	Capacity fading Impedance rise	Alternative conductive salts	Impurities High temp High SoC
	Moisture intrusion	Reaction of conduction salt with water, hydrogen fluoride formation	Decrease in performance	Climate control	High moisture
Separator	Separator destruction	Separator properties and failure modes	-	-	-

* Solid Electrolyte Interphase (SEI) – a passivating protective layer on anode

To have better insight on described processes they are demonstrated in Figure 3.1.

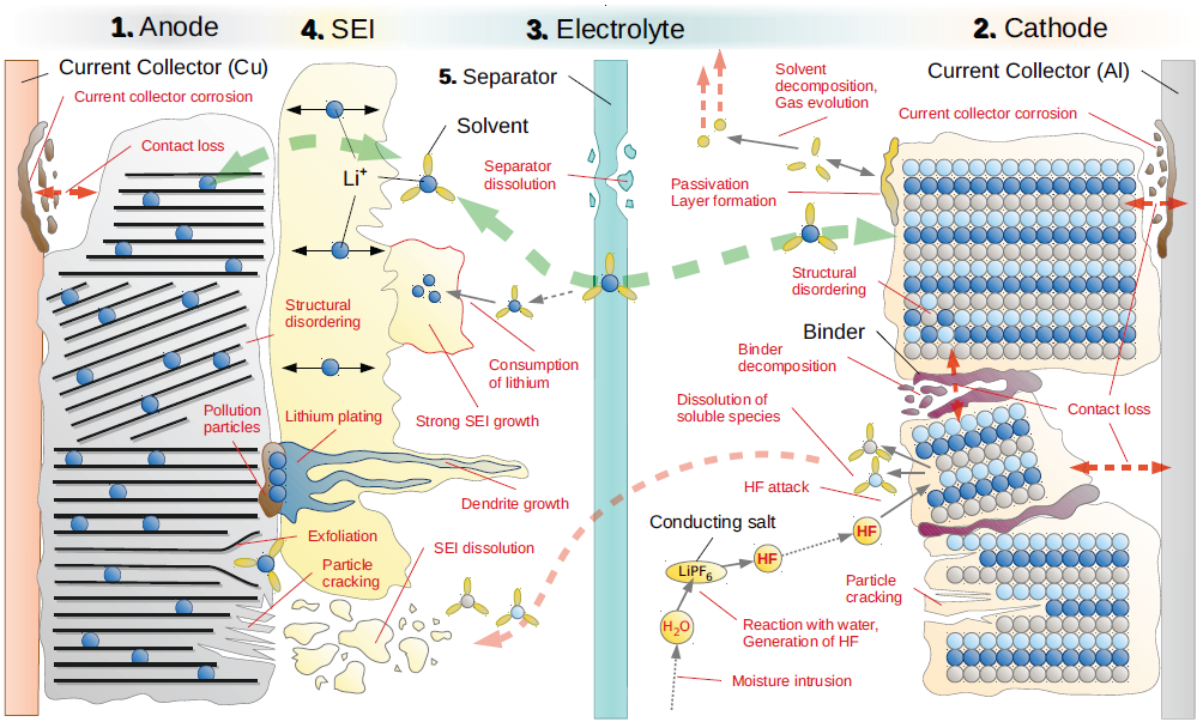

Figure 3.1. Representation of lithium-ion battery aging mechanisms (Schlasza et al. 2014).

Most of the researchers share the opinion that loss of active lithium ions due to their immobilization in the SEI layer is the dominating mechanism responsible to capacity fade. Also, the presence of iron particles inside SEI layer was noted at higher temperatures leading to a reduction in graphite electrode accessibility (Li et al. 2016, 9). It can be concluded that the capacity fading mainly occurs on the electrode/electrolyte interface due to its instability.

Liu et al. (2016) reported that LFP/graphite cells do not experience substantial internal resistance increase after analyzing ageing experimental data. Since today's power electronic devices provide output in BESS and it capable to easily tune output power, this work will neglect the impedance change due to degradation, with more focus on the capacity fade.

It is of great importance for lifetime modelling to figure out how the battery is operating or environment conditions influence the ageing process. In general, lithium-ion cell degradation can be divided into calendar aging and cycle aging.

3.1.1 Degradation due to cycling

After an explanation of ageing mechanisms, it is obvious that capacity fading will occur even if the cell will be operated in ideal conditions due to natural wear off. Normal degradation trend of lithium iron phosphate battery due to cycling can be seen in Figure 3.2.

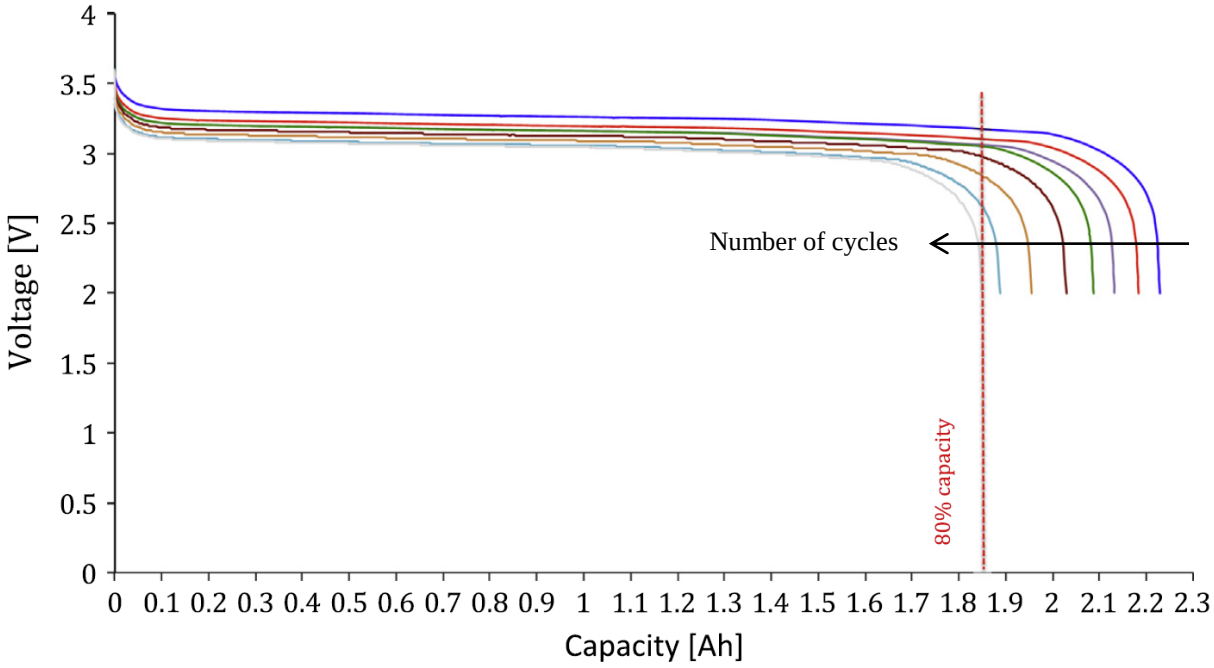

Figure 3.2. An example of capacity is fading due to the cycling of lithium iron phosphate battery.

In real-life applications, cells are not operated in ideal conditions and therefore experience accelerated degradation under several stress factors. These stress factors are widely known from the literature, and their effect will be described below respectively.

Temperature

Just like any other batteries, lithium-ion cells have their optimal temperature operation range. Manufacturers tend to provide very wide range, like for example from -30 °C to +55 °C, however, operating in the margin areas will not only lead to decreased performance but even cause an accelerated degradation. Almost every cycling ageing study provides a pronounced

temperature effect on capacity fading similar to Figure 3.3. It is also worth noting that low temperatures will significantly affect cell capacity too. It will happen by means of another ageing mechanism known as lithium plating resulting rapid capacity fade, mostly during charging.

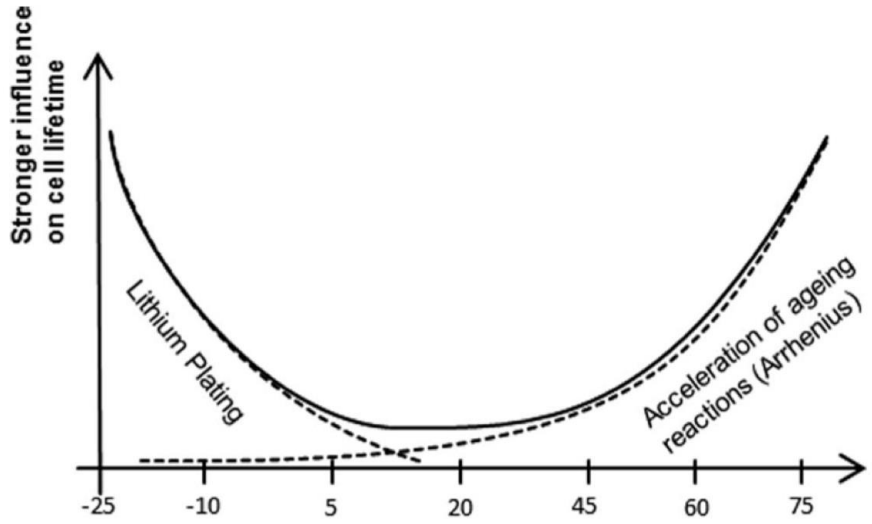

Figure 3.3. Cell lifetime related to operating temperature.

Current rate (C-rate)

Cycling the battery with high currents rates will cause increased power dissipation by ohmic heating on internal resistance. Consequently, that will generate heat and increased temperature leading to high temperature degradation mechanisms described above. Significant voltage drop on resistance can also result in overpotential. Except for that, high currents will also cause extra mechanical stress on the electrodes invoking several ageing mechanisms.

State of charge (SoC)

The high level of SoC means anode of the cell is full of lithium ions and possess a high amount of energy. SEI layer will grow faster in that state. Also, some other ageing mechanisms listed in Table 3.1 will take place. The influence of high SoC is more profound during long storage time,

but the amount of time spent at certain SoC during cycling can play a role in ageing too. Consequently, an impact from high SoC can be mitigated by cycling at lower SoC level, keeping in mind that too low SoC will lead to current collector corrosion.

Obviously, the cell must be operated within SoC range recommended by the manufacturer, and no overcharge or overdischarge should take place. Violation of these limits could lead to severe damage to the cell. The battery management system (BMS) carrying out the operating limits protective functions, i.e. it monitors the SoC, voltage and temperature and in the case of thresholds violation, it can send an alarm message or even shut off the battery. BMS is also responsible for SoC leveling among the cells in the battery pack.

Depth of discharge (DoD)

Many authors and manufacturers present the cycle life of the battery as a function of a number of cycles, but do not specify the details about DoD of that cycling. In the case of evaluating a possible number of cycles until the end of life (EoL), the larger the DoD, the more intercalation, and deintercalation will take place due to natural wear-off leading to loss of lithium and active material (Vetter 2012, 273). Because of that, less full cycles before the EoL are possible than a number of cycles with minor DoD. Figure 3.4 shows an example of expected number of cycles until the end of battery life with different DoD cycling. When the battery is operated with high DoD, it undergoes low and high SoC states which effects were described above.

3.1.2 Degradation due to storage

Lithium-ion cells do not only degrade as a result of utilization. While on rest, SEI layer is exposed to the electrolyte which can slowly enhance its growth. Thermodynamical stability of the components and chemical side reactions inside the cell determine the ageing rate on storage. Under the right conditions, capacity fade can be minimized, but in the case of exposure to elevated temperatures, the activation energy of chemical reactions becomes lower and ageing side reactions occur faster. High SoC is also increasing the reactivity and thus accelerating the capacity fade as mentioned in the previous subsection.

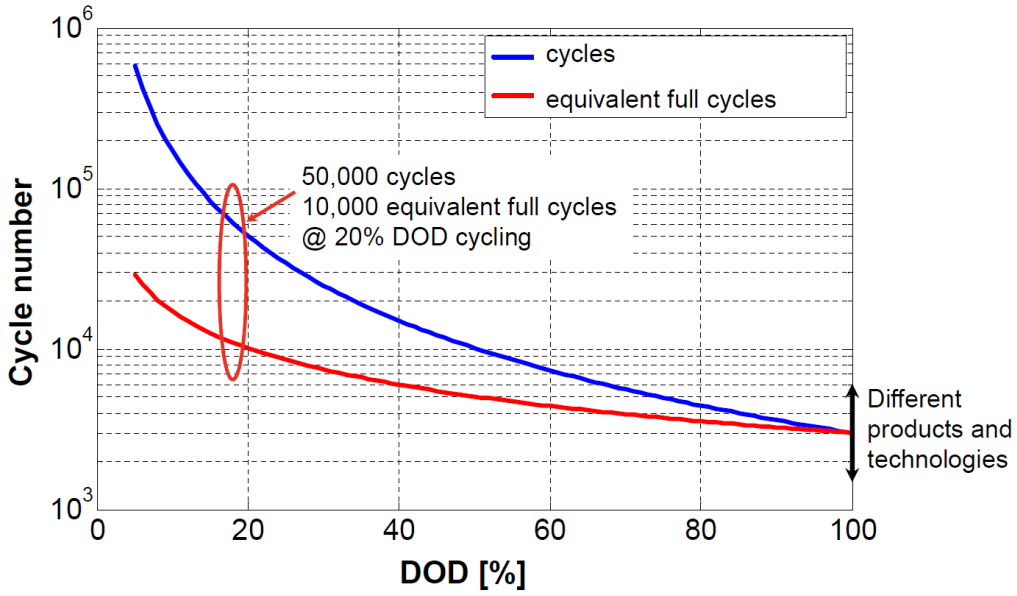

Figure 3.4. An example of expected cycle lifetime as a function of DoD (Sauer 2012, 147).

3.2 Lithium-ion battery lifetime models

There are many approaches for lifetime modeling of lithium-ion batteries exist. Their classification is shown in Figure 3.5. The first approach is usually referred as a post-processing or offline and it is used for assessing the impact of a certain operating scheme on the expected lifetime of the battery. It can be further divided into the counting of the amount of charge through the battery (usually in Ah units or Wh in some cases) and cycles counting method. Both of these methods can only handle the prepared output data, for example from the real system. The second group of methods is called performance degradation models, and they represent the combination of a lifetime model with the performance model. That solution gives the ability to perform on stream calculations and make updates of the performance parameters depending on the degradation rates. There are two major methods exists to estimate the battery performance: the first method represents the equivalent circuit-based models, the second one uses physical equations to describe the chemical kinetics and structural changes of components inside the battery.

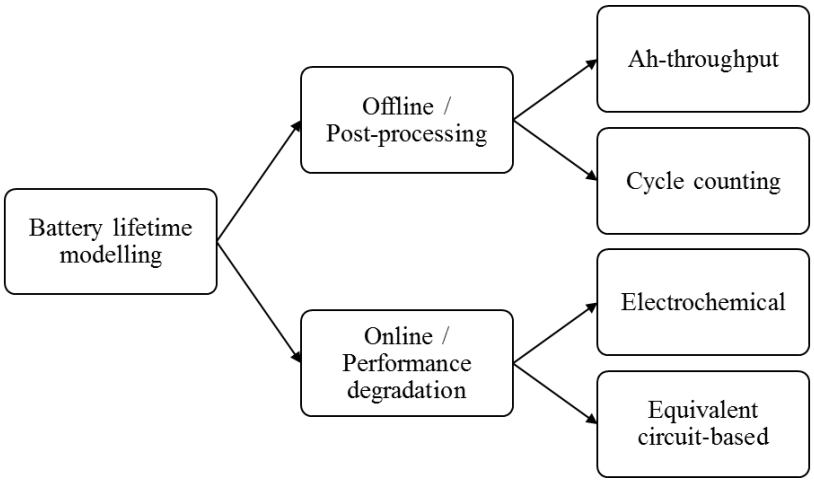

Figure 3.5. Classification of lifetime models.

The goal of this section is to perform a survey of most relevant pure lifetime practical models available to the public, figure out their advantages along with drawbacks and finally compare the outcomes of investigated models with each other. To minimize the divergence in results due to specific chemistries characteristics and discrepancy of cells design, works that were focused on typical cylindrical LFP/graphite cell had been chosen for analysis. The manufacturer datasheet of the cell can be found in Appendix II. This particular cell was selected due to its wide use and sufficient amount of reports among the scientific community. The models which provided full description and characterization with numerical values of coefficients were considered a priority because the end target was to use one of them in the following chapters.

3.2.1 Cycling degradation models

One of the most cited semi-empirical degradation models for LFP cells cycle life is proposed by Wang et al. (2011). The result of the work was the establishment of a mathematical relationship between capacity fade and temperature, C-rate and Ah-throughput.

The model provides a simple Equation 3.1 with variation of pre-exponent factor depending on the C-rate (Table 3.2):

$$Q_{cycling} = B \cdot \exp\left(\frac{-31700 + 370.3 \cdot C_{rate}}{R \cdot T}\right) \cdot \left(Ah_{th}\right)^{0.55} \tag{3.1}$$

$Q_{cycling}$ = capacity loss due to cycling [%]
B = pre-exponent factor
C_{rate} = current rate
R = universal gas constant 8.314 J/molK
T = temperature [K]
Ah_{th} = ampere-hour throughput [A · h]

Table 3.2. Pre-exponent factor dependence on C-rate.

C-rate	C/2	2C	6C	10C
B value	31,630	21,681	12,934	15,512

The main advantage of this model is its simplicity, but it lacks the ability to consider complex cycling profile and SoC influence is neglected. The correlation with experimental data is fair enough, but during the model check, the contradictory question arises. It seems that at the same temperature model results with more damage for C/2-cycling than 2C and 6C, but it has to be the opposite way. Even if temperature correction within the cell due to additional heat been made, the results does not change much (Figure 3.6). This basically means there is no clear relation between current value and degradation rate, except for very high current zone where degradation mechanisms such as lithium plating and rapid SEI-layer growth come into action.

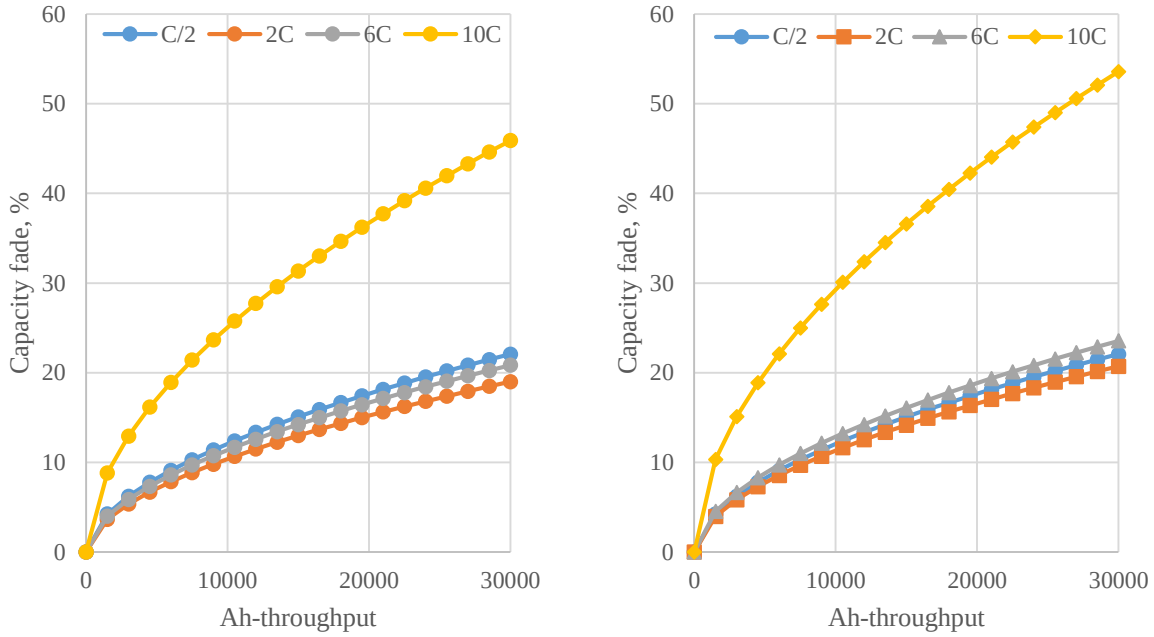

Figure 3.6. Wang et al. (2011) model simulation results for 20ºC a) without temperature correction, b) with temperature correction.

Suri and Onori (2016) modified the previous model, made recalibration and introduced linear dependence on average SoC by values α and β from Table 3.3 instead of pre-exponent factor:

$$Q_{cycling} = (\alpha \cdot SoC + \beta) \cdot \exp\left(\frac{-31500 + 152.5 \cdot C_{rate}}{R \cdot T}\right) \cdot (Ah_{th})^{0.57} \tag{3.2}$$

SoC = state of charge
α = parameter of the severity factor function
β = parameter of the severity factor function

Table 3.3. Values of severity factor function parameters α and β.

	α	β
SoC [%] < 45	2896.6	7411.2
SoC [%] ≥ 45	2694.5	6022.2

Model simulation results on Figure 3.7a clearly show improvement in C-rated dependency. That model should provide better results for applications with pronounced average SoC. It can be noted that values of α and β are greater for < 45% SoC than for ≥ 45% SoC, thus leading to higher degradation rate near the 45% SoC demonstrated on Figure 3.7b. Probably, this is the result of a very few profiles data.

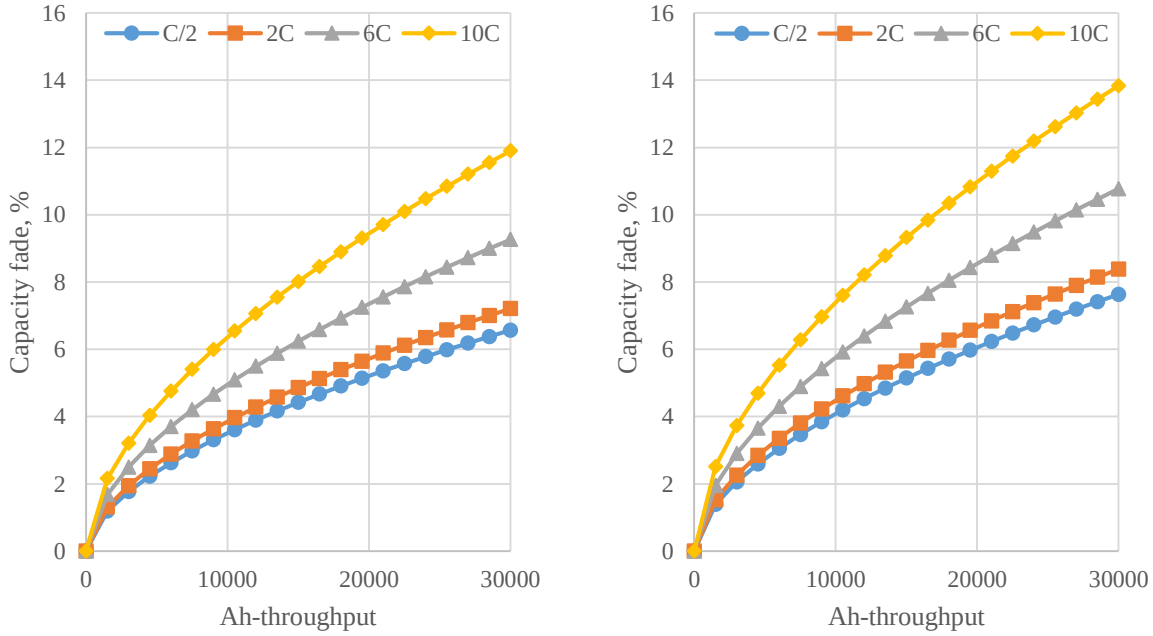

Figure 3.7. Suri and Onori (2016) model simulation results for 20ºC a) 50% SoC, b) 40% SoC.

Yuksel and Michalek (2012) on the other hand simplified the model by Wang et al. (2011) even more. They disposed the C-rate consideration and obtained Equation 3.3 by using a least-squares fit:

$$Q_{cycling} = 1.1443 \cdot 10^{6} \cdot \exp\left(\frac{-4.257 \cdot 10^{4}}{R \cdot T}\right) \cdot \left(Ah_{th}\right)^{0.55} \tag{3.3}$$

Papers by Sarasketa-Zabala et al. (2015, 2016) provide a similar model, but with a focus on DoD swing. He reported that C-rate effect was minimal or had inexplicable trends at certain

DoD levels, for that reason it was neglected. Equations 3.4 and 3.5 compose the overall mathematical model for two ranges of DoD. Unfortunately, he does not provide fitting coefficients, but his experimental results in Figure 3.8 can serve as a reference. The DoD influence presented in this study does not resemble any other models.

$$Q_{cycling} = \left(\gamma_1 \cdot DoD^2 + \gamma_2 \cdot DoD + \gamma_3\right) \cdot b \cdot Ah^{0.87} \quad \{10\% \le DoD \le 50\%\} \tag{3.4}$$

γ_{1-3} = constant fitting parameters
DoD = depth of discharge
b = complex balancing factor that is a function of Ah_{th}

$$Q_{cycling} = \left(\alpha_3 \cdot \exp\left(\beta_3 \cdot DoD\right) + \alpha_4 \cdot \exp\left(\beta_4 \cdot DoD\right)\right) \cdot k \cdot Ah^{0.65} \{DoD < 10\%; > 50\%\} \tag{3.5}$$

α_{3-4} = constant fitting parameters
β_{3-4} = constant fitting parameters

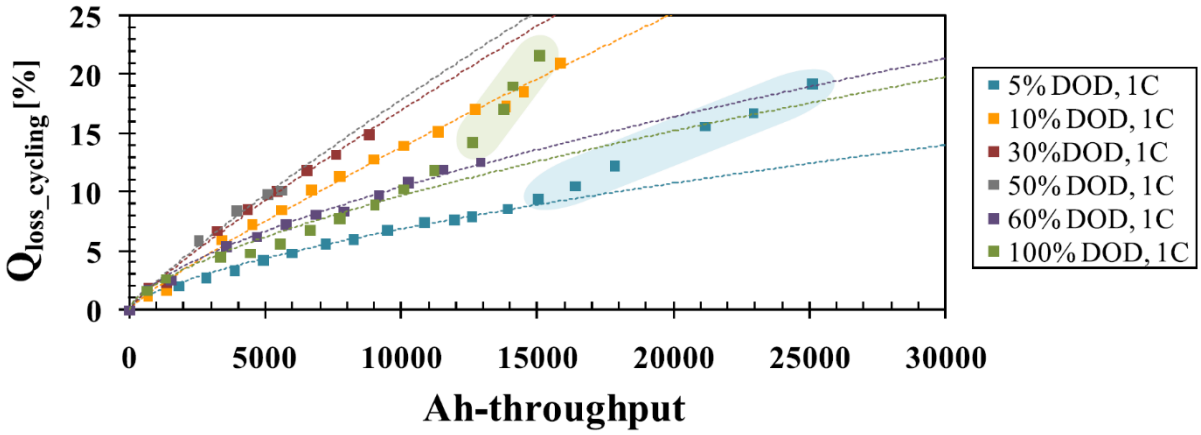

Figure 3.8. Sarasketa-Zabala et al. (2015) experimental and model fitting results for cycling at 1C, 50% middle SoC and 30 °C.

Swierczynski et al. (2015a) investigated lifetime of BESS for integration with a wind turbine. Therefore, an assumption was made that the idling of SoC should be 50% in order to provide power both balancing up and down. Consequently, the SoC factor was neglected in his work.

Moreover, all ageing tests were performed with 4C charge and discharge current to consider worst case scenario and speed up testing phase. Aside from that, temperature and cycle depth were studied. Capacity fade in percent can be calculated with a single function:

$$Q_{cycling} = \left(3.0806 \cdot 10^{-5} \cdot \exp\left(0.03216 \cdot T\right)\right) \cdot \left(0.9049 \cdot \exp\left(-0.00972 \cdot DoD\right)\right) \cdot N_{cyc}{}^{0.5} \quad (3.6)$$

N_{cyc} = number of cycles

DoD = depth of discharge [%]

Model simulations on Figure 3.9 were performed for several DoD levels, and results were converted in Ah-throughput dependency to compare it with previous models.

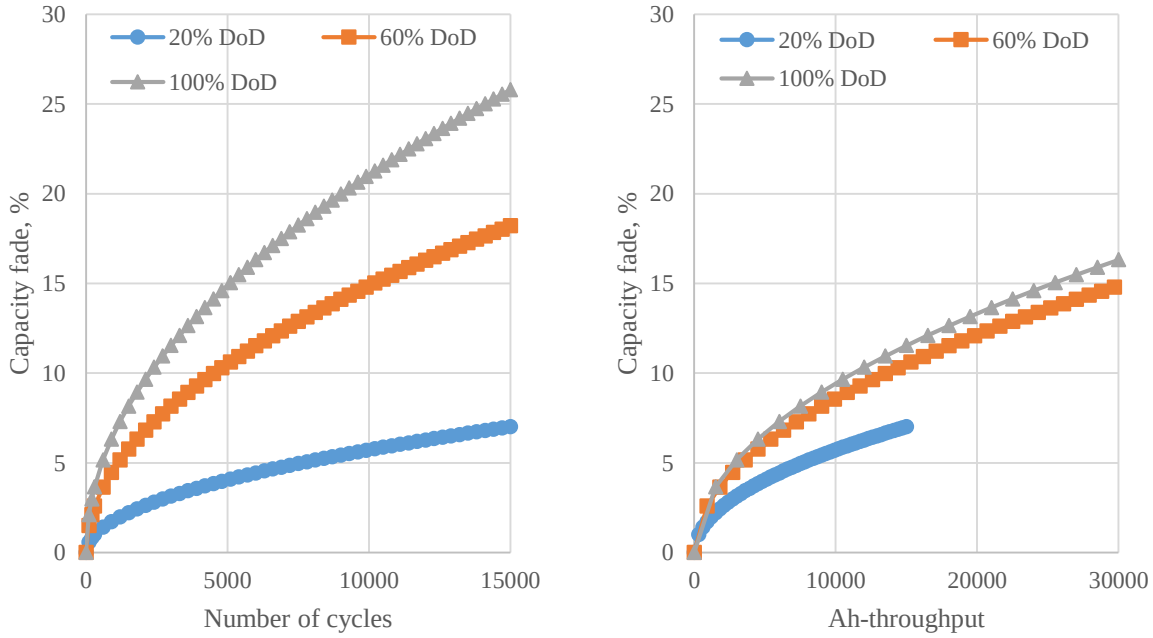

Figure 3.9. Swierczynski et al. (2015a) model simulation results for 20ºC a) number of cycles dependency, b) Ah-throughput dependency.

The same year later Swierczynski et al. (2015b) carried out another paper about lifetime modelling but for electric vehicles application. While all the cycling test cases remained the

same (50% SOC and 4C-rate), the term for DoD consideration and other fitting parameters have changed. Capacity loss due to cycling in updated model can be calculated by Equation 3.7; results were treated the same way to show Ah-dependency and presented on Figure 3.10:

$$Q_{cycling} = 0.00024 \cdot \exp\left(0.02717 \cdot T\right) \cdot 0.02982 \cdot DoD^{0.4904} \cdot N_{cyc}{}^{0.5} \tag{3.7}$$

DoD = depth of discharge [%]

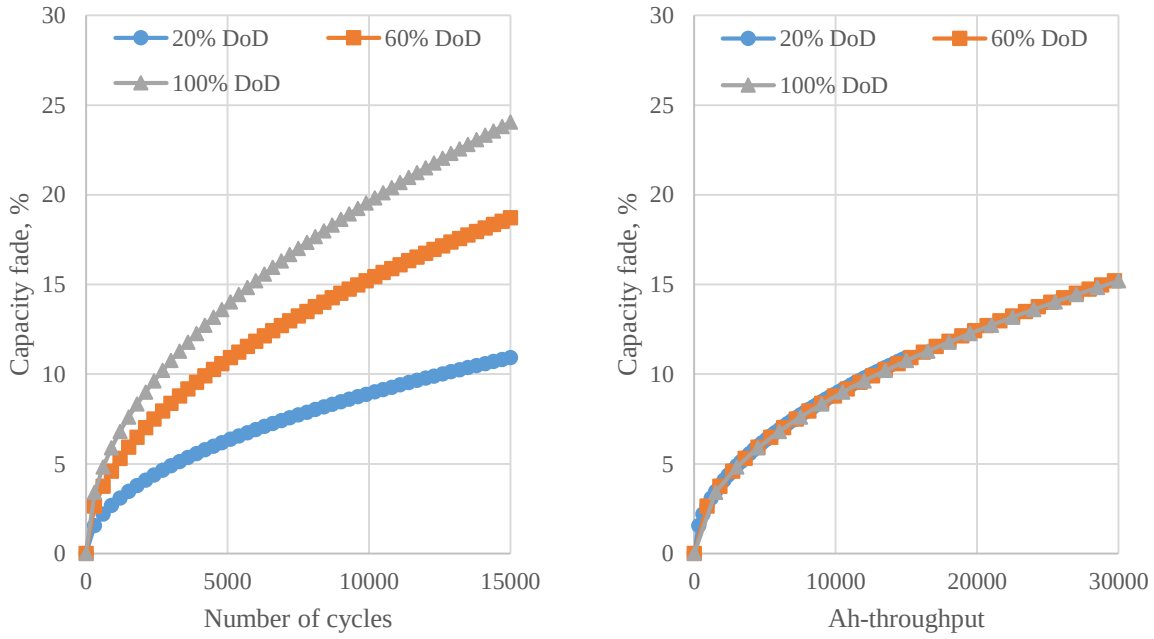

Figure 3.10. Swierczynski et al. (2015b) model simulation results for 20ºC a) number of cycles dependency, b) Ah-throughput dependency.

After conversion from a number of cycles to Ah-throughput value, it is clearly noticeable that curves for different DoD are matching together. Indeed, the assumption that the terms $DoD^{0.4904}$ and $DoD^{0.5}$ can be equated will not contribute a huge error, especially with the fact that results of various models differ significantly, and all estimations are very rough. That will allow to express the function through Ah-throughput in Equations 3.8 – 3.10.

$$Ah_{th} = 2 \cdot N_{cyc} \cdot DoD \cdot Q_{nom} \tag{3.8}$$

$$DoD^{0.5} \cdot N_{cyc}{}^{0.5} = \sqrt{\frac{Ah_{th}}{2 \cdot Q_{nom}}} \tag{3.9}$$

$$Q_{cycling} = 0.00024 \cdot \exp\left(0.02717 \cdot T\right) \cdot 0.02982 \cdot \sqrt{\frac{Ah_{th}}{2 \cdot Q_{nom}}} \tag{3.10}$$

Q_{nom} = cell nominal capacity [Ah]

An interesting way for taking into account more specific cycling conditions was suggested by Millner (2010) and extended by Xu (2013) later on. The model is based on theoretical models of crack propagation in structural materials. The impact of each stress factor expressed in the form of linearized degradation function and simply are multiplied by each other representing total degradation rate of the certain cycle. To count and identify all the cycles, Rainflow cycle-counting algorithm is applied to complex SoC curve, giving out the amplitude (DoD), the mean value (SoC average), begin and end moments of time. Using exact time moments, average temperature and C-rate of each cycle are calculated. Unfortunately, the fitting parameters are determined with experimental data for lithium manganese oxide (LMO) batteries and therefore cannot be used for LFP.

3.2.2 Calendar degradation models

Along with the cycle-life model, Yuksel and Michalek (2012) described calendar ageing of the same LFP/graphite cell with two equations obtained from manufacturer's data:

$$\begin{cases} Q_{storage} = (0.23 \cdot T - 67) \cdot \log 10(t) - (0.3 \cdot T - 88.95), \text{ for } T \le 45°C \\ Q_{storage} = (0.23 \cdot T - 67) \cdot \log 10(t) - (0.013 \cdot T - 2.36), \text{ for } T > 45°C \end{cases} \tag{3.11}$$

$Q_{storage}$ = capacity loss due to storage [%]

t = storage time [days]

The technical data obtained from the manufacturer should always be treated with skepticism. In any case, this model does not take into account the SoC at which battery is stored while this factor plays a huge role in storage degradation.

Another successful model with the empirical expression for predicting capacity fade was made by Grolleau et al. (2014). It considers both temperature and SoC influence in kinetic dependence term *k (T, SoC)* and requires to solve differential Equation 3.12:

$$\frac{dQ_{storage}}{dt} = k_i\left(T, SoC\right)\cdot\left(1+\frac{Q_{storage}(t)}{Q_{nom}}\right)^{-\lambda(T)} \tag{3.12}$$

k_i = kinetic dependence of the capacity fade evolution with T and SoC during storage

λ = transport properties of solvent molecule through SEI layer

$$k(T, SoC) = A(T)\cdot SoC + B(T) \tag{3.13}$$

$$A(T) = k_A \cdot \exp\left(-\frac{Ea_A}{R}\cdot\left(\frac{1}{T}-\frac{1}{T_{ref}}\right)\right) \tag{3.14}$$

$$B(T) = k_B \cdot \exp\left(-\frac{Ea_B}{R}\cdot\left(\frac{1}{T}-\frac{1}{T_{ref}}\right)\right) \tag{3.15}$$

Ea_i = activation energy [kJ×mo^{-1}]

T_{ref} = reference temerature 298 K

Estimated model parameters after non-linear regression of aging data are presented in Table 3.4.

Table 3.4. Estimated model parameters.

Parameter	Temperature		
	30ºC	45ºC	60ºC
λ	3	3	7
k_A	4.39×10^{-5}		
Ea_A	182 kJ mo^{-1}		
k_B	1.01×10^{-3}		
Ea_B	52.1 kJ mo^{-1}		

Besides the cycling degradation model mentioned above, Swierczynski et al. (2015a, 2015b) provide a calendar ageing estimation. Since in the first work, it was considered that the idling SoC of the BESS is equal to 50%, the lifetime of the battery cells in this model is only dependent on the storage temperature and storage time. The final function takes form:

$$Q_{storage} = 4.05 \cdot 10^{-5} \cdot \exp\left(0.035 \cdot T\right) \cdot t^{0.5} \tag{3.16}$$

T = temperature [$°C$]
t = storage time [months]

Second paper also takes into account SoC at which the battery is stored and have totally different fitting function and parameters:

$$Q_{storage} = \left(0.019 \cdot SoC^{0.823} + 0.5195\right) \cdot \left(3.258 \cdot 10^{-9} \cdot T^{5.087} + 0.295\right) \cdot t^{0.8} \tag{3.17}$$

SoC = state of charge [%]
T = temperature [$°C$]
t = storage time [months]

For calendar degradation evaluation Xu (2013) applies the same approach with linearized increment capacity loss multiplied by average temperature and SoC, but as mentioned before the characterization was performed for another cell chemistry.

3.3 Reviewed lifetime models summary

Figure 3.11 and Figure 3.12 demonstrate the most similar cases and conditions for cycling and calendar models respectfully with the addition of some experimental data and mean value curve. The data from calendar models for temperatures other than 20°C can be found in Appendix III.

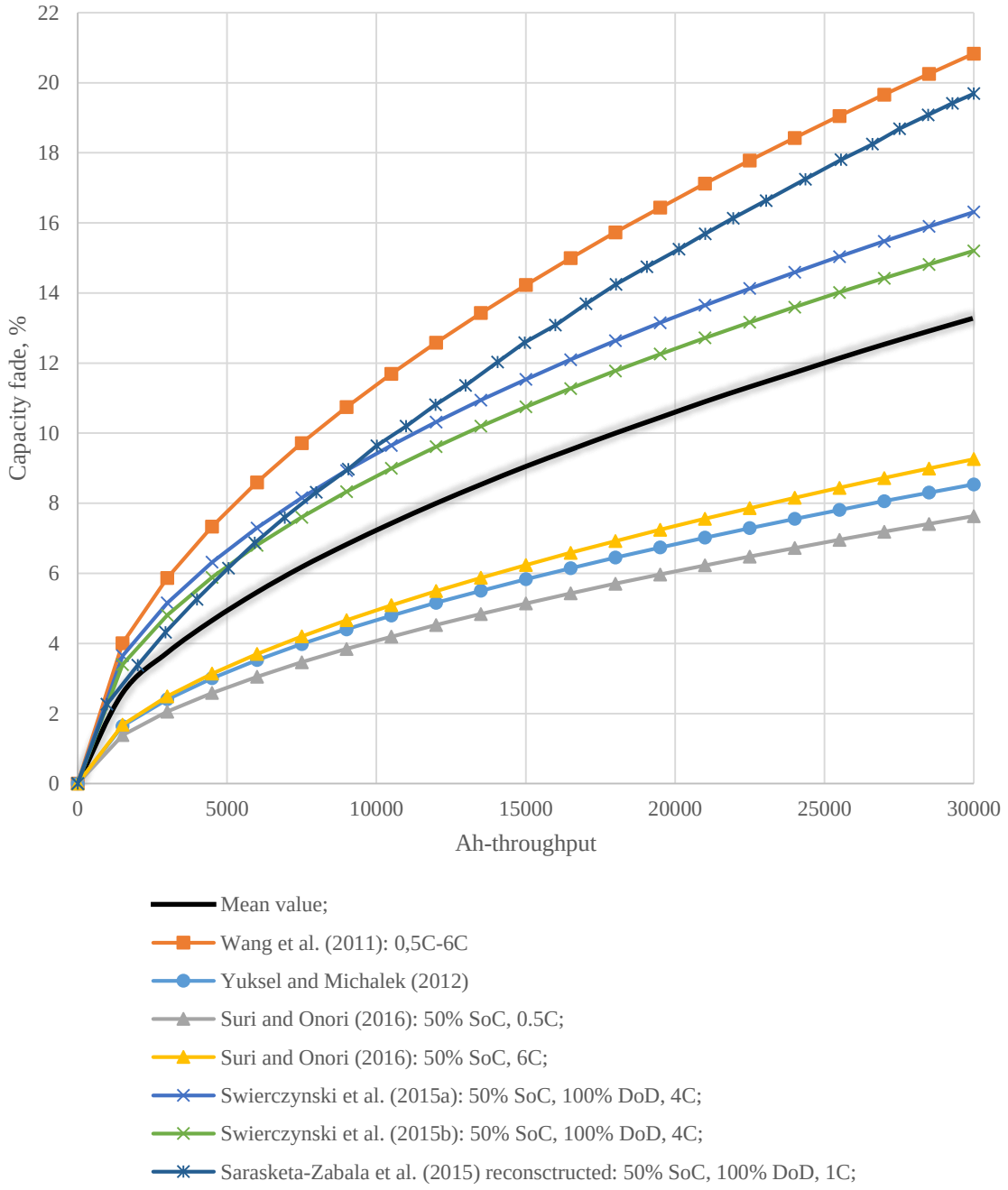

Figure 3.11. Cycling degradation data acquired from examined models and sources (T = 20÷25°C)

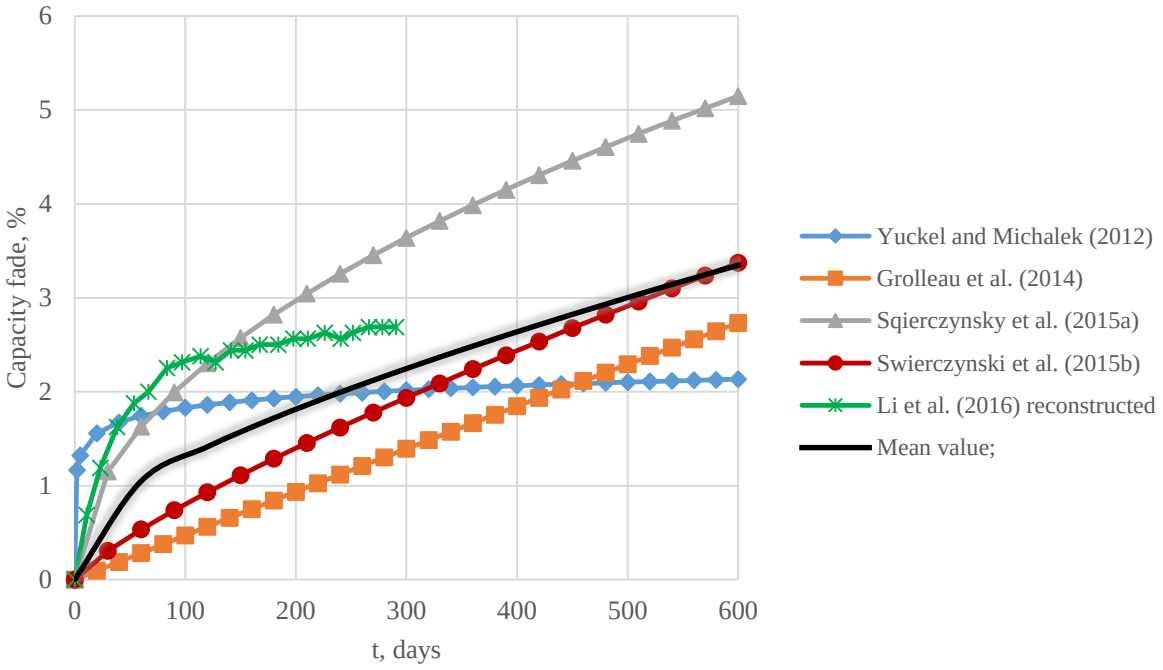

Figure 3.12. Calendar degradation data acquired from examined models and sources (T=20°C, 50% SoC).

Analyzing the results of investigated LFP/graphite cell degradation models, the following conclusions can be drawn:

- Despite the reviewing of models with the same lithium-ion chemistry, the estimations are considerably divergent, which makes the generalization not possible;
- Cycling degradation curves look identical due to similar terms in equations, whereas calendar functions are fundamentally different and do not follow a single trend;
- A variety of models creates difficulties for comparison of their performance since they consider different set of stress factors and making specific assumptions;
- It was noted that almost in every set of conditions both in cycling and calendar, the results from Swierczynsky et al. (2015b) happen to be closer to mean value than other models, consequently it was decided to utilize it in the next chapter;

Selecting the cycling model by Swierczynsky et al. (2015b) comes with certain assumptions. Authors of the work mentioned that the cycling test cases have been performed with a 4C rate, but it is rarely the case in applications like frequency regulation. Consequently, the obtained estimation of BESS lifetime can be too optimistic. However, many studies report that C-rate stress factor can be neglected. For example, Marano et al. (2009) claim that C-rate range under 4C does not introduce to any significant effect unlike currents up to 10C or 15C. As mentioned before, Sarasketa-Zabala et al. (2015) find the effect of C-rate is minimal for some of the tests as shown in Figure 3.13. The capacity degradation trend for the test case with 60% DoD and 2C is not in agreement with the general theory, which implies higher C-rate as a more severe stress factor. On the contrary, the 3.5C cycling case did not demonstrate any signs of accelerated degradation, but 2C degradation rate was definitely enhanced. The case in point could be a cell malfunction or non-linear combined effects of DoD and C-rate, but since there were no additional tests, it was decided to neglect this case and C-rate effect on cycling ageing.

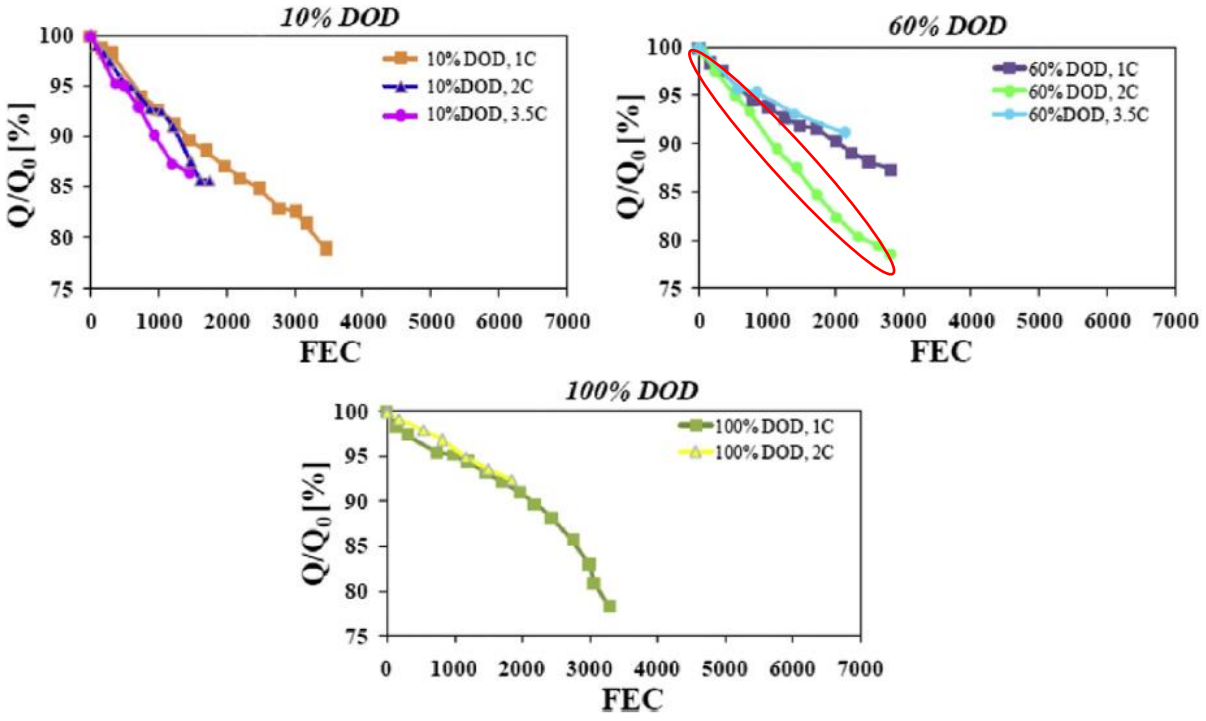

Figure 3.13. C-rate effect on the capacity fade (Sarasketa-Zabala et al. 2015).

Authors also add that the effect of Ah-throughput overlaps the C-rate effect and considered more significant. It was also emphasized previously in Wang et al. (2011) model simulation results that only high C-rates like 10C have pronounced effect. The information described above gives reason to believe that utilizing Swierczynsky et al. (2015b) with C-rates lower than 4C is acceptable and will not cause misconception.

Finally, the important question is how to define overall capacity loss. Only a few works give adequate explanations on how they took into account simultaneous cycling and calendar ageing (i.e. isolating the “pure” cycling effect) on experimental stage (Schmalstieg et al. 2013, Fares 2015). Despite a mentioned uncertainty, the general trend among many researchers (Guenther et al. 2013, Xu 2013, Yuksel and Michalek 2012, Sarasketa-Zabala et al. 2016, Swierczynski et al. 2015b) is assuming that total capacity degradation can be determined by simple sum up of cycling and calendar ageing values, therefore, the same principle will be realized during model implementation.

4 LITHIUM-ION BESS PERFORMANCE DEGRADATION MODEL

The next logical step towards BESS techno-economical analysis is to develop a proper functioning performance model that will be able to evaluate capacity degradation. In Chapter 3, a practical LFP cell lifetime model has been proposed. In this chapter, the missing parts of the BESS performance degradation model will be developed and integrated together.

As it was already mentioned in the previous chapter, the battery performance models serve engineers as a tool to simulate battery dynamic behavior for particular applications and systems. Two major types of these models were categorized earlier:

- Electrochemical models;
- Equivalent circuit-based models;

Although electrochemical models endowed with advantages such as providing high accuracy and comprehension of fundamental physical processes inside the cell, they burden high mathematical complexity and computation power. Moreover, they require a good knowledge of electrochemistry. Since this thesis is written from the perspective of an electrical engineer, electrochemical models are out of this work scope.

The equivalent circuit-based models use electric circuit physical analogs to describe system characteristics of a battery cell. By choosing different combinations of voltage sources, resistors, and capacitors, and characterizing their parameters, circuit-based models are able to describe voltage and capacity behavior of the cell without significant computational complexity. A vast number of circuit models have been developed in the literature, most of them can further be classified into two main groups:

- Lumped-parameter equivalent circuit models;
- Impedance-based models;

A very recent article by Nejad et al. (2016) systematically reviews the lithium-ion battery equivalent circuit models for real-time simulations in terms of their accuracy and demands. The models under investigations include the Combined model, Rint model, two hysteresis models, Randles' model, a modified Randles' model and two resistor-capacitor (RC) network models with and without hysteresis included. The authors also compared the two-RC model with impedance-based type. The impedance-based model allows a direct measurement of system AC-response in any working point and presents a close relation of elements to physic-chemical processes inside the battery. However, in order to properly build that type of model, it requires special equipment for electrochemical impedance spectroscopy (EIS). Overall, the results of the review by Nejad et al. (2016) suggested that the two-RC model structure is an optimum choice for implementation of most battery energy storages and power management strategies. The equivalent circuit two-RC model structure diagram is shown in Figure 4.1.

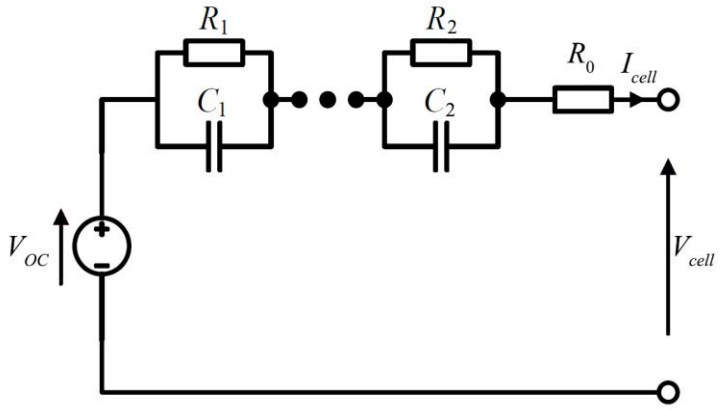

I_{cell} = cell throughput current [A]
V_{cell} = cell terminal voltage [V]
R_0 = cell internal resistance [Ohm]
R_1 = short time transient resistance [Ohm]
C_1 = short time transient capacity [F]
R_2 = long time transient resistance [Ohm]
C_2 = long time transient capacity [F]
V_{OC} = open-circuit voltage [V]

Figure 4.1. The equivalent circuit diagram for the two-RC model.

The self-discharge rate of lithium-ion cells is very low, which is approximately 1-3% per month (Swierczynski et al. 2014, 1), consequently the parasitic branch will be neglected.

Next sections describe the development of lithium-ion BESS model including degradation effects using Matlab®, Simulink™ and Simscape™ modeling environment.

4.1 Battery circuit-based model

The publicly available equivalent circuit model of lithium battery cell with two-RC blocks developed by Huria et al. (2012) was adopted and upgraded for the needs of this thesis. The original model accounts for the dynamic behavior of the cell, including non-linear open-circuit voltage (OCV), passive circuit elements state of charge and inner temperature. Elements of the cell V_{OC}, R_0, R_1, C_1, R_2, C_2 are functions of SoC and temperature. A runtime operation of the model is implemented through coulomb counting technic, i.e. integrating the current flow over time as shown in Equation 4.1.

$$SoC = 1 - \frac{\int_0^t I_{cell}(t)dt}{Q_{nom}} \tag{4.1}$$

Numerical values of the model were estimated for high power NMC cells. Hence, new characterization for LFP cell type is necessary.

4.1.1 Specification of circuit elements

Ding et al. (2012) executed parametrization of corresponding circuit elements for cylindrical LFP/graphite cell. Applying their results will allow integrating performance model with degradation model derived in the previous chapter for the same battery product. Current direction dependency does not have a perceptible effect on results, so it was neglected to avoid immensely high complexity. The circuit elements in models are described by lookup tables. The parameters of passive circuit elements presented in Figure 4.2 and 4.3 were digitized in matrix form with the help of GetData Graph Digitizer software and used in the model.

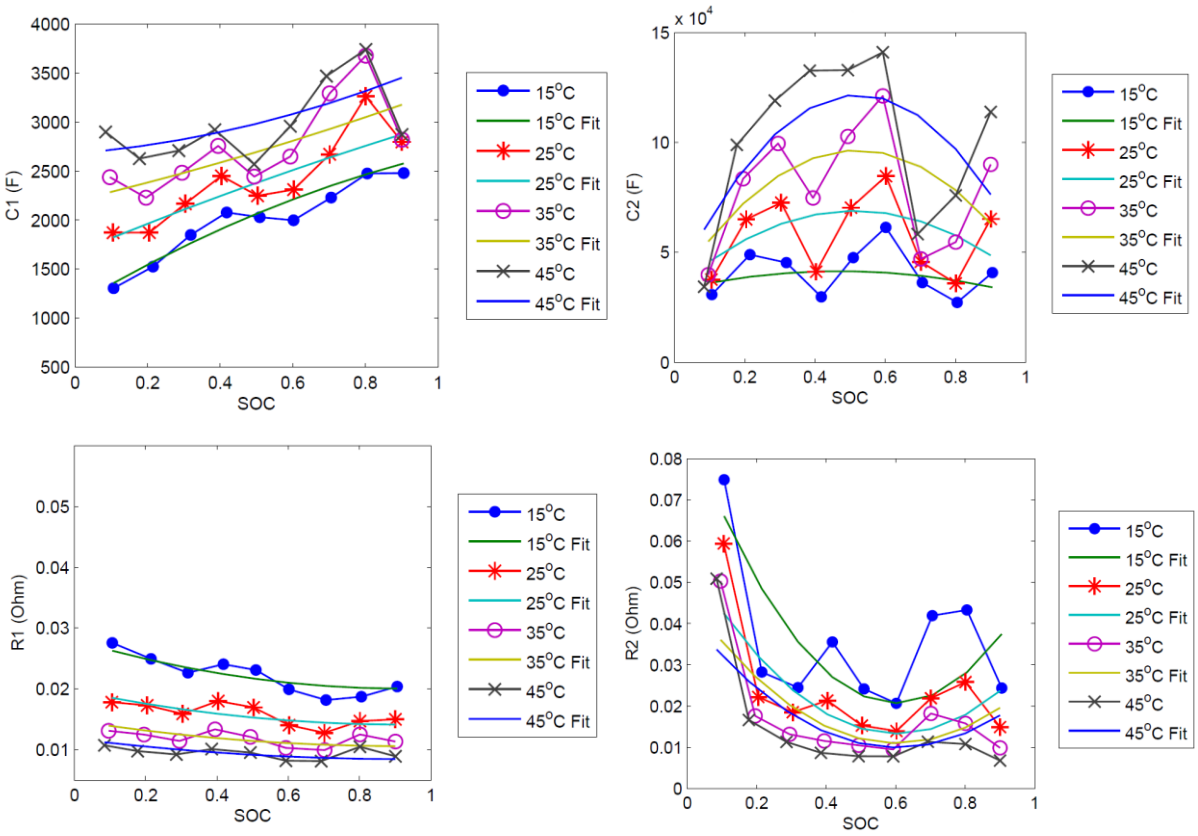

Figure 4.2. Transient passive elements values with dependence from temperature and SoC (Ding et al. 2012).

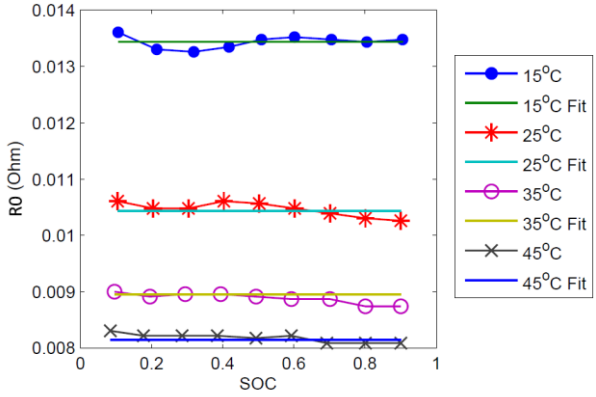

Figure 4.3. Inner resistance values with dependence from temperature and SoC (Ding et al. 2012).

The internal resistance R0 has a minimum dependence on SoC but is highly dependent on temperature. The transient passive elements have both temperature and SoC dependency.

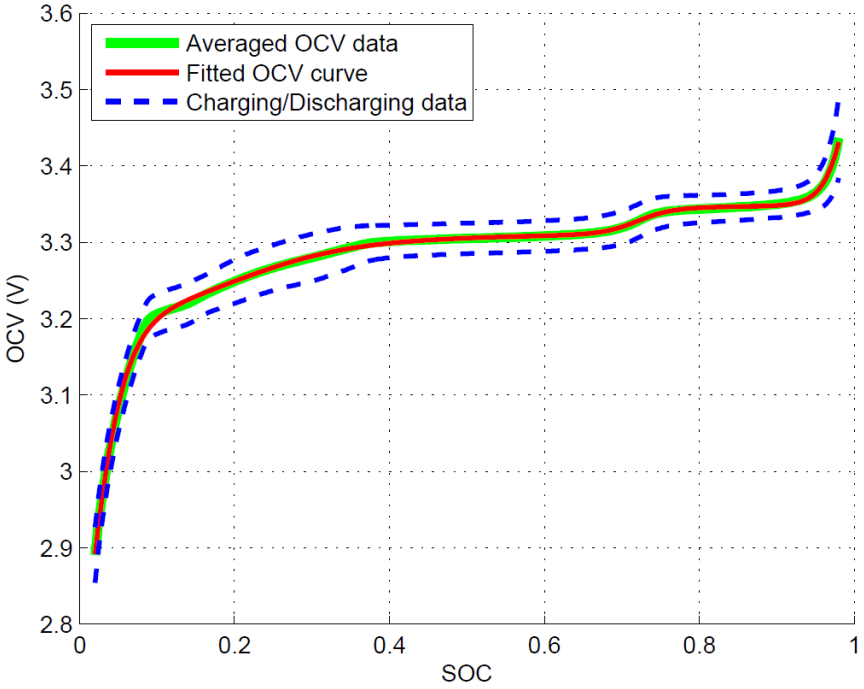

Figure 4.4. The measured charging and discharging OCV as a function of SoC (Weng et al. 2013).

The OCV relation with SoC in LFP cells is a topic for discussion among many researchers. Indeed, LFP cells have very flat charge and discharge curve, so even a small mismatch may cause a large deviation of two values. Some authors observed pronounced hysteresis effect of the OCV during charging and discharging process (Omar et al. 2014, 1579), while others did not.

Weng et al. (2013) proposed a new method of obtaining OCV by taking the average of charging and discharging data, as shown in Figure 4.4. Also, the OCV curve from Weng et al. (2013) paper is based on a lifecycle test data collected from cylindrical LFP cells. Owing to this, Figure 4.4 was used to parametrize OCV look-up table as a function of SoC.

Nominal battery capacity and approximate thermal properties were acquired from manufacturer datasheet presented in Appendix II. Overall summary of model parametrization is embodied within Matlab initialization file and provided in Appendix IV.

4.1.2 General layout of equivalent circuit model

The core equivalent circuit elements were created using Simscape™ simulation tool, and basically, they consist of block parameter estimation part using look-up tables and elementary electrical circuit equations. It has to be noted that original model contained thermal modelling feature based on power dissipation of circuit elements. Figure 4.5 shows the model block set with explanations.

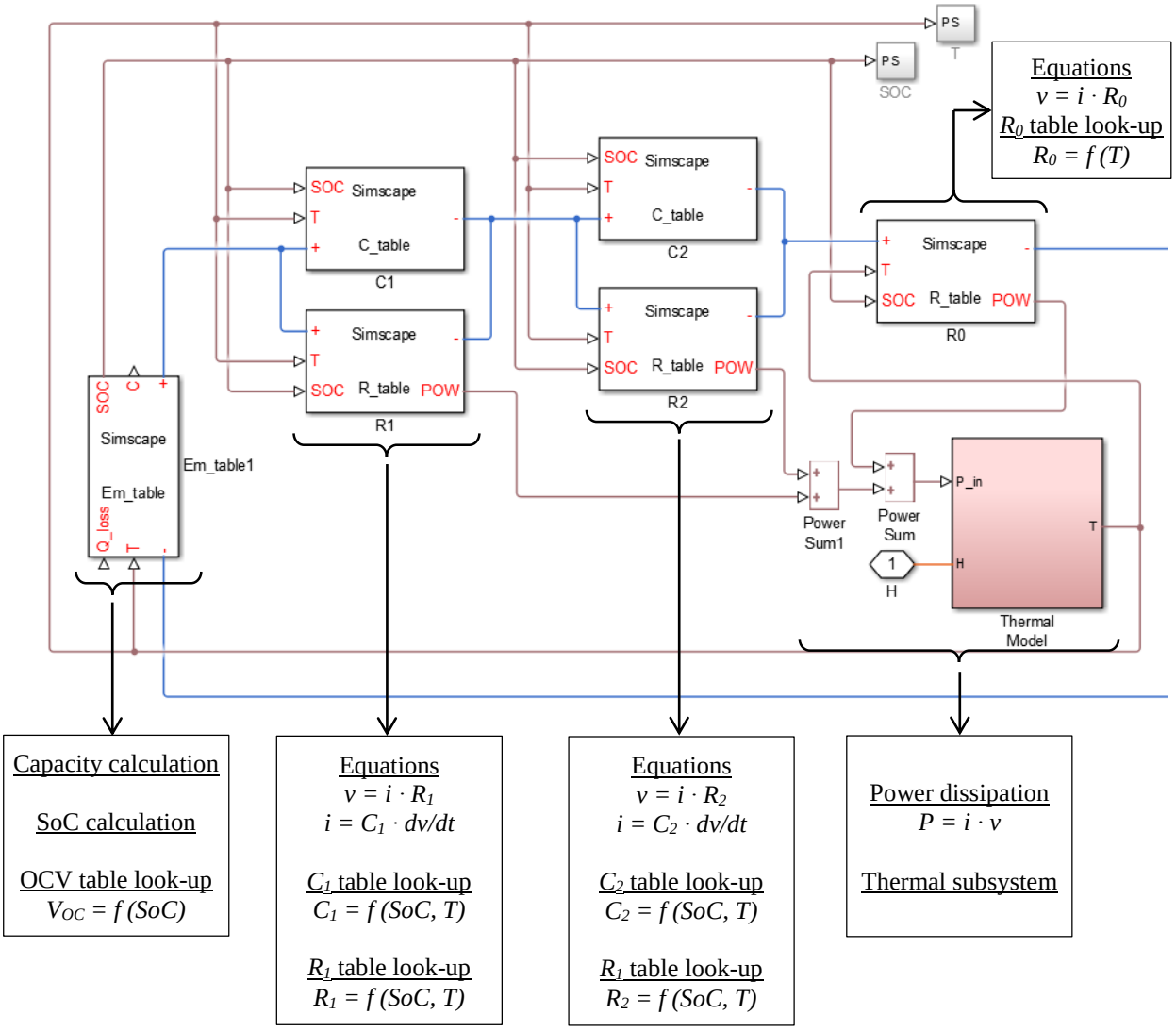

Figure 4.5. The Simscape™ layout of the 2RC battery cell model.

To check the dynamic performance of newly parametrized LFP equivalent circuit model, full charge and discharge with 1C pulse current tests were conducted, and results are demonstrated in Figure 4.6.

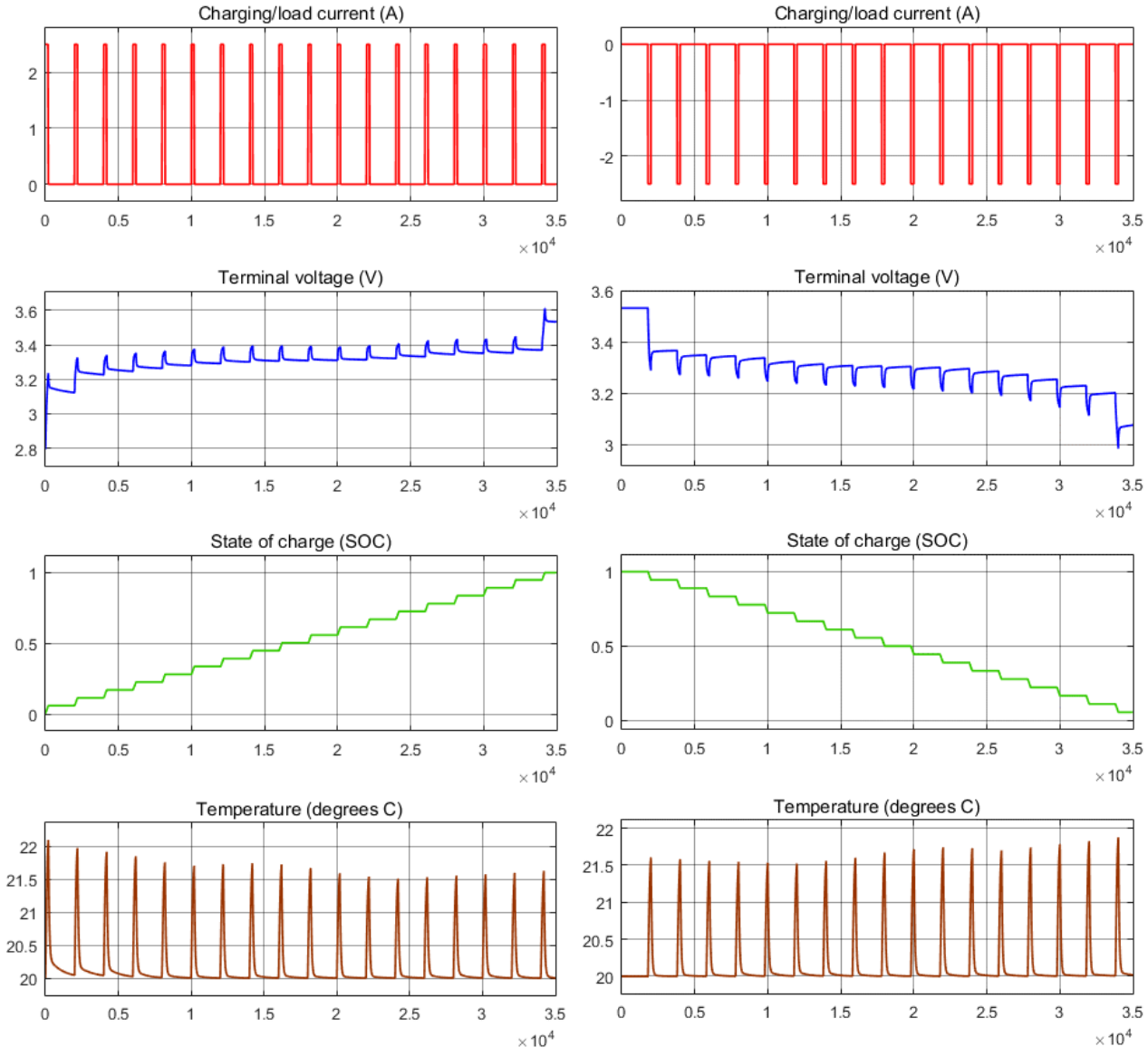

Figure 4.6. The voltage dynamic test of fully a) charging and b) discharging the cell.

4.2 Lifetime model integration

Incorporating degradation rate estimation in performance model of lithium iron phosphate battery is one of the key aspects of present thesis. Based on results from Chapter 3, a model developed by Swierczynsky et al. (2015b) was selected as the best candidate among other options. Total capacity fade due to cycling and calendar simulated setting can be determined from Equations 4.2 – 4.4.

$$Q_{loss} = Q_{cycling} + Q_{storage} \tag{4.2}$$

$$Q_{cycling} = 0.00024 \cdot \exp\left(0.02717 \cdot T\right) \cdot 0.02982 \cdot \sqrt{\frac{Ah_{th}}{2 \cdot Q_{nom}}} \tag{4.3}$$

$$Q_{storage} = \left(0.019 \cdot SoC^{0.823} + 0.5195\right) \cdot \left(3.258 \cdot 10^{-9} \cdot T^{5.087} + 0.295\right) \cdot t^{0.8} \tag{4.4}$$

Q_{loss} = total capacity loss [%]

Capacity degradation can be taken into account based on Equation 3.2. The code of OCV custom block (*Em_table*), where capacity table look-up takes place, can be modified to subtract the capacity loss from nominal capacity as shown in Figure 4.7.

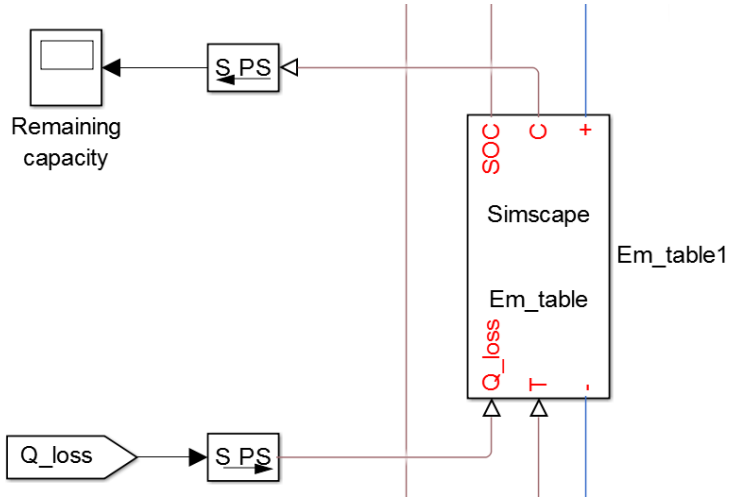

Figure 4.7. Developing dependency of remaining capacity from degradation model output.

Selected lifetime model requires input data such as total Ah-throughput, simulation time, the nominal capacity of the cell and finally average values of temperature and SoC. Since the equivalent circuit model can be highly dynamic, in order to decrease inaccuracy and provide average values of temperature and SoC, continuous RMS value blocks were implemented on continuous input signals. Figure 4.8 introduces lifetime model block set, in addition, the contents of cycling and calendar degradation Matlab functions are available in Appendix V.

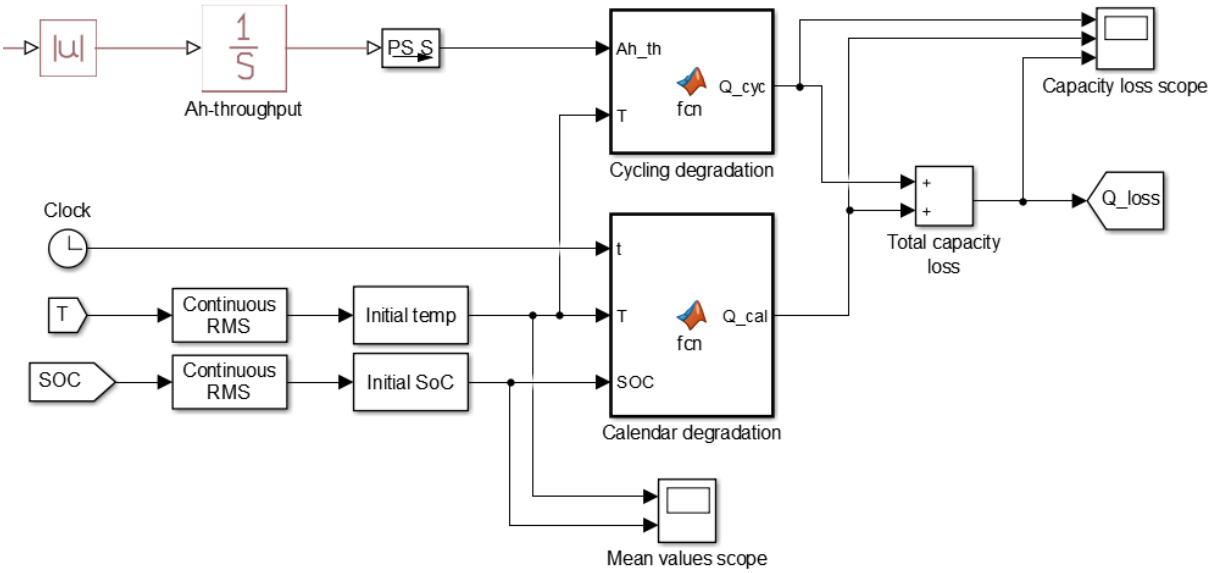

Figure 4.8. The Simulink™ LFP cell lifetime model block set.

4.3 BESS model

Equivalent circuit and lifetime models are developed according to one single cell while BESS contains a large amount of single cells interconnected in series strings which are connected in parallels with each other. Complex battery pack structures introduce additional complications in battery modeling. The research questions of this work did not consider the BMS, power converters or modeling the variation of cells characteristics within the battery pack. Hence, all cells are assumed to be completely identical. In other words, voltage, current, and energy are evenly distributed among the cells. That simplification allows to convert the inputs and outputs

of the cell to a BESS level by simple Equations 4.5 – 4.6. A development from cell to BESS model is shown in Figure 4.9.

$$I_{cell} = \frac{I_{BESS}}{N_{par}} \tag{4.5}$$

$$V_{cell} = \frac{V_{BESS}}{N_{str}} \tag{4.6}$$

I_{BESS} = BESS current [A]
N_{par} = conditional number of parallel strings
V_{BESS} = BESS voltage [V]
N_{str} = conditional number of cells in one string

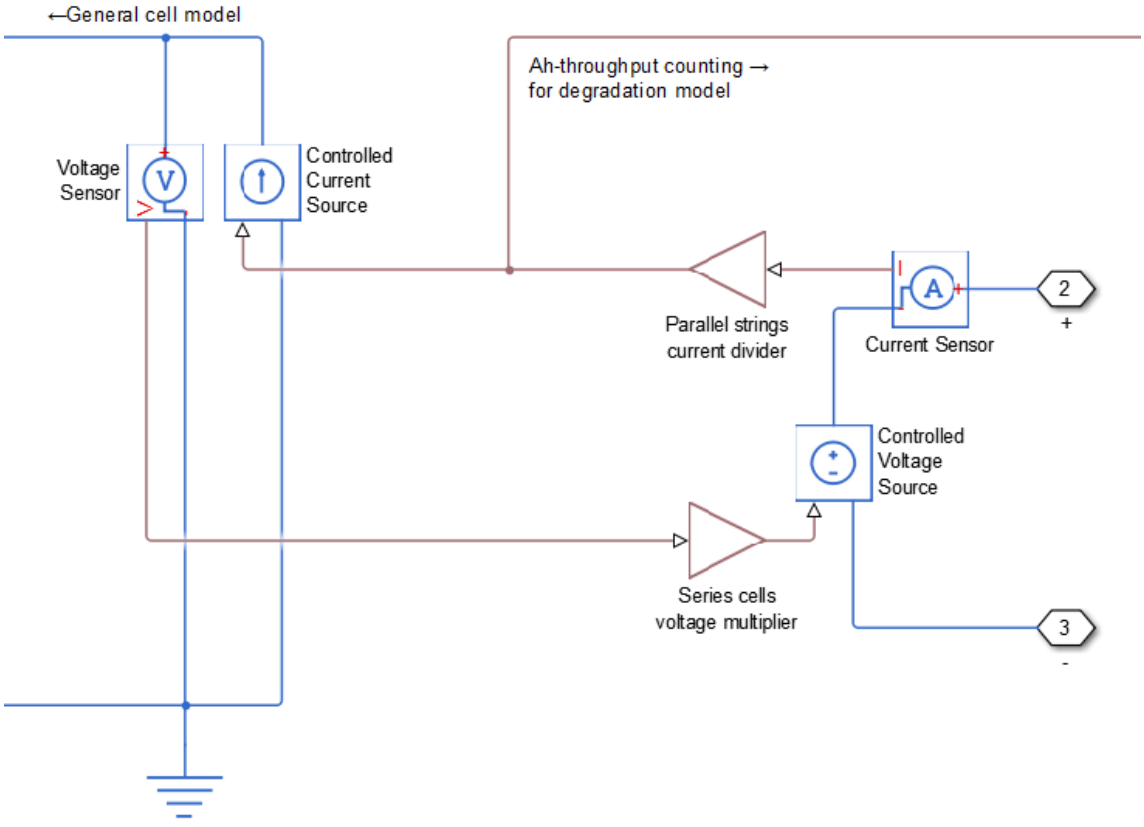

Figure 4.9. The Simscape™ cell - BESS transition block set.

4.4 Simulation system overview

Linking together two-RC equivalent circuit-based model including thermal modeling with previously developed lifetime model and upscaling it to high power BESS level form a complete dynamic simulation system. The main view is presented in Figure 4.10.

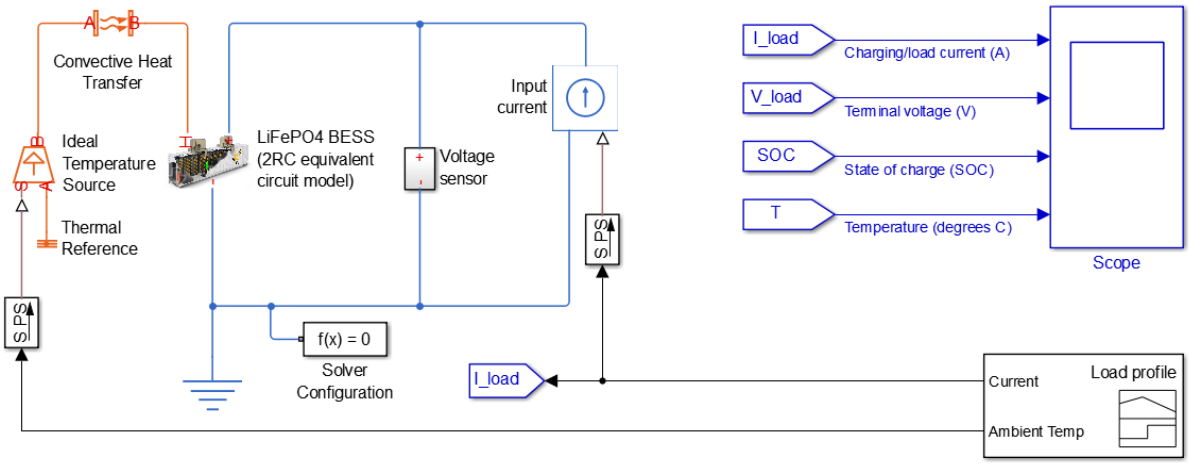

Figure 4.10. Overview of the BESS simulation model.

Besides initialization file containing essential system parameters, the model requires an input current load profile or special control block that will provide the signal. Chapter 5 is dedicated to frequency regulation service; therefore, several control algorithms will be developed to govern the BESS.

5 PRIMARY FREQUENCY REGULATION PROVIDED BY BESS

In recent years' ancillary service markets have been opened by some countries, such as Finland and services like frequency regulation have become profit-making. BESS can be a very useful tool for maintaining system frequency within the desired level. Power electronics inverters with very fast response time within the BESS can provide much faster regulation than Pumped Hydroelectric Storage or Gas Turbine. This is becoming more valuable considering growing trend of time outside the band 49.90 – 50.10 Hz in Nordic countries (ENTSO-E 2011) and hour shift imbalance problems (Barmsnes 2014). Indeed, the frequency histogram of March 2016 measured by Fingrid in Figure 5.1 indicates a big amount of incidents outside the dead-band.

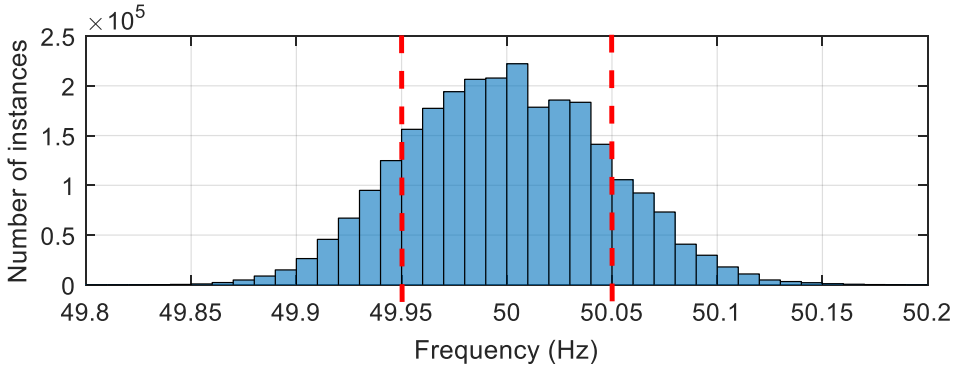

Figure 5.1. Distribution of frequency values in Finland during March 2016.

In order to investigate the techno-economic feasibility of frequency regulation service in this chapter, the concept from Figure 5.2 was employed.

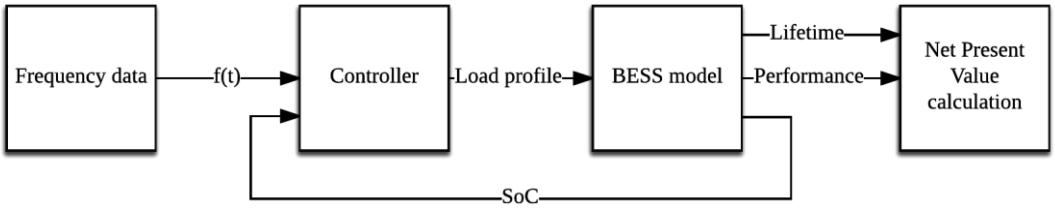

Figure 5.2. The scheme of the BESS frequency regulation service assessment.

5.1 Finland ancillary service markets

In Finland, ancillary service markets are held by national transmission system operator Fingrid. Ancillary services which represent frequency control processes are categorized as reserves. The structure of power reserve markets in Fingrid is presented in Figure 5.3.

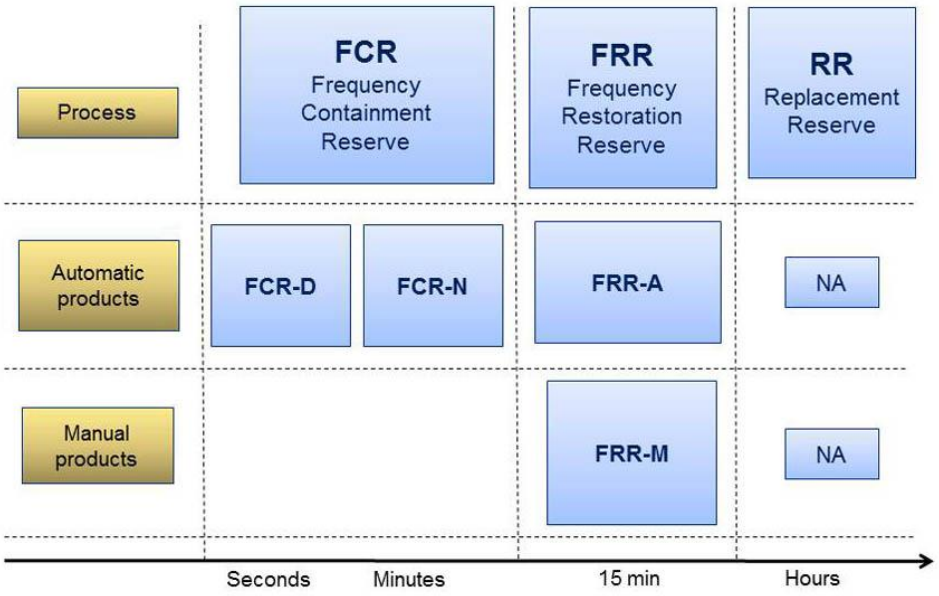

Figure 5.3. Reserve products used in Finland (Fingrid 2016).

Reserves are divided into Frequency Containment Reserves (FCR), Frequency Restoration Reserves (FRR) and Replacement Reserves (RR). FCR are used for the constant control of frequency. The purpose of FRR is secondary control and to relieve FCR units. RR release activated FRR back to a state of readiness in case of new disturbances. FCR are subdivided in Frequency Containment Reserve for Normal operation (FCR-N) and Frequency Containment Reserve for Disturbances (FCR-D). The aim of FCR-N is to maintain the frequency in the normal range of 49.9 – 50.1 Hz. The aim of FCR-D is to replace the production deficit in the case of unexpected disconnection of generation or interconnector. The technical requirements for above mentioned reserves are listed in Table 5.1. (Fingrid)

Table 5.1. The technical requirements for reserve products.

Reserve	Minimum size	Full activation time	Activation frequency	Other
FCR-N	0.1 MW	In 3 min after frequency step change of ± 0,1 Hz	Constantly	Dead band max ±0,05 Hz, droop max 6
FCR-D (Power plant reserves)	1 MW	5 s / 50 % 30 s / 100 %, with frequency 49,50 Hz	Several times per day	
FCR-D (Relay-connected loads)	1 MW	Immediately with frequency 30 s ≤ 49,70 Hz or 5 s ≤ 49,50 Hz	Several times per day	Load can be reconnected to grid when frequency is at least 49.90 Hz for five mins
FCR-D (Idle reserve power machines)	1 MW	Reserve should be activated, when frequency 30 s ≤ 49,70 Hz	Several times per day	Machine can be disconnected from grid when frequency is at least 49.90 Hz for five minutes
FRR-A	5 MW	2 min	Several times per day	automatic
FRR-M	10 MW	max 15 min	Several times per day	manual

Right now there is uncertainty and lack of explanation regarding the question how BESS should be operated in the FCR-D. Additionally, FCR-D requires bigger minimum size, which can be a challenge for BESS, and offers a significantly smaller payment as shown in Figure 5.4. FRR-A and FRR-M require even bigger minimum size and operate with long response time, not utilizing fast response advantage of BESS. Therefore, FCR-N reserve product has suitable requirements for BESS and will provide bigger payments than FCR-D. The corresponding simulations will be performed in the next sections.

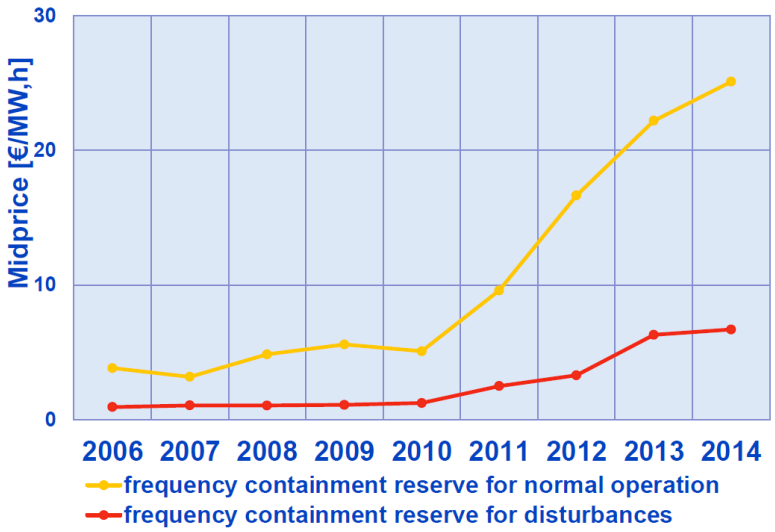

Figure 5.4. Evolution of frequency containment reserves prices in Finland (Fingrid).

5.2 Simulation of BESS at FCR-N

The main goal of the simulations is to observe BESS response to real frequency data, to compare different energy management strategies and to analyse technical constraints. The energy management strategies analysis was made from BESS owner point of view, i.e. to minimize degradation rates and to maximize profits, at the same time fulfilling the TSO requirements.

At the present moment, there is no specific requirements and prequalification rules from Fingrid for reserve providing units with limited capacity such as BESS. In the majority of EU member states and in Finland, the maintaining of FCR full power activation is currently required for a period of 15 minutes. It is assumed that by the end of 15 minutes, the secondary reserves will be fully activated in order to release the primary reserves. That means that required energy storage capacity is the key determining cost factor of the BESS, as it will define the maximum power which can be bidden and the total system investment. The optimal sizing question will be discussed further in the text. During the comparison of control logics, the minimum requirement described above will be used.

In this thesis, the capacity and nominal voltage of the BESS was arbitrary chosen to be 1 MWh and 825 V. The upward (in the case of under frequencies) and downward (in the case of over frequencies) frequency regulations in Finland are not provided separately. Hence the BESS should provide regulation in both directions. Considering the normal distribution of frequency deviation from Figure 5.1, the set point of SoC is assumed to be 50%. However, this is not always the case, because some storages can be utilized with special control strategies. Most of the lithium-ion battery manufacturers highly recommend to operate it within 10 – 90 % SoC range, otherwise a rapid battery degradation will take place. Thus, only 40% of full BESS energy capacity or 0.4 MWh is available to provide 15 minutes' full power regulation service as shown in Figure 5.5. Therefore, the maximum FCR-N bidding power of the unit is defined in Equation 5.1.

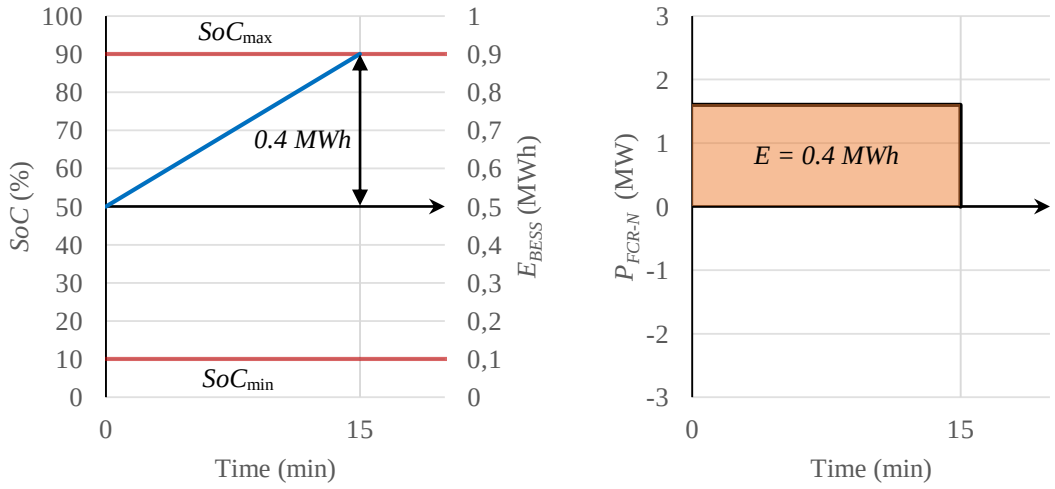

Figure 5.5. Dimensioning requirement graphical representation.

$$P_{FCR-N} = \frac{0.4 \cdot E_{BESS}}{t_{15\text{min}}} = \frac{0.4 \cdot 1}{0.25} \cdot \frac{\text{MWh}}{\text{h}} = 1.6 \text{ MW} \tag{5.1}$$

P_{FCR-N} = FCR-N maximum bidding power [MW]
E_{BESS} = total BESS capacity [MWh]
$t_{15\text{min}}$ = full activation time period requirement [h]

The number of parallel strings and cells in one string of the BESS needed to parametrize the model are presented in Equations 5.2 – 5.3.

$$N_{par} = \frac{E_{BESS}}{V_{BESS} \cdot C_{cell}} = \frac{1}{825 \cdot 2.5} \cdot \frac{\text{MWh}}{\text{V} \cdot \text{Ah}} = 484.84 \approx 485 \tag{5.2}$$

$$N_{str} = \frac{V_{BESS}}{V_{cell}} = \frac{825\ V}{3.3\ V} = 250 \tag{5.3}$$

Also, it has to be mentioned that energy capacity of the battery storage will decrease due to degradation, and maximum bidding power will reduce as well. For example, at 80% state of health (SoH) of the batteries, the regulation capacity will be 0.32 MWh and the maximum bidding power will be 1.28 MW.

5.2.1 Description of control logics

The first control logic implementation represents the most common understanding of the frequency dead-band with center at the nominal frequency 50 Hz. Fingrid's application instruction for the maintenance of FCR (2016) specifies that "reserve unit used in FCR-N shall regulate almost linearly within a frequency range of 49.90 - 50.10 Hz so that the dead band in frequency regulation is at the most 50 ±0.05 Hz." During the time when the frequency is inside the dead-band, if SoC is not equal to initial set point level, the controller will initiate charging or discharging mode to recover the SoC to the reference level. The rate of recovery mode is equal to ±1 p.u. of the current bidding power $P_{FCR\text{-}N}$, if not stated otherwise. The output power of the BESS vs. frequency variation of the first control logic is shown in Figure 5.6. The demonstration of control logic №1 operation during one hour is shown in Figure 5.7.

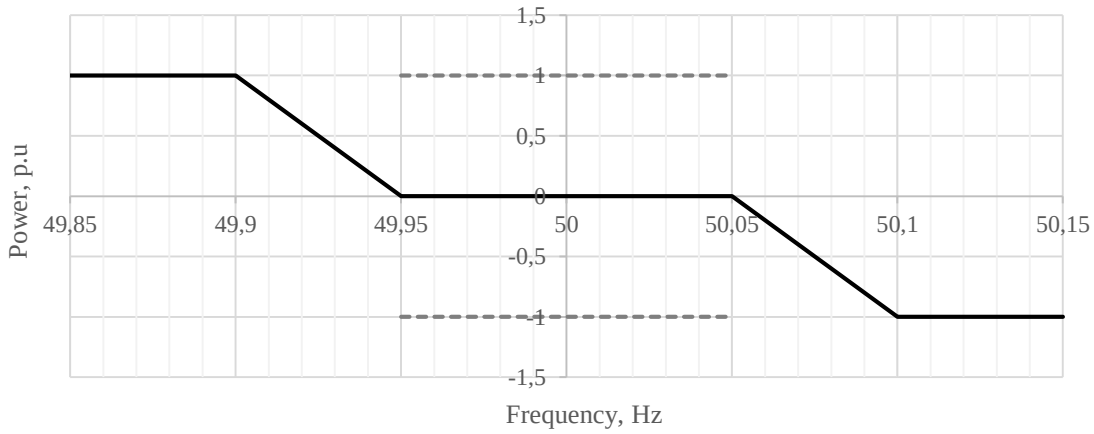

Figure 5.6. Control logic №1 output power vs. frequency variation, ±0.05 Hz dead-band.

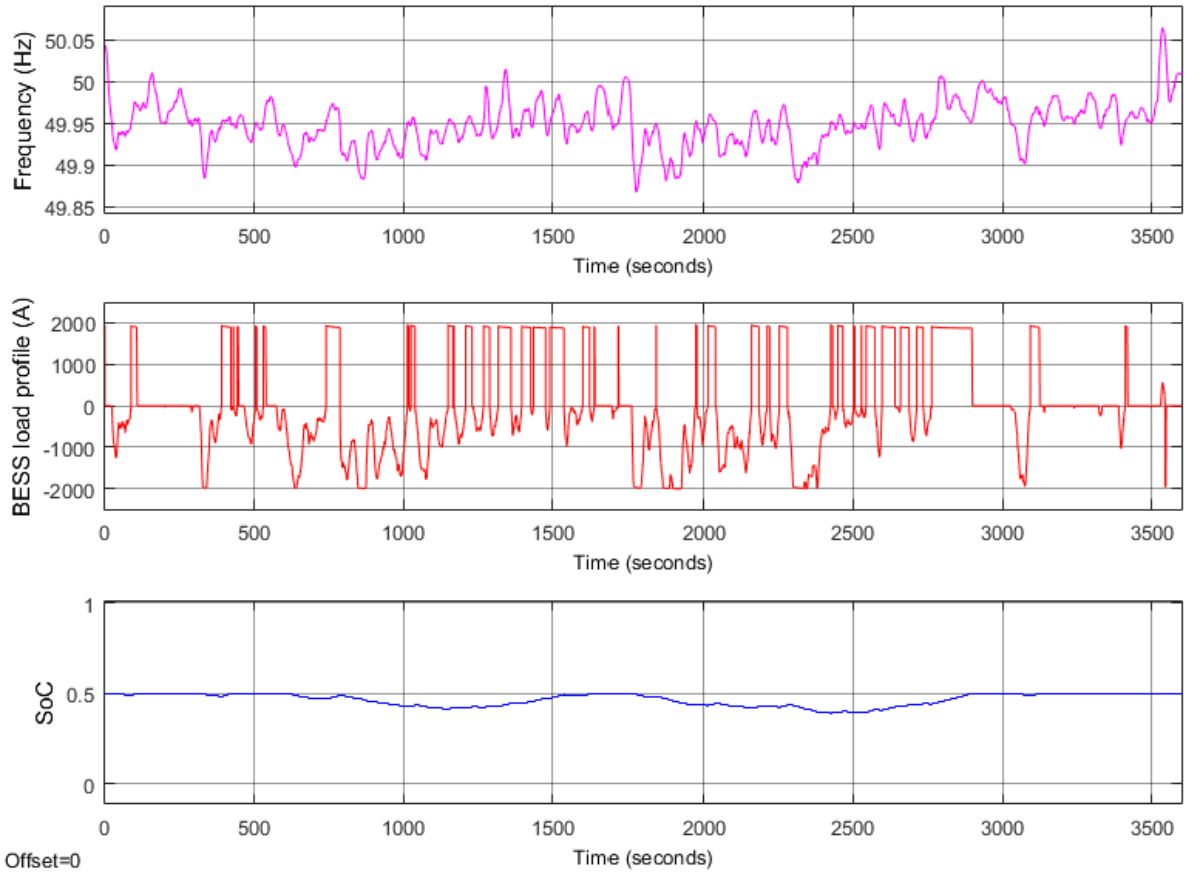

Figure 5.7. Control logic №1 operation (one hour).

European Network of Transmission System Operators for Electricity (ENTSO-E) is discussing the possibility of tightening the dead-band to ±10 mHz. Without a doubt, it will cause implications of more frequent activation of BESS and degradation rate increase. However, the tightening the dead-band can change the market situation or additional payments for BESS can be introduced. The output power of the BESS vs. frequency variation of the second control logic is shown in Figure 5.8. The demonstration of control logic №2 operation during one hour is shown in Figure 5.9.

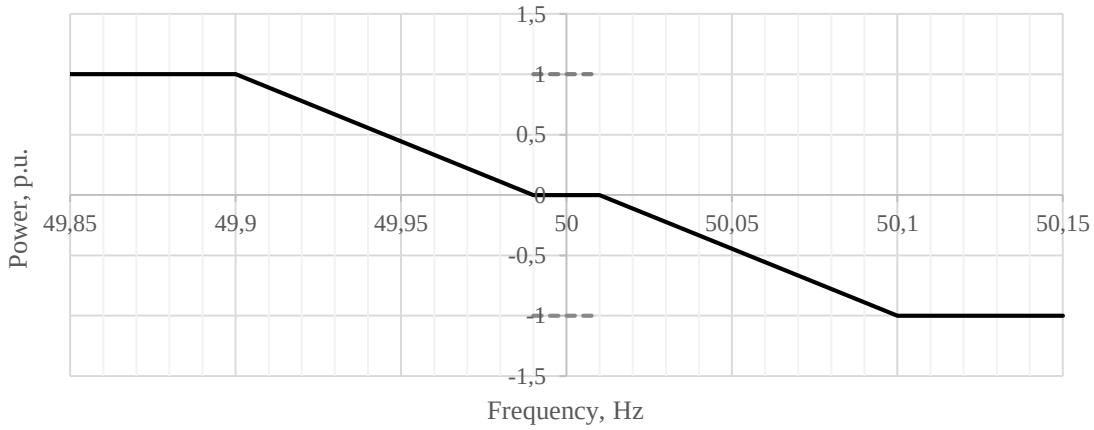

Figure 5.8. Control logic №2 output power vs. frequency variation, ±0.01 Hz dead-band.

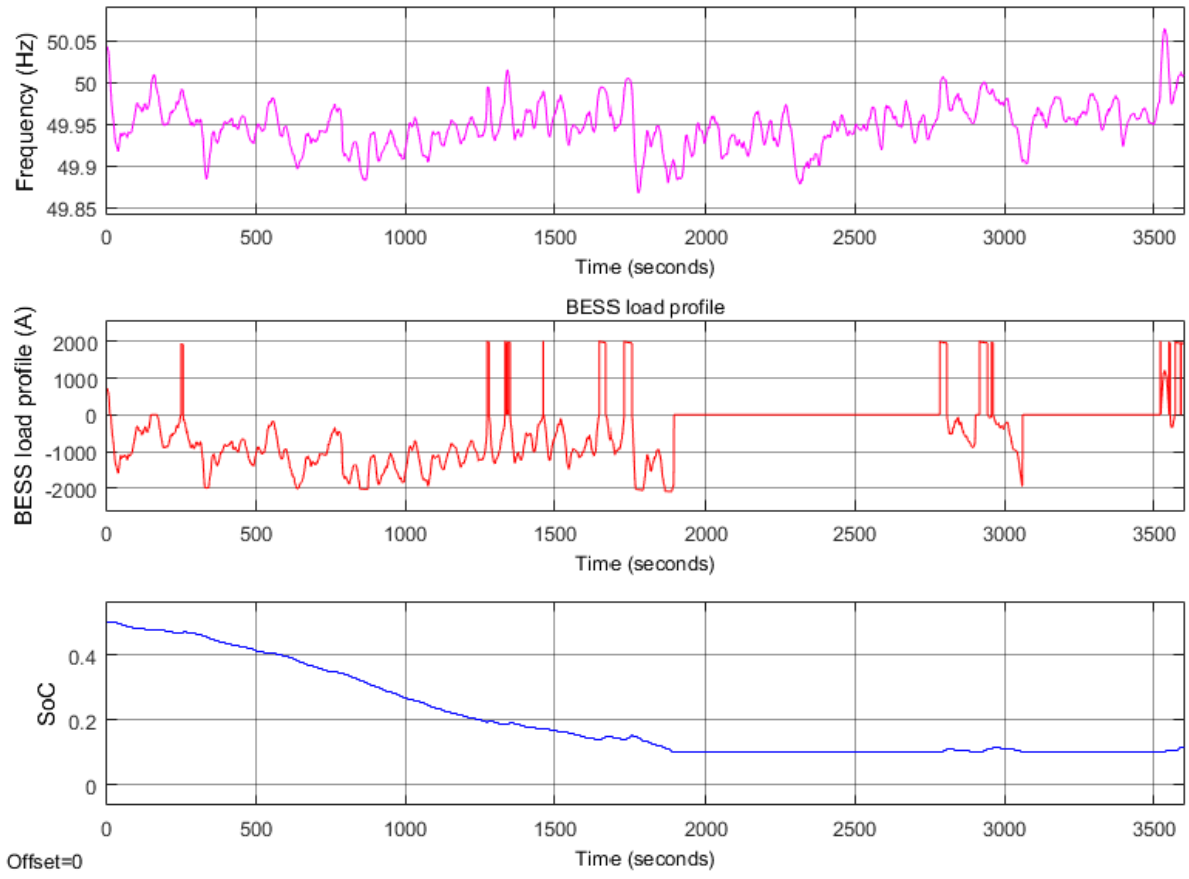

Figure 5.9. Control logic №2 operation (one hour).

Following control logic represent complete absence of dead-band. That case allows evaluating the contribution of dead-band from degradation rate perspective. The output power of the BESS vs. frequency variation of the third control logic is shown in Figure 5.10. The demonstration of control logic №3 operation during one hour is shown in Figure 5.11.

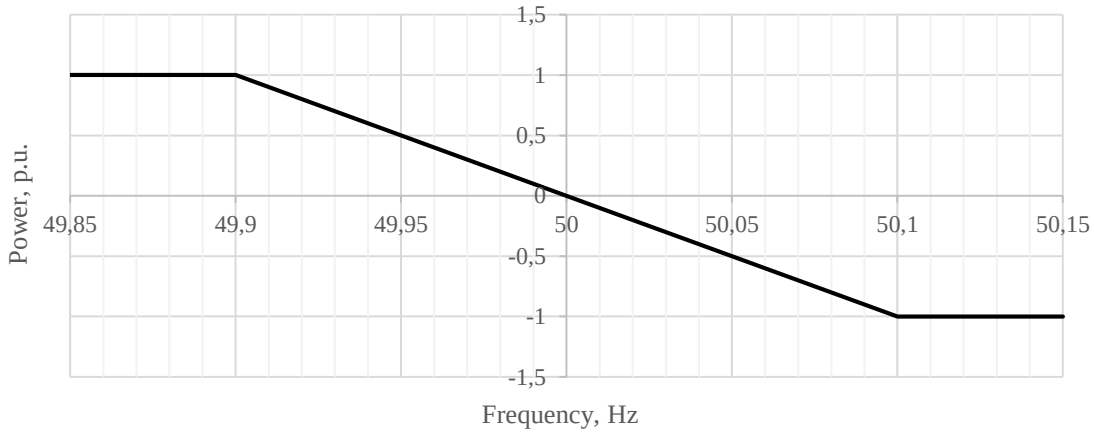

Figure 5.10. Control logic №3 output power vs. frequency variation, no dead-band.

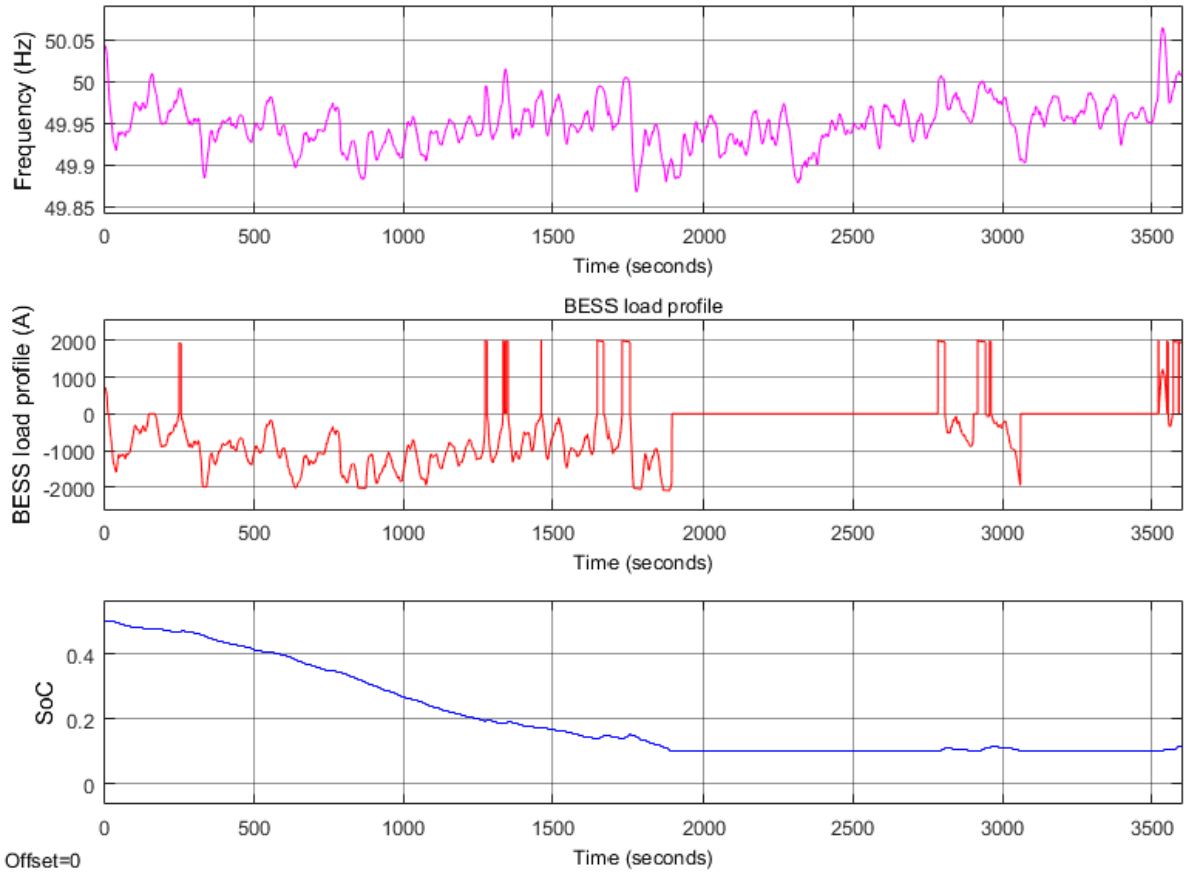

Figure 5.11. Control logic №3 operation (one hour).

The control logic №4 operates with the common dead-band but with the inclusion of 2 sec transport delay block. The idea is to react only if the frequency is out of the dead-band for more than 2 seconds thus ignoring small fluctuations outside the dead-band shorter than 2 sec. Ignoring very short deviations should reduce degradation rates by a certain amount. Although it is obviously favorable by BESS owner, each power activation signal will be delayed and cut off by 2 sec. In fact, it does not violate technical requirements for FCR-N. However, such strategy reduces advantages from BESS for TSO to some extent. The demonstration of control logic №4 operation with custom frequency signal is shown in Figure 5.12.

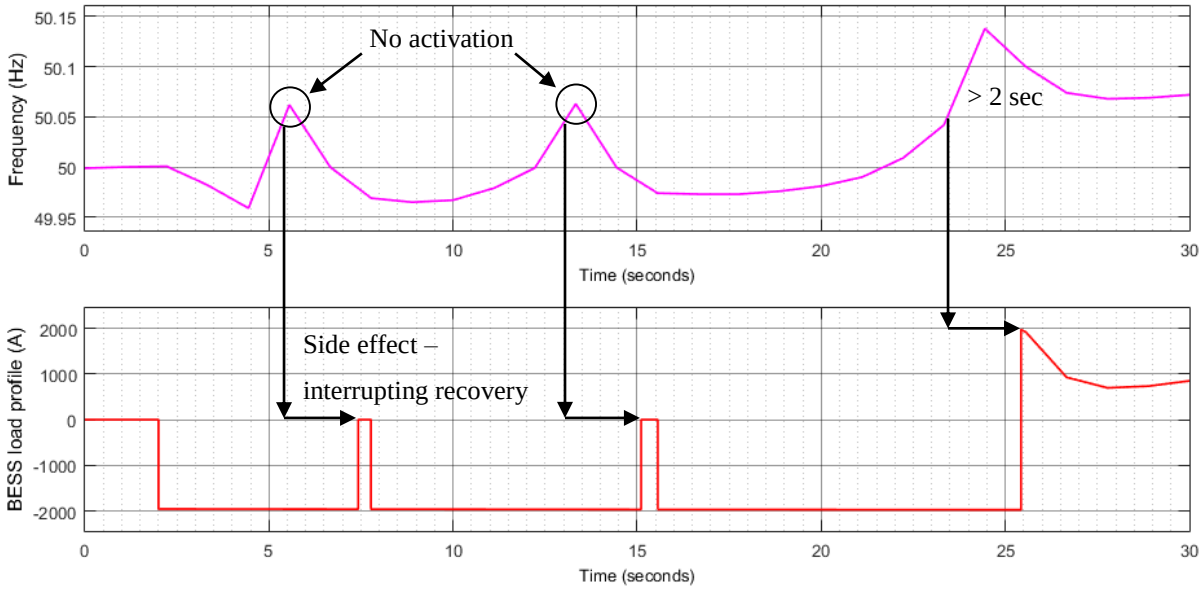

Figure 5.12. Control logic №4 operation (30 sec).

The control logic №5 operates with the common dead-band but introduces a new strategy for recovery mode. There are currently no exact instructions and requirements for how to restore the energy content of FCR units with limited capacity. Based on the fact that frequency signal has a normal distribution, it can be suggested that in ideal case SoC will be regulated toward set point by frequency regulation in opposite direction without additional control. Since the capacity of storage is limited, the recovery control is still necessary. However, it is more reasonable to recover faster near the SoC limits than in set point proximity. Consequently, instead of constant values, recovery power can be described by a function of SoC deviation from the set point. The hybrid strategy approach described by Li et al. (2014) was selected as a reference and adapted for the recovery power as shown in Equations 5.4 and 5.5. The difference between regular and suggested strategy is shown in Figure 5.13. The demonstration of control logic №5 operation during one hour is shown in Figure 5.14.

$$P_{rec\ charge} = \sqrt{\frac{SoC - SoC_{ref}}{SoC_{\min} - SoC_{ref}}} \tag{5.4}$$

$$P_{rec\ discharge} = -\sqrt{\frac{SoC - SoC_{ref}}{SoC_{\max} - SoC_{ref}}} \tag{5.5}$$

$P_{rec\ charge}$ = charge power during recovery [p.u.]

$P_{rec\ discharge}$ = discharge power during recovery [p.u.]

SoC_{ref} = state of charge setpoint

$SoC_{\min}$ = state of charge minimum limit

$SoC_{\max}$ = state of charge maximum limit

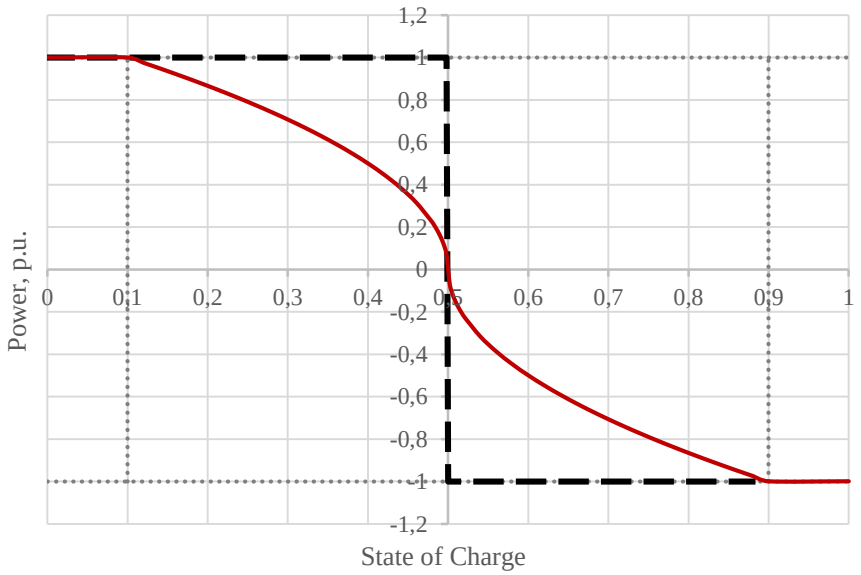

Figure 5.13. Control logic №5 recovery power of the BESS vs. SoC deviation.

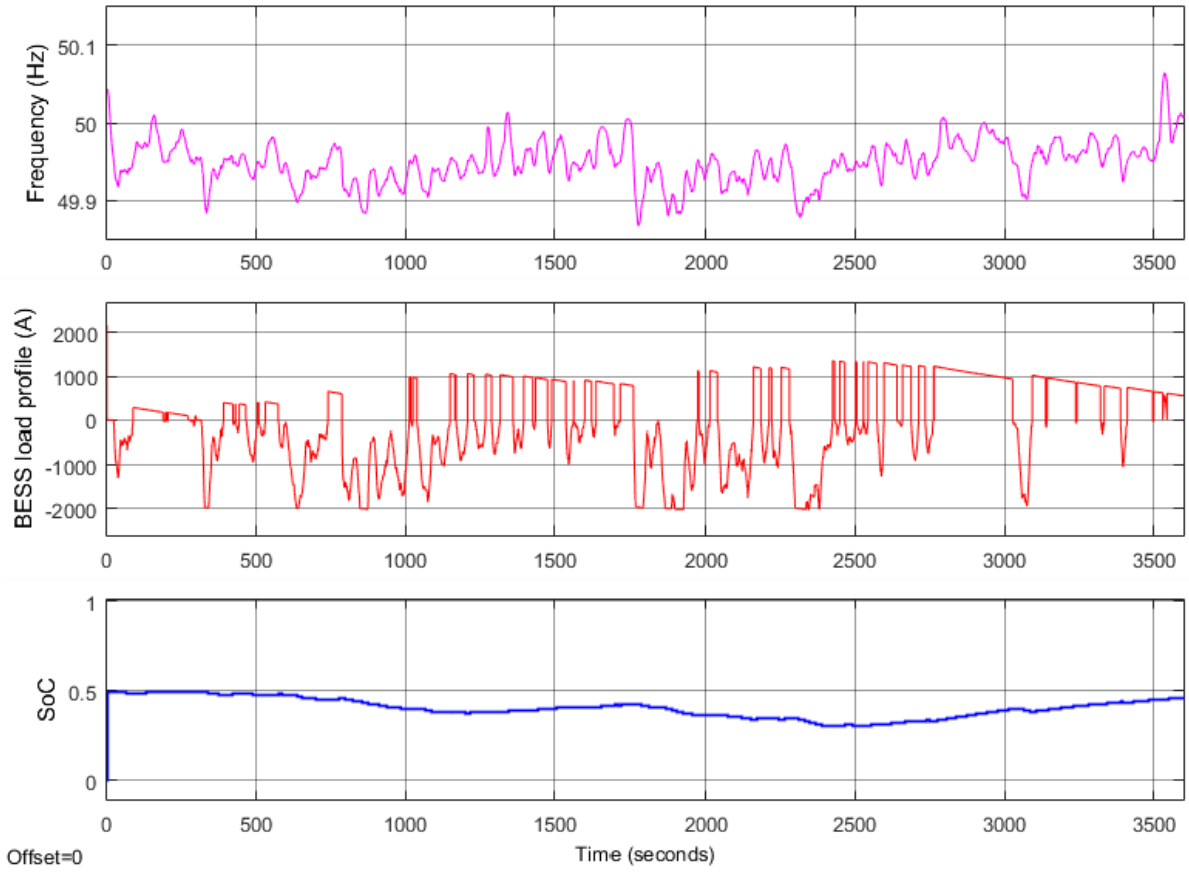

Figure 5.14. Control logic №5 operation (one hour).

The described control logics were implemented in the form of controller blocks that use frequency data and SoC as inputs and gives current charge or discharge signal to BESS model. The layout of developed controller block set in Simulink with control logic №5 can be found in Appendix VI.

5.2.2 BESS dimensioning and the end of life criterion

The dimensioning of the system is the core question for the overall economic feasibility of the BESS. Currently, there is an ongoing enactment process of the new ENTSO-E Network Code (NC) on Load-Frequency Control and Reserves (LFCR) which will introduce specific requirements for energy constrained units (ENTSO-E 2013). Right now the project is passing the approval stage, and it is expected that new code will enter into force in 2017.

According to the draft version of Commission Regulation (2016) establishing a guideline on electricity transmission system operation, all TSOs of Continental Europe (CE) and Nordic synchronous areas shall develop a proposal concerning the minimum activation period to be ensured by FCR providers with limited energy reservoirs. The period determined shall not be greater than 30 or smaller than 15 minutes and shall take full account of the results of the cost–benefit analysis. In the case of frequency deviations that are smaller than a frequency deviation requiring full FCR activation, an equivalent length of time have to be ensured. An FCR providers with limited energy reservoirs should also ensure the recovery of the energy reservoirs in the positive or negative directions at latest within 2 hours after the end of the alert state.

The reason why all TSOs should develop a proposal based on the results of the cost–benefit analysis, is because there are two points of view. As an explanation for the "30 minutes" requirement ENTSO-E (2013) claims that it is based on statistical analysis of frequency deviation patterns and is considered as a compromise between continuous availability and energy reservoir exhaustion risk. On the other hand, many stakeholders are concerned that the "30 minutes" requirement will bring negative effects. They suppose that in the first place it will dramatically increase the cost on the part of FCR provider. Secondly, it could also increase the cost of FCR procurement and the cost of electricity in the European Union since it will limit the potential amount of providers.

Another parameter that influences the investment profitability of BESS is the batteries EoL principle. First of all, there is no determined or prescribed criterion for each application. Usually, the value of 80% is used, which means that battery lost 20% of initial nominal capacity. However, in practice, the effective EoL capacity value might differ from commonly acceptable. For example, operating the BESS until 60% of capacity will limit the maximum bidding power as time goes by and reduce the income, but the time period between the investments in new batteries will increase.

In conclusion, the simulations were performed for a range of capacity time period requirements namely 15, 20, 25 and 30 minutes, with EoL of 80%, 70% and 60% in each examined case. The utilized control logic is justified after comparison in section 5.4.1.

5.3 Methodology

In this section, the methodology used to compare different BESS control strategies and other parameters based on the lifetime estimation and investment profitability is explained.

5.3.1 Lifetime estimation

The model itself does not predict the lifetime of the system; it can only calculate degradation amount during the simulation and set initial SoH. The simulation of several years' time is not an adequate way to get lifetime value because it will take too much time and memory. One month was assumed to be a sufficiently representative period of time. Therefore, the lifetime of the BESS was estimated by fitting the total capacity loss curve with power function and extrapolating it. The example of lifetime estimation process for control logic №1 is presented in Figure 5.15.

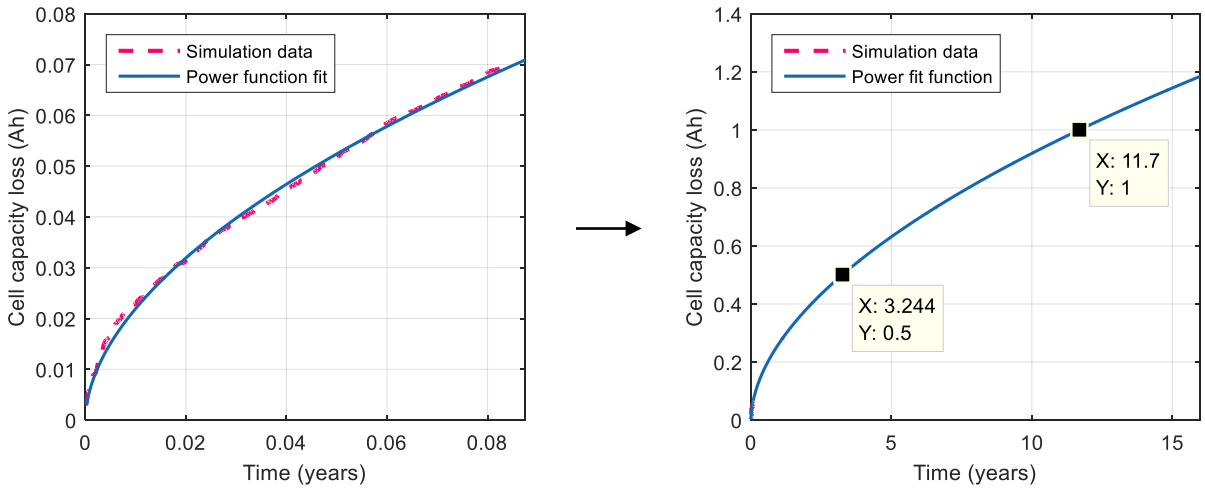

Figure 5.15. BESS lifetime estimation process (Q_{nom}=2.5 Ah, consequently 20% = 0.5 Ah, 40% = 1 Ah).

5.3.2 Assessment of net present value

Economic feasibility of an investment can be estimated by calculating net present value (NPV) as shown in Equation 5.6.

$$NPV = \sum_{i=1}^{n} \frac{C_t}{(1+r)^t} - C_0 \tag{5.6}$$

NPV = net present value [EUR]
C_t = cash flow [EUR]
C_0 = initial investment [EUR]
r = discount rate
t = number of cash flow year
n = number of years for analysis

In actuality, the installed costs of BESS comprises several components. Besides the batteries, the system must include power conditioning and transformation equipment, interfaces and controls, physical housing, cooling system and other necessary equipment. In addition, the project engineering, installation, operations and maintenance costs should be considered too. Therefore, the reported costs of energy storage are only estimates. GTM Research (2016) reports at year-end 2015 a system price of large-scale lithium-ion BESS within an estimated range of 700 - 1200 $/kWh. For the following NPV assessment, the installation price of 900 EUR/kWh were assumed.

Annual income is based on a yearly agreement with Fingrid for providing FCR-N service. The capacity fee in 2016 is 17.42 €/MW,h and assumed to be the same for the following years. The reserve plans are made for 24 h every day, so total annual time is 8760 h. The fines for unavailability are calculated in accordance with Fingrid (2016) rules: *"Reserve Holder shall pay Fingrid 50 per cent of the above price, in other words, 8.71 €/MW,h, in compensation for capacity not supplied."* As mentioned before, the remaining capacity of the BESS is gradually fading, and so the maximum bidding power is reducing. Since the agreement is concluded at the

beginning of the year, to ensure its' obligations at the end of the year the FCR-N provider should make a contract for volume expected by the end of the year.

The investment profitability was calculated for a period of estimated lifetime with a discount rate of 5%. The example of cash flows and NPV assessment for 1.6 MW / 1 MWh BESS with 60% EOL criterion and control logic №1 employed is shown in Table 5.2 and Figure 5.16.

Table 5.2. BESS cash flows and NPV calculation.

Year	Remained capacity, MWh	Max bidding power, MW	Installed costs, EUR	Income, EUR	Penalty costs, EUR	Cash flow, EUR	Present value factor	Present value of cash flow, EUR	Cumulative NPV, EUR
0	1.00	1.60	-900 000	0	0	-900 000	100%	-900 000	-900 000
1	0.89	1.43	0	215 202	-1 592	213 611	95%	203 439	-696 561
2	0.85	1.35	0	203 623	-1 506	202 117	91%	183 326	-513 235
3	0.81	1.29	0	194 542	-1 439	193 103	86%	166 810	-346 425
4	0.78	1.24	0	186 779	-1 381	185 398	82%	152 527	-193 898
5	0.75	1.20	0	179 869	-1 330	178 539	78%	139 890	-54 008
6	0.72	1.15	0	173 571	-1 284	172 287	75%	128 563	74 556
7	0.70	1.12	0	167 739	-1 241	166 499	71%	118 328	192 883
8	0.67	1.08	0	162 280	-1 200	161 079	68%	109 025	301 908
9	0.65	1.04	0	157 126	-1 162	155 964	64%	100 535	402 444
10	0.63	1.01	0	152 229	-1 126	151 103	61%	92 764	495 208
11	0.61	0.98	0	147 552	-1 091	146 461	58%	85 633	580 840
11.7	0.60	0.96	0	101 076	-748	100 328	57%	56 690	**637 530**

The total amount of energy throughput is 2597.72 MWh, and price of electricity is 40 EUR/MWh with battery efficiency 95%, then possible losses can be estimated in Equation 5.7. The value of losses is too small compared to NPV, so it can be neglected.

$$C_{loss} = V_{BESS} \cdot Ah_{th} \cdot c_{loss} \cdot \eta = 825 \cdot 3148755 \cdot 40 \cdot 10^{-6} \cdot 0.05 = 5195.5 \text{ EUR} \quad (5.7)$$

C_e = loss due to efficiency [EUR]

c_e = electricity price [EUR/MWh]

η = battery efficiency [%]

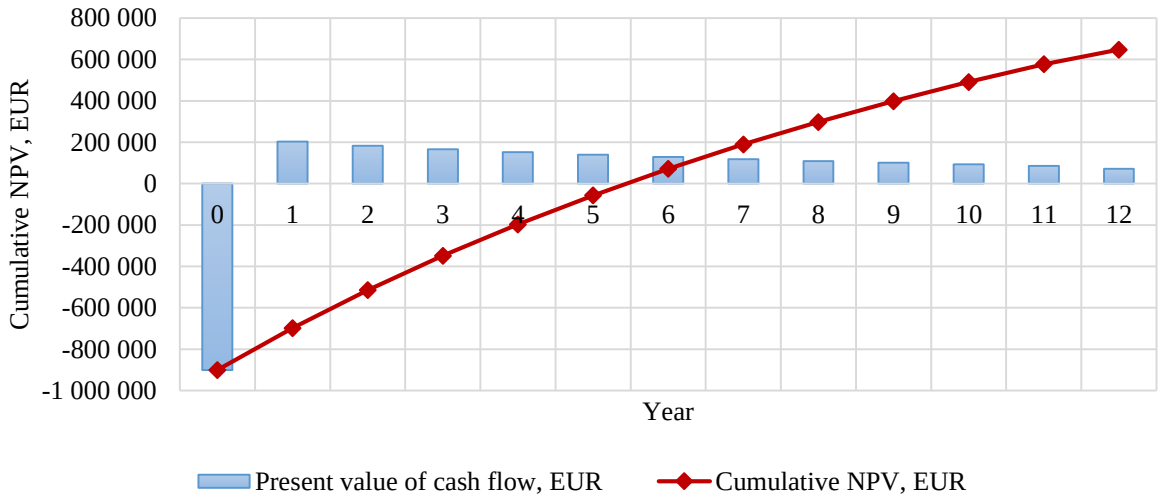

Figure 5.16. BESS present values graph.

5.4 Simulation results

Five control logics described above were simulated using the real frequency data profile of March 2016 measured at 400 kV substations at different locations in Finland, with 1 second sample time. The rated power and energy capacity of the BESS was set to 1.6 MW and 1 MWh consequently. The ambient temperature of the batteries assumed to be 20°C.

5.4.1 Comparison of control logics

Figure 5.17 shows the resulting SoC graphs of the BESS during simulations, and Figure 5.18 shows the evolution of cell capacity loss curves for different control logics.

The strategies worked as expected except №2 and №3. The capacity loss of strategy without a dead-band is smaller than with a ±0.01 Hz dead-band. That can be explained due to the longer idling periods in control strategy №3 and can be seen on the SoC graphs. Notwithstanding the degradation rates, control logics №2 and №3 activate the BESS too often and therefore have problems with the frequent reaching of the SoC limits which calls into question the applicability

of such strategies. It means that reduction of the dead-band will have a huge effect on BESS sizing and overall profitability unless the compensation payments will be introduced.

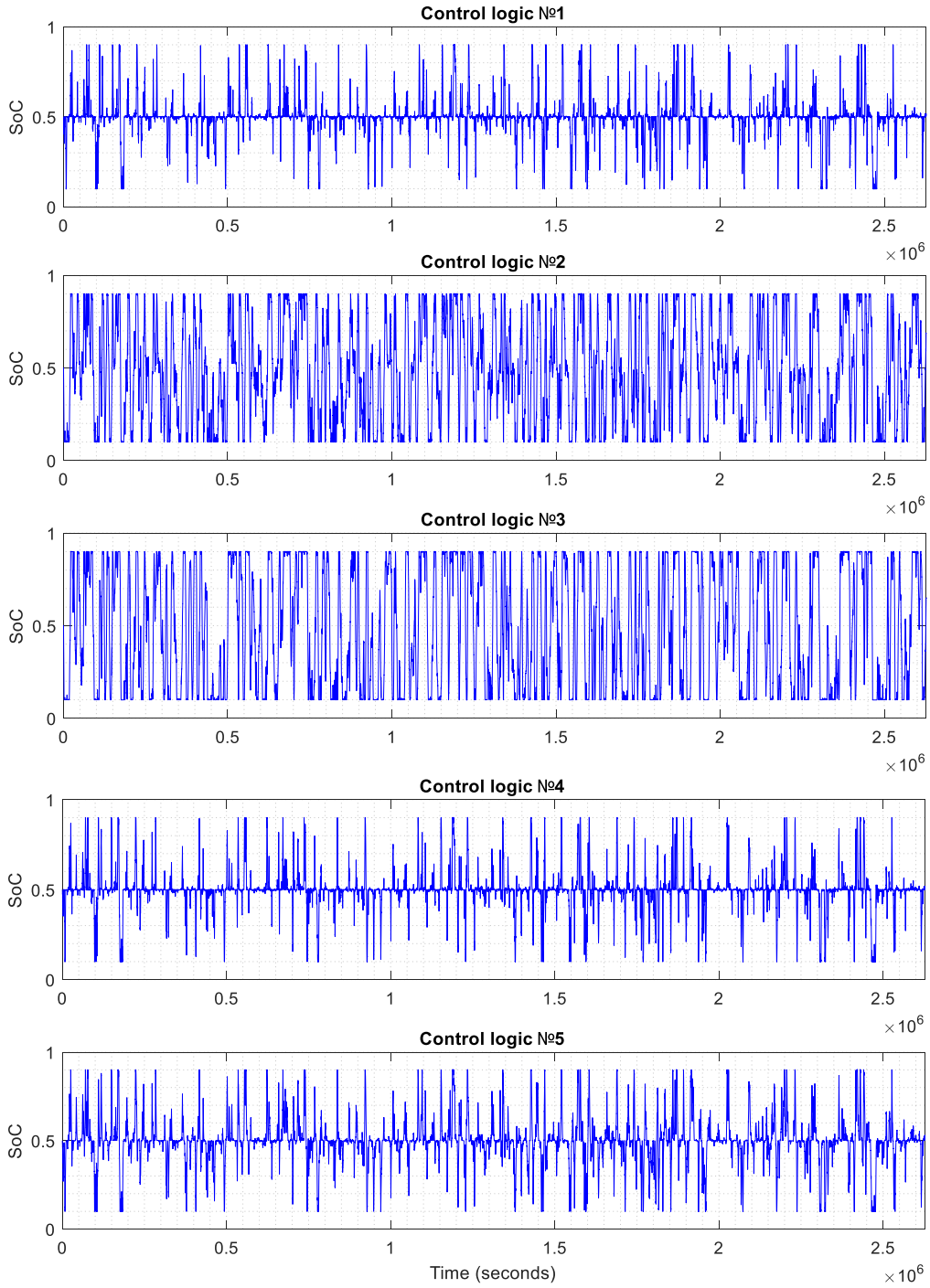

Figure 5.17. SoC simulation results for different control logics (one month period).

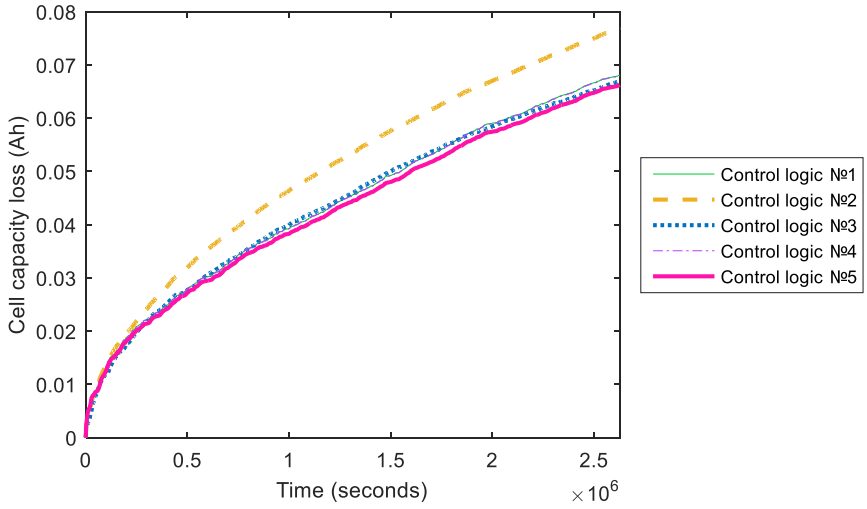

Figure 5.18. Cell capacity loss simulation results for different control logics.

The lifetime until 80% SoH and corresponding NPV of BESS are presented in Table 5.3.

Table 5.3. Results and comparison of the control logics.

Control logic	Lifetime, years	SoC saturation idling time per month, h	Net present value, EUR
№1	3.244	10.64	-306 617
№2	2.446	132.82	-563 533
№3	3.562	254.11	-583 298
№4	3.25	10.73	-305 692
№5	3.37	12.97	-287 488

The suggested 2 seconds “ignoring-delay” approach in control strategy №4 provided only 925 EUR gain of NPV. Such a slight difference cannot be considered as a clear improvement and therefore it will not be utilized in further simulations.

Control logic №1 fulfills its function without a problem, but simplified recovery strategy leads to shorter lifetime compared to smooth recovery in control logics №5. The cause of larger degradation in logic №1 is because SoC level recovers too fast even if the deviation is not so huge. Although slower recovery increases the risk of BESS exhaustion and leads to longer SoC

saturation idling time, the benefits from prolonged lifetime is more valuable for the BESS owner than the cost of unavailability fines.

In conclusion, the control logic №5 have shown the highest NPV in the analysis among other candidates and hence it will be employed in the further analysis.

5.4.2 Sensitivity analysis

The requirement obligating FCR providing a unit to activate full capacity for a specific period of time is basically a way to limit the power-to-energy ratio (MW/MWh rating). For following cases, the energy capacity of the BESS assumed to stays the same as 1 MWh. By substituting the different time period in Equation 5.1, the maximum bidding powers of 15, 20, 25 and 30 minutes' requirements are 1.6 MW, 1.2 MW, 0.96 MW and 0.8 MW, consequently.

The simulations were performed using control logic №5 and EoL range 50-80%. Results are presented in Table 5.4. NPV and cash flows calculations for the most representative cases can be found in Appendix VII.

Table 5.4. Lifetime and cost-benefit estimation of simulated cases.

Full activation time period requirement, min	Maximum bidding power, MW	SoC saturation idling time per month, h	EoL, %	Lifetime, years	Net present value, EUR
15	1.6	12.97	80	3.37	-287 488
		13.05	70	7.12	207 324
		13.09	60	12.13	673 281
		13.14	50	18.28	1 043 467
20	1.2	7.69	80	4.11	-340 634
		7.73	70	8.65	92 736
		7.75	60	14.67	479 251
		7.80	50	22.08	770 554
25	0.96	4.62	80	4.73	-385 814
		4.64	70	9.90	-3 657
		4.67	60	16.73	318 585
		4.72	50	25.07	552 587
30	0.8	3.05	80	5.32	-423 374
		3.06	70	11.09	-83 497
		3.09	60	18.67	198 069
		3.13	50	27.91	391 671

To have a better visual understanding of the dependencies, the surface plot of NPV with two variables is presented in Figure 5.19.

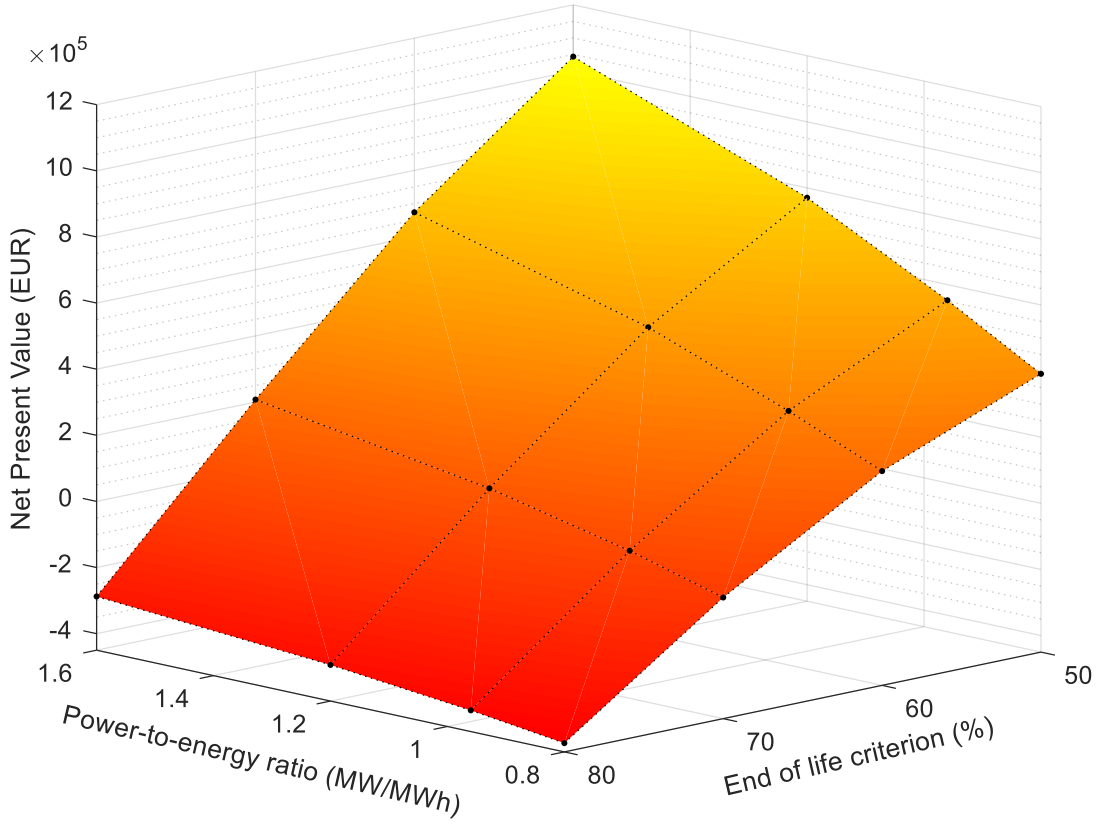

Figure 5.19. NPV surface plot with power-to-energy and EoL variables.

Firstly, there is a clear pattern of how EoL criterion is affecting the NPV of the BESS project. The dependency is non-linear, with more NPV for lower EoL principle. Indeed, the specific of frequency regulation unit is that it can make new contracts every year for the smaller amount of reserve power. However, in real life BESS cannot be employed until it will lose all 100% of the capacity. Naumann et al. (2015) explain that at a certain point of a lifetime, new nonlinear aging mechanisms can be revealed. The results would be a strong decrease of capacity and a strong increase of internal resistance, i.e. decrease of battery efficiency. That phenomenon greatly depends on cell chemistries and prior use conditions. Currently, there is no adequate

understanding of how the second-life batteries (SoH < 80%) should be operated correctly. Now it is one of the questions, which has drawn the attention of the scientific community because using second-life batteries in unassuming applications can significantly reduce the costs. In the meantime, this thesis assumes that operating batteries under 60% of nominal capacity are not possible.

Secondly, the investment profitability is decreasing with the lower power-to-energy ratio, i.e. raising the level of full power active time requirement will negatively affect the value of energy storages on FCR markets. Nevertheless, the model demonstrated a positive NPV for a quite big area of cases. Figure 5.20 shows how the surface plot results from Figure 5.19 represented in the way so it can be seen what combination of variables will produce positive NPV. It goes without saying that economics of the system depends on many other factors and the transition between “profitable” and “not profitable” should rather be perceived as smooth.

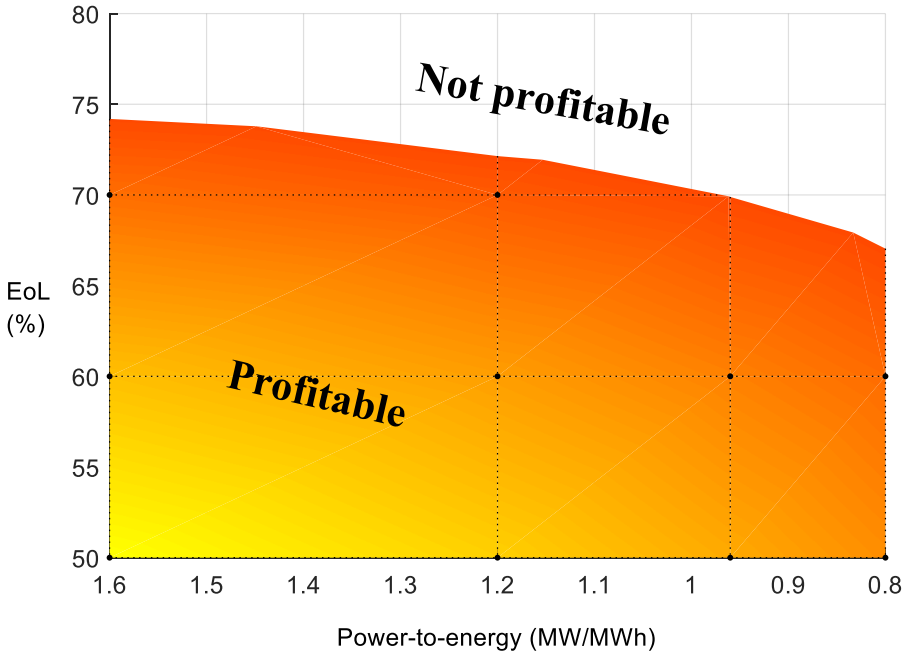

Figure 5.20. Gradient area of the positive NPV estimation.

As it was mentioned in Section 5.2.2, many stakeholders have an opinion that the doubling of full activation time requirement will severely decrease the profitability of limited energy storages. Whereas the results of the conducted simulations show that NPV of cases with 80% EoL, which is probably the most common approach, have a quite small impact from power-to-energy ratio change. On the other hand, the influence of EoL criterion on NPV is rather big.

At last, the price of the lithium-ion batteries has a direct impact on the NPV. Many academic sources in the past claimed economic unreasonableness due to high prices. After a long price development process, it seems that prices reached the level when it can bring profits with certain assumptions. Figure 5.21 and 5.22 show the relationship between system installed costs and NPV of BESS ranging from 15 min to 30 min requirements duration for 80% and 60% EoL criterion respectively.

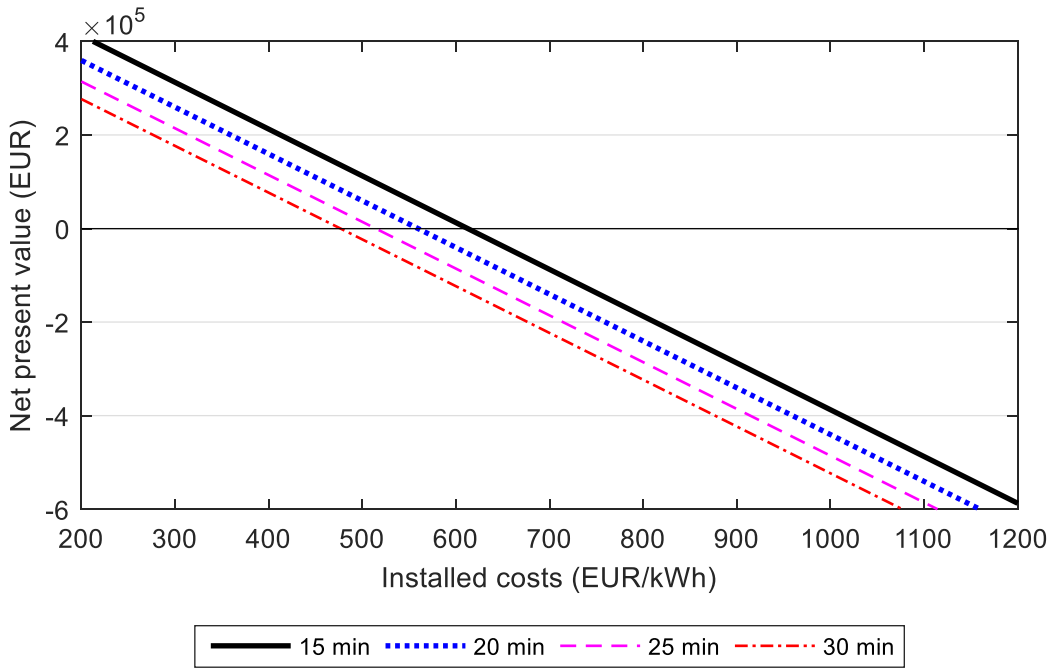

Figure 5.21. NPV sensitivity analysis with the variable system installed price (80% EoL).

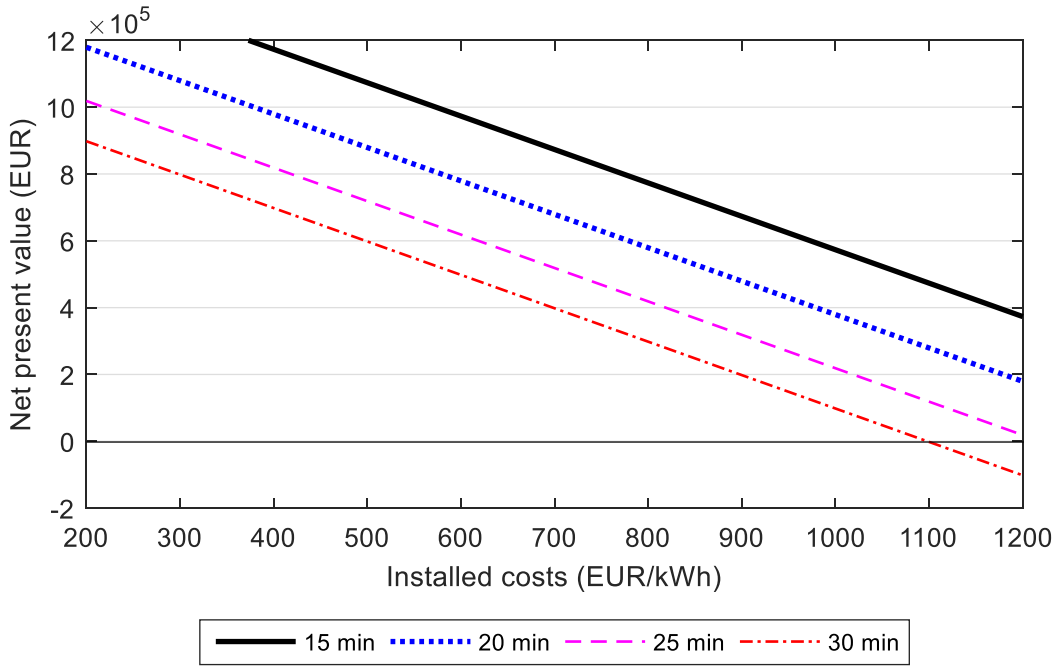

Figure 5.22. NPV sensitivity analysis with the variable system installed price (60% EoL).

It can be observed that, based on developed model and all other considerations with common 80% EoL approach, it would require further price reduction approximately in half. While the 60% EoL criterion is theoretically justifying the BESS with the current price values.

6 CONCLUSION

The presented study has investigated technical and economic aspects of lithium-ion BESS in grid-scale applications from the point of view of BESS owner (operator). In general terms, it required a comprehensive analysis of literature, employment, and development of the models, as well as relevant methodologies.

Lithium-ion technologies are considered as viable solutions for many high power or high energy applications and represent a broad family of chemistries each with their own features and properties. This thesis particularly justified and considered LFP cells type in conjunction with selected application. One of the main challenges of working with electrochemical cells is the appropriate lifetime estimation and understanding the phenomena behind the aging processes. It becomes essentially vital in order to form a link from operating conditions to lifetime and eventually the economic feasibility of a BESS. This thesis provided the literature review with necessary up-to-date background information about lithium-ion cells, including the main features, development progress, and aging mechanisms. An adequate LFP cell lifetime model was selected as a result of the publically available models comparison.

On the next stage, the study developed a practical lithium-ion BESS model with the ability to describe dynamic performance behavior and to estimate degradation effects. The model was implemented in Matlab/Simulink modeling environment. It was found to perform its functions accurately and effectively. To demonstrate the use of the developed model, it was employed for simulation of primary frequency regulation provided by BESS.

The feasibility assessment of providing the frequency regulation using BESS in Finland was selected as a study case. The relevance and demand of such a service in Nordic countries were emphasized. To perform a BESS control management based on frequency input data, five different control logics were implemented and described in details. The control logics comparison found the strategy proposed in this thesis to have advantages over the traditional fixed droop. The questions related to the application such as BESS dimensioning, EoL criterion,

overall system costs, lifetime estimation and economic assessment were discussed. Results from the techno-economic analysis revealed profitable and implementable system cases.

6.1 Future work

There are many possibilities for further improvement and to continue the presented research. One of the improvements can refer to developing more advanced lifetime model, which will consider more stress factors or increase the overall estimation accuracy. Regarding the equivalent circuit-based model, the coulumbic counting SoC estimation method can be improved by more advanced methods. The resistance increase and efficiency of the battery can be also taken into account.

The control strategies for BESS operated at frequency regulation can be improved, or optimized or even invented the novel approaches. The more advanced and accurate economic evaluation methods can be utilized. Other state markets can be investigated as well. The BESS benefits increase by combining different provided services and how it influence on the service quality and requirements is very interesting and relevant topic. Also mentioned in the text, the potential of utilizing second-life batteries could bring significant costs decrease, but it needs to be also investigated from the technical point of view.

It would be interesting to investigate the case feasibility of BESS providing frequency regulation at conventional power plants. For example in Russia, all power plants have to participate in frequency regulation, except some nuclear plants. Participating in frequency regulation means certain units are not working with optimal efficiency, therefore losing possible profits. Instead, power plants could meet the regulation commitments with the help of BESS while operating the generator units with optimal cost-efficient level.

REFERENCES

A123 LiFePO4 cylindrical cell [Online]. Available: http://www.a123systems.com/LiFePO4-battery-cell.htm

Barmsnes Kjell A. 2014. The Nordic Balancing Market, experiences and future developments.

Brodd Ralph J. as editor. 2013. Batteries for Sustainability. Selected Entries from the Encyclopedia of Sustainability Science and Technology. Springer-Verlag New York. ISBN 978-1-4614-5791-6

De-Leon Shmuel. 2010. High Power Rechargeable Lithium Battery Market. IFCBC Meeting.

Ding Yi et al. 2012. Parameterization and Validation of an Integrated Electro-thermal LFP Battery Model. ASME 2012 5th Annual Dynamic Systems and Control Conference. 11 pages.

Dinger A. et al. 2010. Batteries for Electric Cars. Challenges, Opportunities, and the Outlook to 2020. The Boston Consulting Group.

ENTSO-E. Exchange of balancing services international workshop Jan 2011.

Eyer Jim, Corey Garth. 2010. Energy Storage for the Electricity Grid: Benefits and Market Potential Assessment Guide. Sandia report. Available: http://www.sandia.gov/ess/publications/SAND2010-0815.pdf

Fang W., Kwon O.J., and Wang C.Y. 2010. Electrochemical-thermal modeling of automotive Li-Ion batteries and experimental validation using a three-electrode cell. Int. J. Energy Res. vol. 34, pp. 107-115.

Fares Leo Robert. 2015. A Framework to Model and Optimize the Operation of Lithium-Ion Energy Storage in Electricity Markets, and an Assessment of Lithium-Ion Energy Storage in

Texas. Doctoral thesis. Faculty of the Graduate School of The University of Texas at Austin. 221 pages.

Feng Xue, Gooi Hoay Beng, Chen Shuaixun. 2015. Capacity fade-based energy management for lithium-ion batteries used in PV systems. Electric Power Systems Research, vol. 129, pp. 150–159.

Fingrid. 1 January 2016a. Application instruction for the maintenance of frequency controlled reserves. Appendix 2 to the Yearly Agreement and Yearly Market Agreement for Frequency Controlled Normal Operation Reserve and Frequency Controlled Disturbance Reserve.

Fingrid. 2016b. Yearly Agreement No. XX/2016 For Frequency Controlled Normal Operation Reserve and Frequency Controlled Disturbance Reserve.

Fingrid. 2016c. [Online]. Available: http://www.fingrid.fi/en/company/Pages/default.aspx

Fitzgerald Garrett et al. 2015. The Economics of Battery Energy Storage: How multi-use, customer-sited batteries deliver the most services and value to customers and the grid. Rocky Mountain Institute. Available: http://www.rmi.org/electricity_battery_value

Goodenough J.B. et al. 1980. LixCoO2 (0<x<-1): A new cathode material for batteries of high energy density. Materials Research Bulletin vol. 15, issue 6, pp. 783-789.

Grolleau Sébastien et al. 2014. Calendar aging of commercial graphite/$LiFePO_4$ cell - Predicting capacity fade under time dependent storage conditions. Journal of Power Sources, vol. 255, pp. 450-458.

GTM Research and the Energy Storage Association (ESA). 2016. U.S. Energy Storage Monitor: 2015 Year in Review Executive Summary. Available: https://forms.greentechmedia.com/Extranet/95679/forms.aspx?msgid=074fe914-6e56-4b44-8959-8dc46ab58ea6&LinkID=CH00095679eR00000420AD&Source=sidebar

Guenther Clemens et al. 2013. Model-based investigation of electric vehicle battery aging by means of vehicle-to-grid scenario simulations. Journal of Power Sources, vol. 239, pp. 604-610.

Gulbinska Malgorzata K. as editor. 2014. Lithium-ion Battery Materials and Engineering. Current Topics and Problems from the Manufacturing Perspective. Springer-Verlag. ISBN 978-1-4471-6548-4.

Huria Tarun et al. 2012. High Fidelity Electrical Model with Thermal Dependence for Characterization and Simulation of High Power Lithium Battery Cells. IEEE. 8 pages.

Idaho National Laboratory, September 2010. “Battery Test Manual for Plug-In Hybrid Electric Vehicles”.

International Energy Agency. 2014. Technology Roadmap: Energy storage. [Online]. Available: https://www.iea.org/publications/freepublications/publication/technology-roadmap-energy-storage-.html

Kassem M. et al. 2012. Calendar aging of a graphite/$LiFePO_4$ cell. Journal of Power Sources, vol. 208, pp. 296–305.

LAZARD'S Levelized cost of storage analyis - version 1.0. 2015. [Online]. Available: https://www.lazard.com/media/2391/lazards-levelized-cost-of-storage-analysis-10.pdf

Li Xinran et al. 2014. Modeling and Control Strategy of Battery Energy Storage System for Primary Frequency Regulation. International Conference on Power System Technology (POWERCON 2014).

Li Dongjiang et al. 2016. Degradation Mechanisms of C6/LiFePO4 Batteries: Experimental Analyses of Calendar Aging. Electrochimica Acta, vol. 190, pp. 1124–1133.

Lin Cheng et al. 2015. Aging Mechanisms of Electrode Materials in Lithium-Ion Batteries for Electric Vehicles. Journal of Chemistry, Volume 2015, Article ID 104673, 11 pages.

Liu Ping et al. 2010. Aging Mechanisms of LiFePO4 Batteries Deduced by Electrochemical and Structural Analyses. Journal of The Electrochemical Society, vol. 157 pp. 499-507.

Luo Xing et al. 2015. Overview of current development in electrical energy storage technologies and the application potential in power system operation. Applied Energy, vol. 137, pp. 511-536.

Mahlia T. M. I. et al. 2014. A review of available methods and development on energy storage; technology update. Renewable and Sustainable Energy Reviews vol. 33, pp. 532–545.

Marano et al. 2009. Lithium-ion batteries life estimation for plug-in hybrid electric vehicles. Vehicle Power and Propulsion Conference. IEEE, pp. 536-543

MIT Electric Vehicle Team, 2008. “A guide to understanding battery specifications." [Online]. Available: http://web.mit.edu/evt/summary battery specications.pdf

Nejad S., Gladwin D.T., Stone D.A.. 2016. A systematic review of lumped-parameter equivalent circuit models for real-time estimation of lithium-ion battery states. Journal of Power Sources, vol. 316, pp. 183-196.

Nitta Naoki et al. 2015. Li-ion battery materials: present and future. Materials Today, vol. 18, number 5, pp. 252-264.

Omar Noshin et al. 2014. Lithium iron phosphate based battery – Assessment of the aging parameters and development of cycle life model. Applied Energy, vol. 113, pp. 1575–1585.

Oudalov Alexandre, Chartouni Daniel, and Ohler Christian. 2007. Optimizing a Battery Energy Storage System for Primary Frequency Control. IEEE Transactions on power systems, vol. 22, no. 3, pp. 1259-1266.

Padhi A. K., Nanjundaswamy K. S. and Goodenough J. B.. 1997. Phospho-olivines as Positive-Electrode Materials for Rechargeable Lithium Batteries. J. Electrochem. Soc. vol. 144, issue 4, pp. 1188-1194.

Prosini Pier Paolo. 2011. Iron Phosphate Materials as Cathodes for Lithium Batteries. The Use of Environmentally Friendly Iron in Lithium Batteries. Springer-Verlag. ISBN 978-0-85729-745-7.

Sarasketa-Zabala E. et al. 2014. Cycle ageing analysis of a $LiFePO_4$/graphite cell with dynamic model validations: Towards realistic lifetime predictions. Journal of Power Sources, vol. 275, pp. 573-587.

Sauer Dirk Uwe. 2012. Lithium-Ion Batteries Technology, Performance, Aging Mechanism and Performance Modeling. Lecture slides from Industrial/Ph.D. course @ Aalborg University.

Schlasza Christian et al. 2014. Review on the aging mechanisms in Li-ion batteries for electric vehicles based on the FMEA method. Transportation Electrification Conference and Expo (ITEC).

Schmalstieg Johannes et al. 2013. From Accelerated Aging Tests to a Lifetime Prediction Model: Analyzing Lithium-Ion Batteries. EVS27 International Battery, Hybrid and Fuel Cell Electric Vehicle Symposium.

Skea J., Nishioka S. 2008. Policies and practices for a low-carbon society. Modelling long-term scenarios for low carbon societies. Climate Policy, vol. 8, pp. 5-16.

Swierczynski Maciej et al. 2014. Investigation on the Self-discharge of the LiFePO4/C Nanophosphate Battery Chemistry at Different Conditions. ITEC Asia-Pacific. 6 pages.

Swierczynski Maciej et al. 2015a. Lifetime and economic analyses of lithium-ion batteries for balancing wind power forecast error. Int. J. Energy, vol. 39, pp. 760–770.

Swierczynski Maciej et al. 2015b. Lifetime Estimation of the Nanophosphate LiFePO4/C Battery Chemistry Used in Fully Electric Vehicles. IEEE Transactions on Industry Applications, vol. 51, no. 4, pp. 3453-3461.

The National Petroleum Council (NPC). 2013. Advancing technology for America's transportation future. Chapter 13 - Electric. pp. 1-69.

Walawalkar Rahul, Apt Jay, Mancini Rick. 2007. Economics of electric energy storage for energy arbitrage and regulation in New York. Energy Policy, vol. 35, issue 4, pp. 2558–2568.

Wang John et al. 2011. Cycle-life model for graphite-$LiFePO_4$ cells. Journal of Power Sources, vol. 196, pp. 3942–3948.

Weng Caihao, Sun Jing, Peng Huei. 2013. An Open-Circuit-Voltage Model Of Lithium-Ion Batteries For Effective Incremental Capacity Analysis. ASME 2013 Dynamic Systems and Control Conference. 8 pages.

Vetter J. et al. 2005. Ageing mechanisms in lithium-ion batteries. Journal of Power Sources, vol. 147, pp. 269–281.

Yoshino Akira. 2014. Development of the Lithium-Ion Battery and Recent Technological Trends. Lithium-Ion Batteries Advances and Applications, pp. 1-19.

Yuksel Tugce, Michalek Jeremy. 2012. Evaluation of the Effects of Thermal Management on Battery Life in Plug-in Hybrid Electric Vehicles.

Zhuang Weidong, Lu Shigang, Lu Huaquan. 2014. Progress in materials for lithium-ion power batteries. International Conference on Intelligent Green Building and Smart Grid (IGBSG).

Zidar Matija et al. 2016. Review of energy storage allocation in power distribution networks: applications, methods and future research. IET Gener. Transm. Distrib., vol. 10, iss. 3, pp. 645–652.

Appendix I. Battery cell terminology

Cell capacity

Nominal capacity (Q_{nom}) represents capacity labeled on cell specification by the manufacturer. Remaining capacity (Q_r) represents the accessible capacity of the cell. The remaining capacity of the new cell should be equal to nominal capacity. Faded capacity (Q_{loss}) represents capacity lost due to degradation.

State of health (SoH)

The term state of health (SoH) is used to describe the state of the cell between the beginning of life (BoL) and end of life (EoL). The value of 100% means the cell with full nominal capacity and value of 0% means the cell without the ability to store any energy.

State of charge (SoC)

The state of charge (SoC) indicates a percentage of active charge stored in the cell at certain moment of time

Cycle

In general, the cycle is described as a sequence of a discharge followed by a charge or vice versa. Full cycle indicates a complete discharging and charging event with 100% DoD (i.e. emptying and refilling the whole capacity). The term equivalent full cycle is defined by the amount of energy processed through the battery with any DoD swing divided by the nominal capacity.

Current rate (C-rate)

The C-rate is the current scaled to the nominal capacity of a cell stated by the manufacturer (MIT Electric Vehicle Team 2008, 1). A current discharge rate of 1C means that battery cell

will be discharged from SoC = 100% to SoC = 0% in 1 hour. For example, for a cell with a nominal capacity of 100 Ah, 1C current will be 100 A.

Open-Circuit Voltage (OCV)

The OCV of the cell is defined as the voltage between terminals in the state of electrochemical equilibrium with no load applied. The OCV strongly depends on the SoC at any moment of time.

Appendix II. Lithium-ion cell used in model development

Nanophosphate® High Power Lithium Ion Cell ANR26650m1-B

A123 SYSTEMS

KEY FEATURES AND BENEFITS

- Excellent abuse tolerance and superior cycle life from A123's patented Nanophosphate® lithium ion chemistry
- High power with over 2,600 W/kg and 5,800 W/L, 10 seconds, 50% SOC
- High usable energy over a wide state of charge (SOC) range

ANR26650m1-B Cell Specifications	
Cell Dimensions (mm)	ø26 x 65
Cell Weight (g)	76
Cell Capacity (nominal/minimum, Ah)	2.5/2.4
Voltage (nominal, V)	3.3
Internal Impedance (1kHz AC typical, mΩ)	6
HPPC 10 Sec Discharge Pulse Power 50% SOC	200 W
Recommended Standard Charge Method	1C to 3.6V CCCV, 45 min
Recommended Fast Charge Method to 80% SOC	4C to 3.6V CC, 12 min
Maximum Continuous Discharge (A)	70
Maximum Pulse Discharge (10 seconds, A)	120
Cycle Life at 10C Discharge, 100% DOD	>1,000 cycles
Operating Temperature	-30°C to 55°C
Storage Temperature	-40°C to 60°C

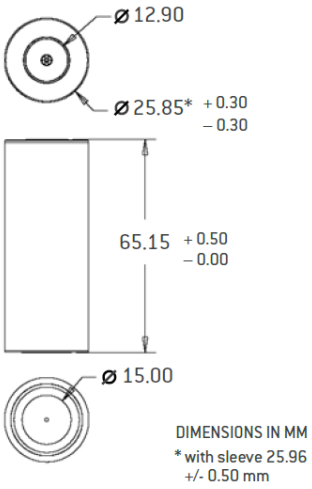

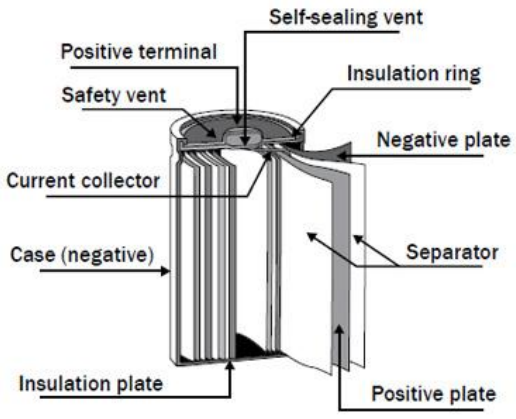

Appendix III. Calendar degradation models additional data

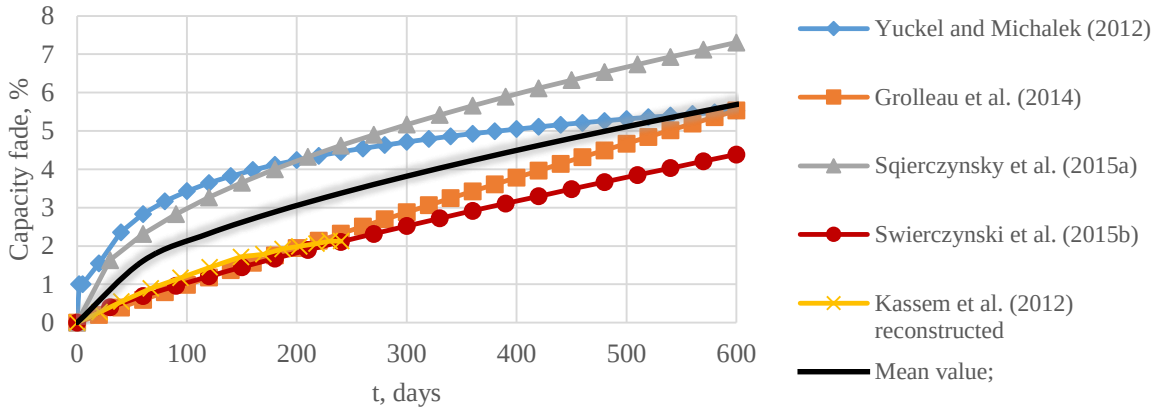

Figure C.1. Calendar degradation data acquired from examined models and sources (T=30°C, 50% SoC).

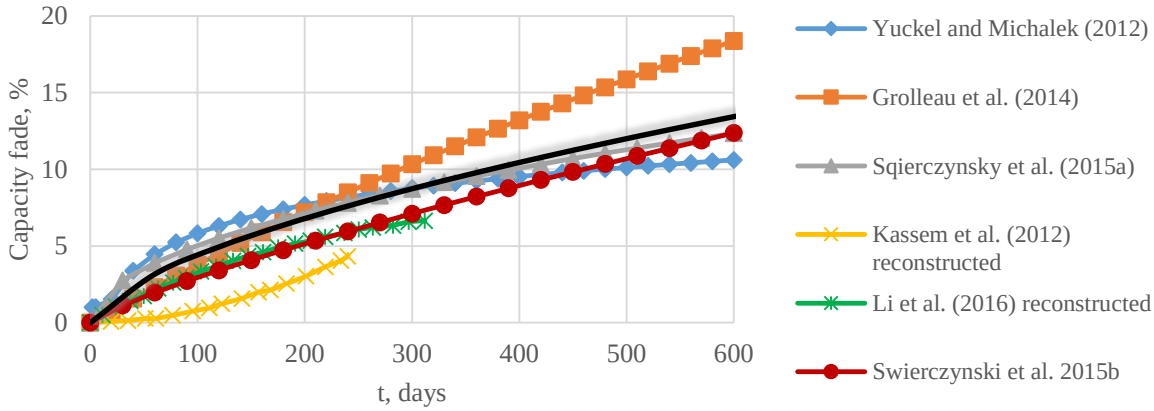

Figure C.2. Calendar degradation data acquired from examined models and sources (T=45°C, 50% SoC).

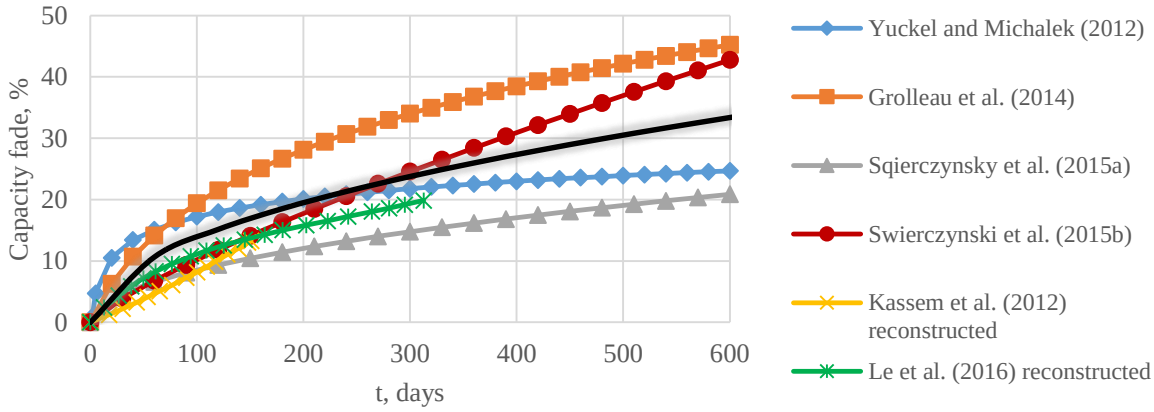

Figure C.3. Calendar degradation data acquired from examined models and sources (T=60°C, 50% SoC).

Appendix IV. Model initialization file

```
% Initialization file for ssc_lithium_cell_2RC_BESS
% Parameters of A123 system's ANR26650 LiFePO4/graphite cell
%
% Copyright 2012 The MathWorks, Inc.
% With upgrades from Ignatev Eduard (edd-ign@mail.ru)

%% BESS size

% Number of parallel strings
N_par = 485; % 485 for 1212.5 Ah (1000 kWh) total capacity

% Number of cells in one string
N_str = 250; % 250 for 825 V nominal voltage

% FCR-N bidding power
P_fcr = 1.6e6; % W

%% Initial Conditions

% State of Health
SOH = 1; %0..1

% Charge deficit
Qe_init = 1.25; %Ampere*hours

% Ambient Temperature
T_init = 20 + 273.15; %K

%% Lookup Table Breakpoints

SOC_LUT = [0 0.025 0.05 0.1 0.2 0.3 0.4 0.5 0.6 0.7 0.8 0.9 0.95 0.975 1]';
Temperature_LUT = [15 25 35 45] + 273.15;

%% Em Branch Properties (OCV, Capacity)

% Nominal battery capacity
Capacity_nom = [
    2.50  2.50  2.50  2.50]; %Ampere*hours

Capacity_LUT = Capacity_nom .* SOH; %Ampere*hours

% Em open-circuit voltage vs SOC rows and T columns
Em_LUT = [
    2.730  2.730  2.730  2.730
    2.933  2.933  2.933  2.933
    3.079  3.079  3.079  3.079
    3.204  3.204  3.204  3.204
    3.250  3.250  3.250  3.250
    3.283  3.283  3.283  3.283
```

```
    3.300  3.300  3.300  3.300
    3.306  3.306  3.306  3.306
    3.309  3.309  3.309  3.309
    3.322  3.322  3.322  3.322
    3.346  3.346  3.346  3.346
    3.351  3.351  3.351  3.351
    3.369  3.369  3.369  3.369
    3.414  3.414  3.414  3.414
    3.532  3.532  3.532  3.532
]; %Volts

%% Terminal Resistance Properties

% R0 resistance vs SOC rows and T columns
R0_LUT = [
    0.0134  0.0104  0.0090  0.0082
    0.0134  0.0104  0.0090  0.0082
    0.0134  0.0104  0.0090  0.0082
    0.0134  0.0104  0.0090  0.0082
    0.0134  0.0104  0.0090  0.0082
    0.0134  0.0104  0.0090  0.0082
    0.0134  0.0104  0.0090  0.0082
    0.0134  0.0104  0.0090  0.0082
    0.0134  0.0104  0.0090  0.0082
    0.0134  0.0104  0.0090  0.0082
    0.0134  0.0104  0.0090  0.0082
    0.0134  0.0104  0.0090  0.0082
    0.0134  0.0104  0.0090  0.0082
    0.0134  0.0104  0.0090  0.0082
    ]; %Ohms

%% RC Branch 1 Properties

% R1 Resistance vs SOC rows and T columns
R1_LUT = [
    0.0296  0.0181  0.0135  0.0111
    0.0296  0.0181  0.0135  0.0111
    0.0290  0.0180  0.0134  0.0109
    0.0279  0.0178  0.0131  0.0107
    0.0255  0.0172  0.0125  0.0097
    0.0233  0.0160  0.0115  0.0092
    0.0240  0.0179  0.0134  0.0100
    0.0233  0.0169  0.0122  0.0095
    0.0200  0.0141  0.0103  0.0082
    0.0184  0.0128  0.0100  0.0082
    0.0188  0.0146  0.0125  0.0103
    0.0204  0.0150  0.0114  0.0089
    0.0216  0.0151  0.0111  0.0086
    0.0223  0.0151  0.0110  0.0085
    0.0223  0.0151  0.0110  0.0085
    ]; %Ohms
```

```
% C1 Capacitance vs SOC rows and T columns
C1_LUT = [
      1076    1758    2616    3155
      1132    1796    2560    3080
      1182    1834    2522    3023
      1308    1877    2447    2911
      1527    1877    2241    2641
      1852    2172    2485    2710
      2078    2447    2760    2923
      2021    2253    2447    2579
      2003    2322    2648    2961
      2228    2673    3286    3474
      2479    3267    3668    3743
      2479    2804    2817    2873
      2479    2629    2648    2729
      2479    2566    2591    2685
      2479    2510    2560    2654
]; %Farads

% R2 Resistance vs SOC rows and T columns
R2_LUT = [
    0.1260  0.1079  0.0946  0.0830
    0.1133  0.0877  0.0830  0.0728
    0.1024  0.0774  0.0728  0.0628
    0.0752  0.0596  0.0503  0.0510
    0.0284  0.0221  0.0176  0.0167
    0.0247  0.0186  0.0133  0.0114
    0.0354  0.0212  0.0115  0.0086
    0.0240  0.0156  0.0106  0.0079
    0.0207  0.0141  0.0095  0.0076
    0.0422  0.0220  0.0181  0.0112
    0.0433  0.0258  0.0157  0.0107
    0.0245  0.0149  0.0099  0.0069
    0.0164  0.0099  0.0079  0.0059
    0.0112  0.0080  0.0072  0.0058
    0.0058  0.0064  0.0066  0.0058
    ]; %Ohms

% C2 Capacitance vs SOC rows and T columns
C2_LUT = [
       270     540     809    1619
      8633   11331   12140   12410
     16727   21313   22662   22122
     31025   38040   39658   34532
     49101   65018   83633   98471
     45594   72572   99550  119245
     29946   41547   75000  132734
     48022   70414  102788  133004
     61781   84982  121133  141097
     36421   46403   47482   59353
     27248   35881   55036   76079
     40737   65288   89838  114119
```

```
     47482   82824  109802  135162
     52068   91996  123291  146493
     60701  102518  144604  159442
    ]; %Farads


%% Thermal Properties

% Cell dimensions and sizes
%cell_thickness = 0.0084; %m
cell_width = 0.026; %m
cell_height = 0.065; %m
cell_radius = 0.013; %m

% Cell surface area
% cell_area = 2 * (...
%     cell_thickness * cell_width +...
%     cell_thickness * cell_height +...
%     cell_width * cell_height); %m^2
cell_area = 2 * 3.14 * cell_height * cell_radius; %m^2

% Cell volume
cell_volume = 3.14 * cell_height * cell_radius^2; %m^3

% Cell mass
cell_mass = 0.076; %kg

% Volumetric heat capacity
% assumes uniform heat capacity throughout the cell
% ref: J. Electrochemical Society 158 (8) A955-A969 (2011) pA962
cell_rho_Cp = 2.04E6; %J/m3/K

% Specific Heat
cell_Cp_heat = cell_rho_Cp * cell_volume; %J/kg/K

% Convective heat transfer coefficient
% For natural convection this number should be in the range of 5 to 25
h_conv = 20; %W/m^2/K
```

Appendix V. Degradation functions contents

```
function Q_cyc = fcn(Ah_th, T, Capacity_nom)
%#codegen

%Initial capacity [Ampere*hours]
Cap_init = Capacity_nom(2);

%Calendar degradation function [Ampere*hours]
Q_cyc = 0.00024 * exp(0.02717 * (T + 273.15)) * 0.02982 ...
* sqrt(abs(Ah_th) * 100 / (3600 * 2 * Cap_init)) *
Cap_init/100;
```

```
function Q_cal = fcn(t, T, SOC, Capacity_nom)
%#codegen

%Initial capacity [Ampere*hours]
Cap_init = Capacity_nom(2);

%Calendar degradation function [Ampere*hours]
Q_cal = (0.019 * (abs(SOC) * 100)^0.823 + 0.5195) ...
* (3.258 * 10^(-9) * abs(T)^5.087 + 0.295) ...
* (t * 3.8 * 10^(-7))^0.8 * Cap_init/100;
```

Appendix VI. Controller Simulink block set of control logic №5

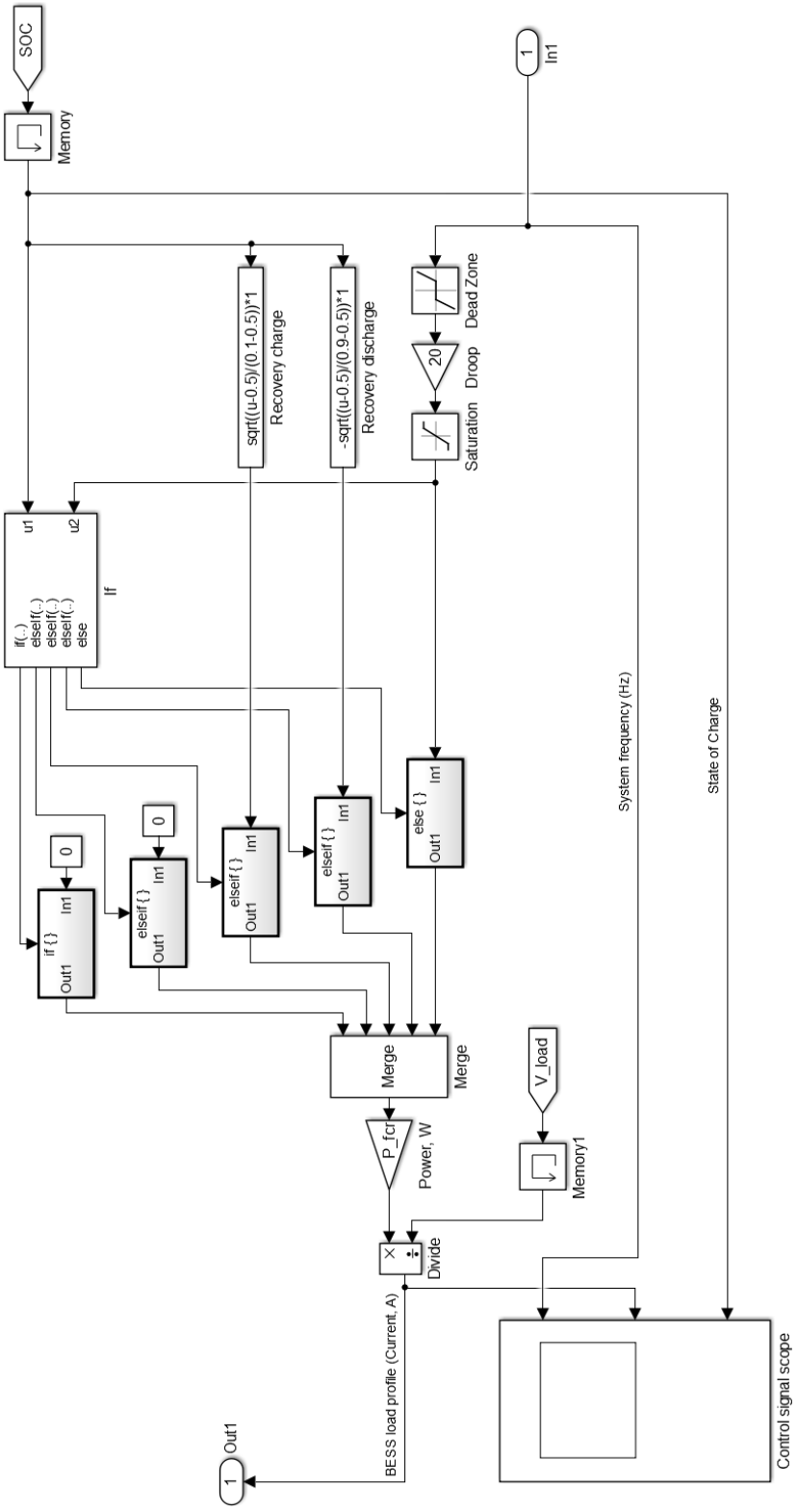

Appendix VII. Representative cases NPV calculation

Table VII.1. BESS cash flows and NPV calculation (1.6 MW/1 MWh; EoL - 60% SoH; control logic №5).

Year	Remained capacity, MWh	Max bidding power, MW	Installed costs, EUR	Income, EUR	Penalty costs, EUR	Cash flow, EUR	Present value factor	Present value of cash flow, EUR	Cumulative NPV, EUR
0	1.00	1.60	-900 000	0	0	-900 000	100%	-900 000	-900 000
1	0.90	1.43	0	215 033	-1 945	213 088	95%	202 941	-697 059
2	0.85	1.36	0	203 711	-1 842	201 868	91%	183 101	-513 958
3	0.81	1.30	0	194 828	-1 762	193 066	86%	166 778	-347 181
4	0.78	1.25	0	187 233	-1 693	185 539	82%	152 644	-194 537
5	0.75	1.20	0	180 470	-1 632	178 838	78%	140 124	-54 413
6	0.73	1.16	0	174 305	-1 576	172 729	75%	128 893	74 480
7	0.70	1.12	0	168 596	-1 525	167 071	71%	118 735	193 215
8	0.68	1.09	0	163 251	-1 476	161 774	68%	109 495	302 710
9	0.66	1.06	0	158 204	-1 431	156 773	64%	101 058	403 767
10	0.64	1.02	0	153 409	-1 387	152 021	61%	93 328	497 095
11	0.62	0.99	0	148 829	-1 346	147 483	58%	86 230	583 326
12	0.60	0.96	0	144 436	-1 306	143 130	56%	79 700	663 026
12.13	0.60	0.96	0	18 704	-169	18 535	55%	10 256	**673 281**

Table VII.2. BESS cash flows and NPV calculation (1.6 MW/1 MWh; EoL - 80% SoH; control logic №5).

Year	Remained capacity, MWh	Max bidding power, MW	Installed costs, EUR	Income, EUR	Penalty costs, EUR	Cash flow, EUR	Present value factor	Present value of cash flow, EUR	Cumulative NPV, EUR
0	1.00	1.60	-200 000	0	0	-200 000	100%	-200 000	-200 000
1	0.90	1.43	0	215 033	-1 945	213 088	95%	202 941	2 941
2	0.85	1.36	0	203 711	-1 842	201 868	91%	183 101	186 042
3	0.81	1.30	0	194 828	-1 762	193 066	86%	166 778	352 819
3.37	0.80	1.28	0	71 003	-642	70 361	85%	59 693	**412 512**

Table VII.3. BESS cash flows and NPV calculation (0.8 MW/1 MWh; EoL - 60% SoH; control logic №5).

Year	Remained capacity, MWh	Max bidding power, MW	Installed costs, EUR	Income, EUR	Penalty costs, EUR	Cash flow, EUR	Present value factor	Present value of cash flow, EUR	Cumulative NPV, EUR
0	1.00	0.80	-900 000	0	0	-900 000	100%	-900 000	-900 000
1	0.92	0.74	0	111 942	-235	111 707	95%	106 388	-793 612
2	0.88	0.71	0	107 436	-225	107 210	91%	97 243	-696 369
3	0.85	0.68	0	103 880	-218	103 662	86%	89 547	-606 822
4	0.83	0.66	0	100 829	-212	100 617	82%	82 778	-524 044
5	0.81	0.65	0	98 105	-206	97 899	78%	76 706	-447 338
6	0.79	0.63	0	95 616	-201	95 415	75%	71 200	-376 137
7	0.77	0.61	0	93 307	-196	93 111	71%	66 172	-309 965
8	0.75	0.60	0	91 141	-191	90 950	68%	61 559	-248 407
9	0.73	0.59	0	89 094	-187	88 908	64%	57 311	-191 096
10	0.72	0.57	0	87 147	-183	86 964	61%	53 389	-137 707
11	0.70	0.56	0	85 285	-179	85 106	58%	49 760	-87 947
12	0.69	0.55	0	83 498	-175	83 323	56%	46 397	-41 550
13	0.67	0.54	0	81 776	-172	81 604	53%	43 277	1 726
14	0.66	0.53	0	80 112	-168	79 944	51%	40 377	42 103
15	0.65	0.52	0	78 501	-165	78 337	48%	37 681	79 785
16	0.63	0.51	0	76 938	-161	76 776	46%	35 172	114 957
17	0.62	0.50	0	75 417	-158	75 259	44%	32 835	147 792
18	0.61	0.49	0	73 936	-155	73 781	42%	30 658	178 450
18.67	0.60	0.48	0	48 886	-103	48 784	40%	19 619	**198 069**

Table VII.4. BESS cash flows and NPV calculation (0.8 MW/1 MWh; EoL - 80% SoH; control logic №5).

Year	Remained capacity, MWh	Max bidding power, MW	Installed costs, EUR	Income, EUR	Penalty costs, EUR	Cash flow, EUR	Present value factor	Present value of cash flow, EUR	Cumulative NPV, EUR
0	1.00	0.80	-900 000	0	0	-900 000	100%	-900 000	-900 000
1	0.92	0.74	0	111 942	-235	111 707	95%	106 388	-793 612
2	0.88	0.71	0	107 436	-225	107 210	91%	97 243	-696 369
3	0.85	0.68	0	103 880	-218	103 662	86%	89 547	-606 822
4	0.83	0.66	0	100 829	-212	100 617	82%	82 778	-524 044
5	0.81	0.65	0	98 105	-206	97 899	78%	76 706	-447 338
5.32	0.80	0.64	0	31 131	-65	31 066	77%	23 964	**-423 374**